CARDIFF UNIVERSITY

SCHOOL OF ENGINEERING

Thesis Titled:

Laboratory Characterisation of Soil Ionisation under Impulse Voltages

By

Alseddig E. Elzowawi

Thesis submitted in fulfilment of the requirements for the degree of Doctor of Philosophy, 2016

DECLARATION

This work has not previously been accepted in substance for any degree and is not concurrently submitted in candidature for any degree.

Signed…………………….…… (Candidate) Date…...................................

STATEMENT 1

This thesis is being submitted in partial fulfilment of the requirements for the degree of PhD

Signed…………………….…… (Candidate) Date…...................................

STATEMENT 2

This thesis is the result of my own work/investigation, except where otherwise stated. Other sources are acknowledged by explicit references.

Signed…………………….…… (Candidate) Date…...................................

STATEMENT 3

I hereby give consent for my thesis, if accepted, to be available for photocopying and for inter-library loan, and for the title and summary to be made available to outside organisations.

Signed…………………….…… (Candidate) Date…...................................

STATEMENT 4

I hereby give consent for my thesis, if accepted, to be available for photocopying and for inter-library loans after expiry of a bar to access previously approved by the Graduate Development Committee.

Signed…………………….…… (Candidate) Date…...................................

ACKNOWLEDGEMENT

I would like to express my very great appreciation to my supervisors Professor. A. Haddad and Professor. H. Griffiths for their invaluable guidance and feedback to navigate throughout the research. It has been a great honour to work with Prof. Haddad, and I have learnt a lot from his wide knowledge and wisdom.

I would like to thank all the staff members of the Advanced High Voltage Engineering Research Centre and Morgan-Botti Lightning Laboratory for their support, and the time they have given me. Also the staff members of the school of engineering for the service and friendly environment.

I would like to offer my special thanks to my motherland Libya, the ministry of the Libyan higher education and the University of Misurata for the scholarship to pursue my postgraduate study, which has been a step forward and a significant change to my entire life.

My thanks are also extended to all my colleagues in the group for their discussion and friendship, especially during the weekly presentations. To all my friends, especially those who kept in touch for the study period.

I would like to express my deep gratitude to all my family back home in Libya for the great love, encourage and support, especially my mum who was her prayers enlightening my way.

Lastly, special thanks to my family here in the UK, my beloved wife for the sincere love, support and long patience. To my son for the happiness he brought to my heart.

ABSTRACT

Since the discovery of the soil ionisation phenomenon in the earthing systems under high lightning current, there have been tremendous investigations studying this ambiguous phenomenon. Some aspects are still not yet fully addressed, which some of them were considered in this thesis, such as visualizing the phenomenon, soil ionisation delay times, propagation velocity, and breakdown stages in dry porous materials, the initiation and propagation of the soil ionisation in two-layer soil with different moisture contents and thicknesses.

Therefore, a special test cell has been developed to facilitate the various laboratory tests conducted in this study. The rig has a rod-plane electrode configuration. A transparent dielectric tube installed between the electrodes, as the samples were placed in this tube. Glass bubble material and sand were used as tests media throughout the study.

In this thesis, a new methodology was used to visualise the phenomenon in a new dielectric porous material under fast and slow impulse voltages. The correlation between the recorded videos and the discharge waveforms was a major achievement. It provided significant results, exhibiting the dynamic developments of the discharge throughout the applied impulse. Various discharge scenarios were visualised with a new sample configuration, which was prepared especially for this investigation, and showed great outcomes.

Due to the high performance of new sample configuration, and in order to understand the ionisation process in the dry layer, multi-point voltage measurement technique was utilised to acquire the potential in the ionised zone in the dry layer. The measured voltages tracked the initiation and propagation of the soil ionisation in the dry layer. The velocity of the propagation was also investigated. Two delay times were obtained, which represented the various initiation and propagation stages of the ionisation until the dry layer breakdown. The new sample arrangement was also simulated with a proposed equivalent circuit that presented a satisfactory agreement with the real test performance.

Several scenarios were examined to study the initiation and propagation of the soil ionisation in two-layer sand under lightning surges. Multi-point voltage measurement technique was also used to trace the ionisation in both layers. Similar breakdown stages to those in glass bubble material were found. The soil ionisation was found to initiate and propagate in the lower wet sand layer after the breakdown of the upper dry sand layer. The amount of water and the thickness of both layers were found to have a great impact on the initiation and propagation of the ionisation phenomenon in both layers of the sample.

PUBLICATIONS

1. **A. Elzowawi,** A. Haddad and H. Griffiths, 'Discharge in Glass Bubbles under Impulse Voltage', Seventh Universities High Voltage Network, UHVnet 2014, Colloquium on Sustainable HV and UHV Networks The Interdisciplinary Challenge, 15-16 Jan 2014, Surrey University 2014. (**Poster**)

2. **A. Elzowawi,** A. Haddad and H. Griffiths, 'Review: Techniques Used in Visualization of Electric Discharge in Soil', the sixth ENGIN conference, Cardiff school of engineering, 18-20 June 2014, Gregynog.

3. **A. Elzowawi,** A. Haddad and H. Griffiths, 'Visualization of Electric Discharge in Porous Materials', International Conference on High Voltage Engineering and Application 2014, 8 - 11 September 2014, Poznan, Poland.

4. **A. Elzowawi**, A. Haddad and H. Griffiths, 'Ionisation under Impulse in Two-Layer Wet and Dry Soil Sample', eighth Universities High Voltage Network, UHVNet 2015, Colloquium on HVDC Power Transmission Technologies, 14-15 Jan 2015, Staffordshire University 2015. (**Poster**)

5. **A. Elzowawi,** A. Haddad and H. Griffiths, 'Visualization of the Ionisation Phenomenon in Porous Materials under Lightning Impulse', 9th Asia-Pacific International Conference on Lightning (APL), 23-26 June 2015, Nagoya, Japan.

6. **A. Elzowawi**, A. Haddad, H. Griffiths and D. Clark, 'Investigation of Impulse Discharges in Two-Layer Wet and Dry Soil Sample', 19th International

Symposium on High Voltage Engineering (ISH), 23-28 Aug 2015, Pilsen, Czech Republic.

7. **A. Elzowawi,** A. Haddad, H. Griffiths and D. Clark**,** 'Investigation of Soil Ionisation Propagation in Two-Layer Soil Samples', 50th International Universities Power Engineering Conference (UPEC), September 1-4, 2015, Stock on Trent, UK.

TABLE OF CONTENT

LIST OF FIGURES

xiii

Chapter One

Introduction

1.1 Background

The earthing system is one of the most important elements in the safety and protection system in any electrical power network. Its purpose is to protect people and reduce the damage caused by various faults that occur in the grid. Lightning strikes on transmission and distribution lines and towers are extremely powerful faults that present a serious hazard, which can cause significant damage and losses, due to the high current values injected into the network. Protection devices and earthing systems divert these currents to the ground to be dissipated safely. This requires good earthing systems that offer low impedance paths for the diverted currents. However, earthing systems perform differently under high impulse current excitation, creating a nonlinear

behaviour in the soil around the earthing electrodes. This distinct behaviour is characterised by the considerable reduction of the soil impulse impedance under high impulse currents. [1]. The impedance reduction can be explained by the initiation of the soil ionisation phenomenon, which occurs inside the voids between the soil grains surrounding the ground electrode. Based on this, numerous investigations have been carried out to examine the reasons behind this peculiar phenomenon, which has led to the development of theory explaining the impulse currents into the soil [1]. Therefore, more research is required to study the soil ionisation phenomenon to develop more efficient earthing systems in order to achieve safer power networks.

1.2   Soil Ionisation Phenomenon

In 1929, Towne observed a phenomenon in the soil around a concentrated earthing rod electrode under high impulse currents excitation. He noticed that the soil resistivity had dropped to a lower value compared to the steady state value. This resistivity reduction was attributed to the soil ionisation phenomenon that occurred in the soil [2]. This phenomenon is of great benefit to earthing systems; it reduces the impulse impedance, allowing the current to dissipate more quickly in the soil and so reduces the earth potential rise (EPR). Since then, a considerable amount of literature has been published on this complex phenomenon in terms of several angles and various features; for example, determining the critical electric field value that is responsible for the initiation of the phenomenon under various electrode arrangements [3-6], determining the effect of some factors on the discharge process, such as water content, grain size, dimension and configuration of the electrode, polarity of the applied voltage [7-11], studying the soil breakdown

phenomenon and initiation and propagation of the streamers [12-16], using models and circuits to verify and predict the behaviour of the system taking account of the ionisation phenomenon [17-21], photographic studies to obtain visual pictures of the discharge development under different conditions [22-26].

Water content is considered the main element affecting the resistivity of the soil. The soil resistivity can vary from a low number of Ohms per metre in wet soil to a high number of kilo-Ohms per metre for dry soil, depending on the differences in the grain size, moisture percentage, soil type, and salt content. Based on the above, soil ionisation could have different critical electric fields before initiation, and different resistivity reductions after initiation [6, 11]. In addition, if the water content is very high (saturated soil), soil ionisation cannot be initiated, since the voids between the grains are full of water and not air, as was found in [20]. Nor et al. [27, 28] performed several tests to find the relation between the steady state resistance and the impulse resistance. The investigation revealed that the degree of soil ionisation effect relies on the DC resistances (R_{dc}): the smaller the value of (R_{dc}) is, the lesser the impact of the ionisation phenomenon on the soil will be.

Despite the long history of the discharge process in the soil surrounding the earthing electrodes, it is still a major area of interest within the field of earthing systems. From the literature, it has been observed that imaging soil ionisation could reveal significant information about the ionisation process. Nevertheless, the imaging techniques already in use produce very limited views of the phenomenon, and they cannot record the dynamic changes of the discharge. Therefore, in this study, a different methodology is employed to

take images of the soil ionisation around the high voltage electrode. Moreover, soil ionisation initiation and propagation processes and the breakdown stages in two-layer soil have still not been fully addressed. Consequently, laboratory tests are conducted in this work to investigate the factors affecting the soil ionisation and the breakdown process in two-layer sand samples with different water contents.

1.3 Thesis Scope and Objectives

This thesis studies and explores the different characterises of the soil ionisation phenomenon, such as visualising the phenomenon around the electrode, its impact on dry porous media, the initiation and propagation of the phenomenon in dry porous materials, and the initiation and propagation of soil ionisation in two-layer soil. Therefore, the following objectives are considered:

- An extensive review of the soil ionisation concerning different aspects that greatly influence the phenomenon and visual techniques used to record the phenomenon.

- Visualisation of the electric discharge phenomenon in a dry glass bubble material under lightning and switching impulse voltages.

- Investigation of the soil ionisation impact on the dry porous media used in this research under lightning voltage.

- Investigation of the initiation and propagation stages of the soil ionisation phenomenon in dry porous dielectric materials.

- Investigation of the streamer velocity during the propagation through the dry porous materials.

- Investigation of the soil ionisation initiation and propagation in a wet soil layer below a dry soil layer after the breakdown of the latter layer.

- Investigation of the initiation and propagation of the soil ionisation phenomenon in two wetted sand layers with different moisture contents.

- Study of the effect of the layers thickness in a two-layer soil sample on the initiation and propagation of the soil ionisation in both layers.

1.4 Contributions

- Extensive literature of the soil ionisation characterisation and visualisation.

- Proposed new porous material (glass bubble material) and a novel two-layer arrangement of the test sample was prepared, to investigate characteristics and dynamic development of soil ionisation.

- Evidence of soil ionisation was obtained through a new correlated voltage and current measurements and high-speed camera imaging of the ionisation phenomenon.

- A new technique using a multi-point voltage measurement along the path of the discharge current was proposed and successfully applied.

- Using the multi-point voltage measurement technique, the variable velocity of the ionisation discharge propagation is quantified for the first time.

- Soil ionisation initiation and propagation in two-layer sand samples with different water contents was investigated and classified under lightning impulse voltages.

1.5   Thesis Content

This thesis is organised into seven themed chapters including the current chapter, which describes the phenomenon, the objectives of the thesis, and the contributions of the research. A list of references is placed at the end of the thesis with full details of all cited references. A brief description of each chapter is as follows:

Chapter 2

In this chapter, the previous work related to this research is reviewed. This includes the causes of the nonlinear behaviour of the soil under high impulse currents, the critical electric field and the factors influencing its value, soil breakdown initiation and the resulting delay time, and various definitions of the impulse impedance. It also includes the circuit models proposed to simulate the soil under impulse voltages considering the ionisation phenomenon, imaging soil ionisation around the electrodes with the utilized techniques, and finally, the soil ionisation initiation and propagation processes in multilayer soil under diverse conditions.

Chapter 3

This chapter presents the methodology followed to achieve the objective of the thesis. In addition, it provides a practical description of the generators, the visual techniques, the measurement equipment, the test circuit, the porous material used as test media, and the test rig built for the project. The rod-plane electrode configuration in the test cell was also simulated using finite element software (COMSOL Multiphysics) to study the electric field behaviour. Then, the test cell was examined with resistive salt water to investigate the behaviour

of the rig under the applied impulse voltages. Finally, a comparison was made between lightning discharges in the glass bubble material and sand in order to compare the behaviour of both materials.

Chapter 4

This chapter presents and discusses the visual investigations carried out to record the discharge phenomenon in the dielectric porous glass bubble material under lightning and switching impulse voltages. A resistivity test was performed to determine the glass bubble resistivity. A special sample arrangement and high-speed cameras were utilised to facilitate the imaging process. The recorded videos of the discharges were then correlated with the applied voltage and the current flowing through the sample. A microscopic imaging process was also carried out on the glass bubble filaments, which are thought to be formed by the current flow in the dry material.

Chapter 5

Due to the remarkable performance of the new sample configuration used with the visual study, as discussed in the previous chapter, this chapter considers the subsequent electrical examination, which was implemented to investigate the behaviour of the wet glass bubble material and the impact of the ionisation phenomenon on the dry glass bubble material. The propagation of the soil ionisation and the breakdown steps were also studied in the dry material. Furthermore, an equivalent circuit of the sample was proposed and simulated by a transient software program. Finally, a comparison was made to summarize the main differences between the lightning and the switching discharges in glass bubble material.

Chapter 6

The sixth chapter discusses the initiation and propagation of soil ionisation in two-layer soil samples under lightning impulse voltage. These layers contain various moisture contents. Two voltage probes were installed at different positions in the sample to track the ionisation phenomenon in both layers. Various scenarios were considered in this chapter, such as soil ionisation propagation in dry sand, the initiation of the ionisation phenomenon in the wet sand below a dry sand layer, and two wetted layers with distinctive water percentages. A comparison between the discharge in dry and wet porous materials was accomplished. Lastly, thermal calculations was carried out to determine the energy required to achieve the thermal effect under lightning impulse.

Chapter 7

This chapter presents a general discussion of the findings of all the experiments performed during this research. The main conclusions are also discussed and summarized. To conclude the thesis, several recommended suggestions for future works are listed in this chapter.

Chapter Two

Soil Ionisation in Earthing Systems:

Literature Review

2.1   Introduction:

In electrical power systems, ground is utilised as a sink allowing fault and lightning currents to be drained and dissipated safely and quickly. This is achieved using what are called earthing systems. Therefore, these systems divert the fault currents from the system to the ground, to protect people from injury and the system in general from damage and losses. However, any earthing system must provide a low resistivity path for these currents to be diffused into the ground. To design a system that will allow impulse current dissipation process into the soil is considered difficult due to the nonlinear

behaviour of the soil surrounding the earthing electrodes under high impulse currents [11]. It is well known that soils are porous materials that consist of a mixture of many different substances, such as nonconductive variable sized grains, air voids, different water percentages, salts and minerals, stones, and other materials like organic substances. These components combine to make the soil an inhomogeneous medium. Air will fill the gaps among the soil grains in dry soil conditions; in this case, the dry soil is a good dielectric material, whereas in wet soil, air with water will occupy the voids to construct a vast net, which could produce conducting channels. These channels provide the soil with its conductivity and reduce its resistivity. Soil conductivity widely varies depending on the water and salt content, and the size of the grains. Moreover, the grains usually have different sizes, such as fine soil, medium soil, and coarse soil, according to the BS1377 standard [29]. Different particle shapes will create irregular air cavities inside the soil [6, 8, 30]. However, in many studies, to eliminate the complexity of the non-uniformity of the soil when proposing and studying soil models, soil has been assumed to be a homogenous and isotropic medium [31-34].

2.2   Soil Impulse Behaviour

It has been concluded from the experimental laboratory work implemented in [7, 11, 20] that the nonlinear behaviour of soil commences once the current jumps to a second peak, while the voltage is decaying. This additional current peak is due to the resistivity reduction in the soil in the vicinity of the electrode. However, it was thought the resistivity reduction was due to either the soil ionisation (electrical process) or thermal process or to both processes. The second current peak raises two different resistances, the first is the pre-

ionisation resistance (R_1), which is caused by the first current peak and the soil properties, and the second parameter is the post-ionisation resistance (R_2), which is related to the second current peak. Thus, due to the soil ionisation, (R_1) is always greater than (R_2). The two current peaks and the applied impulse voltage are depicted in Figure 2-1 [11, 20]. In this figure, there are also two different delay times generated by the second crest, these times are: time lag (t_1), which is the time of the ionisation onset, while the time (t_2) is the time lag for the second current peak [11]. Besides the second current peak, other criteria reported in [2, 35] to identify the occurrence of soil ionisation in the soil neighbouring the earthing electrode. For instance, when the I-V curves start to form loops in the shape of (⌀), then it is confirmed that the ionisation phenomenon has been initiated.
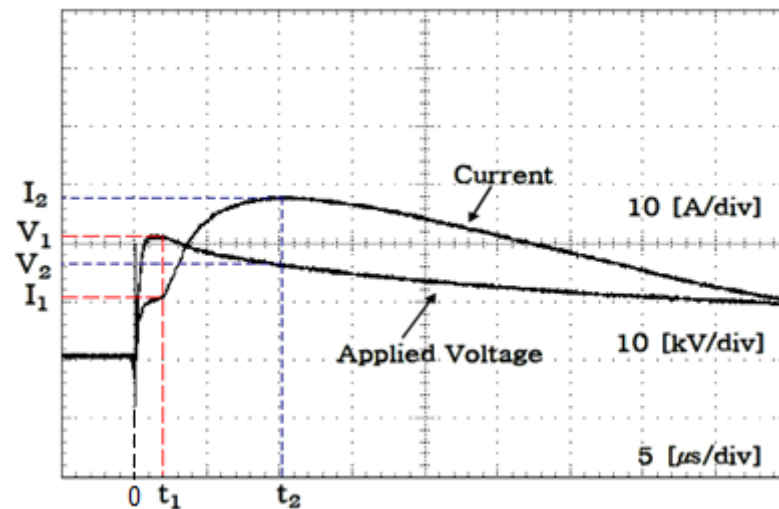
Figure 2-1: voltage and current traces with initiation of soil ionisation phenomenon under lightning impulse voltage (modified from [11])

The other condition is the time lag between the rise time of both the voltage and the current, the time to the current peak increases with the increase in the applied voltage at the initiation of the soil ionisation, whereas the front time of

the voltage does not change. Moreover, soil ionisation can also be observed by examining the impulse impedance behaviour, so when the impulse impedance is lower than the steady state impedance, then it is known that the ionisation phenomenon has initiated in the soil. For the uniform electric field, soil ionisation is initiated with the occurrence of the breakdown, the current sharply increases and the voltage collapses at the same moment as the ionisation phenomenon occurs. Soil resistivity reduction caused by the ionisation phenomenon is thought to offer a great benefit in decreasing the earth potential rise (EPR). The value of the critical electric field controls the degree of the soil resistivity reduction [36]. However, it was reported in [37] that the degree of the resistivity reduction or the soil ionisation effect depends on the magnitude of the DC resistance (R_{dc}); meaning that if (R_{dc}) is low, then the degree of ionisation is low (slight resistivity decrease) as well. These two claims should not contradict each other, because it has been found that as the water content increases to a certain limit, which reduces (R_{dc}), the critical electric field decreases as stated in [8].

In one well-known study, Liew and Darveniza [34] have developed a significant dynamic model to describe the behaviour of soil excited by lightning surges. This model was based on series of tests on different vertical rods installed in different soils (gritty light clay, sand and gravel mix and loamy sand). impulse current were applied in a range of (1 kA- 20 kA) with different wave shapes between 6-16 μs and 18-54 μs. The soil resistivity profile was plotted against the current density to examine the performance of the soil including the nonlinear ionisation phenomenon. The soil resistivity produced a hysteresis with a time variant during the discharge. From the model, three steps were

identified in the whole discharge process as shown in Figure 2-2. The first step
(a) is called 'no ionisation', when the resistivity is still constant before the onset
of ionisation. The second stage (c) (ionisation zone) is when the current
density exceeds the critical value (J_c), and then the soil ionisation is initiated,
leading to a fall in the resistivity with an exponential curve. The last step (b) is
when the current density is decreasing below the critical value; hence, the soil
resistivity is recovering to the original value 'deionisation zone'. Due to the
complexity of the soil ionisation phenomenon, some assumptions have been
made, such as, considering soil to be an isotropic and homogeneous medium,
and assuming there is a uniform ionisation zone around the electrode.
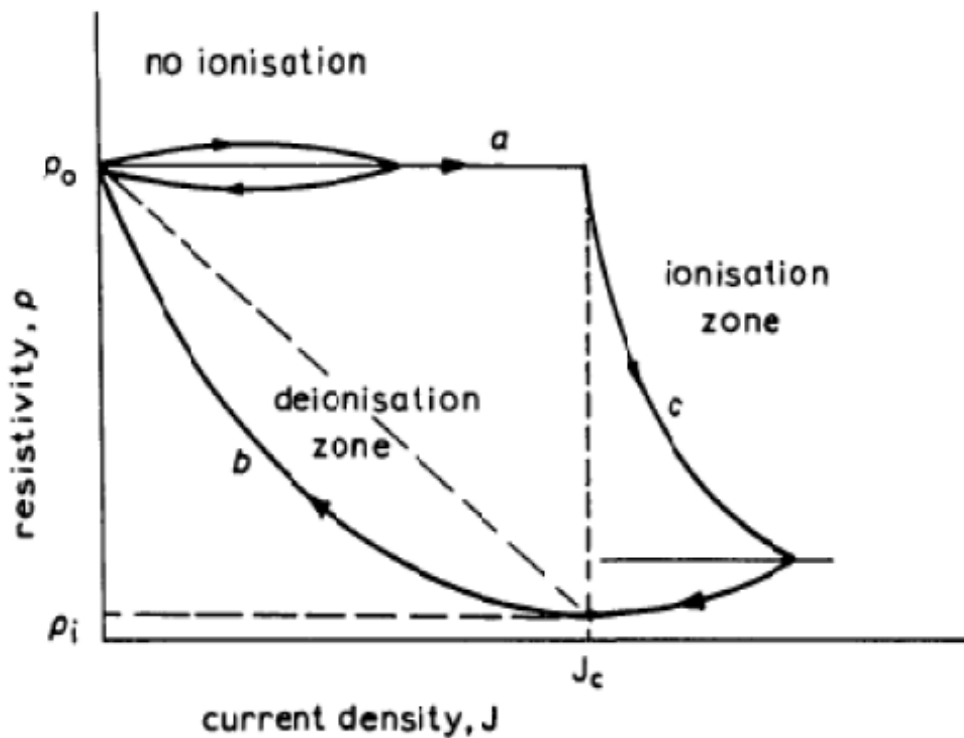
Figure 2-2 resistivity profile during the impulse [34]

Once the discharge occurs, the electric field will have the greatest value at the
surface of the electrode. This value will decrease as it proceeds away from the
electrode through the soil. If the shape of the electrode changes, the ionised

area around the electrode will change too, but the ionisation mechanism does not change. It is very difficult to predict the shape of the ionisation zone. Thus, it was assumed that these zones can be uniform whereby [36, 38] adopted a range of forms for electrodes and for ionised zones near them for use in soil ionisation models to facilitate the calculations of the soil resistivity and the electric field [30, 38].

2.2.1 Electrical Process

The majority of researchers and authors studying earthing systems consider soil ionisation process, which occurs in the air pockets inside the soil, as the predominant mechanism that creates the nonlinear behaviour of the soil under high impulse current excitation [2]. The ionisation process begins when the applied electric field is sufficiently intense to ionise the air filling the spaces among the soil particles. The field in these voids will be enhanced due to the relative permittivity differences between the air and the soil. Once the air is ionised and converted from an insulating medium to a conductive medium, then the resistivity of the soil drops significantly, in some cases causing the current to jump to a second crest. In addition, during the current decay, another phenomenon starts to take effect, which is opposite to the ionisation process. This is the deionisation process, where the ionised soil recovers and regains the original resistivity value through this process, as described in Liew and Darveniza's model [11, 20, 30, 34].

In a key study, Flanagan et al. [16] performed an experiment using a parallel plated cylindrical soil sample with 0.5 cm separation under a 10 kV pulser. The test was carried out under two conditions. The first was with air, while the second was with SF_6 gas, so the sample was submerged in SF_6. It was

observed that the breakdown voltage was much higher in the case of SF_6 than in air, which was attributed to the higher breakdown threshold of SF_6. This was a clear indication that soil ionisation is the reason behind the reduction in soil resistivity, supporting the theory of the electrical process.

In a follow-up study in 1983, the same team as in the previous study [39] conducted another investigation using SF_6 gas. A special mechanism was employed to replace the air in the soil sample with SF_6 gas. The soil was placed in a plastic tube measuring 56 cm diameter; the ground electrode was a circular plate, while the active electrode was a sphere electrode. Coarse sand wetted with tap water was considered to ease the exchange of the gases in the sample. The outcome of this study offers strong evidence that soil ionisation is responsible for the breakdown under impulse voltages, where the ratio of the critical electric field of air and SF_6 is around 2.5, since the breakdown threshold of SF_6 gas is about 2.5 times that for air.

Later, in 1986, Snowden et al. [13] implemented tests similar to the above investigations, also using SF_6 gas, and compared the results with the test results under air. However, the test configuration was completely different, and the mechanism of the placement of the gases into the soil sample was also changed. The test rig was a Plexiglass tube 2.5 cm in diameter. Both electrodes were copper plugs sealed to both ends of the tube. The ground plug had a pin in the centre extended inside the tube to initiate the breakdown. Six voltage transducers were installed in the tube to measure the voltage along the sample. In order to avoid drying the soil, the gas was bubbled by water, it was then sent flowing through the gas ports into the tube, where the soil sample was placed. Dry and wet sands with different water contents were

examined. With the dry sand, similar results were observed, as the SF_6 gas increased the electric field threshold value of the breakdown, where the streamer was found to initiation at 62kV while with the SF_6 was 75kV. Conversely, as more water was added to the sample, the SF_6 gas did not tend to have an impact on the discharge. This result was unexpected and contradicted the conclusions of Flanagan's tests. However, Mousa [36] had argued that the procedure of replacing the gases was not effective, as it may easily have led to an incomplete gas exchange; also replacing the air with SF_6 in the sample with the bubbling technique seemed to introduce a high percentage of moisture in the SF_6 gas, which could have reduced the dielectric strength of this gas.

According to [40, 41], in dry soil, the ionisation phenomenon was considered the main reason for the drop in the resistivity of the soil when the high impulse voltage was applied. There are no water channels in the soil to conduct the current and increase the temperature by generating resistive heating. Moreover, after changing the impulse polarity, the resistivity reduction changed accordingly, which supports the ionisation hypothesis, whereas the thermal effect might not be affected by the polarity change. These two studies investigated soil ionisation in dry soil with a cylindrical electrode configuration. Positive and negative lightning impulses were applied to a dry medium grain sand sample. The resistances obtained under the positive polarity were found to be smaller than those under the negative polarity, which was attributed to the greater current under the positive surges. In addition, U_{50} of the breakdown voltage level was found 67.9 kV under positive impulses, and 69.6 kV under negative impulses. These voltage values corresponds to the electric field

values of 35.2 kV/cm and 36 kV/cm respectively. The authors attributed that to the generated higher local space charge under positive impulse than under negative impulse.

2.2.2   Thermal Effect during Impulse Discharge

In the literature, authors have attributed the thermal effect in the discharge to the resistive heating ($I^2 \times R$) due to the current flow in water channels, shunting the wet soil grains [11, 37, 40, 41]. This heating leads to an increase in the conductivity of the water, which then contributes to the decrease in the soil's resistance. The low energy absorption based on the moisture content and the type of minerals and salts may enhance the ionic conductivity. However, in the case of excessive heating during the discharge, water evaporation may occur, which will dry some areas, leading to a reduction in the conductivity and then an increase in the soil resistivity. Therefore, the produced heat will either result in an increase or decrease in the soil resistivity depending on the energy absorption, which is very difficult to predict. Leadon et al. [39] highlighted that once the resistivity of the water decreases with the resistive heating, thermal instability created by the heating rate non-uniformity might occur, driving the current to flow in a few channels that have lower resistivity. If the water temperature continues to rise up to boiling point, then the breakdown is presumed to occur. Moreover, they viewed that the thermal process is a plausible main reason for the soil breakdown in saturated soil, but between the dryness and the moisture saturation, the electrical and thermal processes are competing with one another to dominate the discharge process.

Lee et al. [11] conducted a series of tests with a hemispherical test rig. Various water percentages were selected. As a result, two current peaks were

observed during the discharge. The reduction in the pre-ionisation resistance (R_1) was attributed to the thermal process, which resulted from the current conduction, due to the increase in the ion's mobility if no evaporation had occurred, whereas the reduction in the post-ionisation resistance (R_2) was attributed to the field enhancement process (soil ionisation).

In 1982, van Lint and Erler [14] carried out a vital investigation with a pulser that generated long impulse waves of up to 1 ms. The samples consisted of wetted sands with different moisture contents. A very long streamer initiation delay time (1500 μs) was observed. The authors thought that field enhancement theory was not able to offer an explanation for this long time lag. Thus, the instability of the thermal resistance of the water was believed to concentrate the current stream in specific water filaments, leading eventually to steam bubbles in that filament. In the presence of electric field, these bubbles could be converted to plasma.

Furthermore, Snowden and Erler [42], implemented another investigation supporting the thermal process theory. Impulse current waves of more than 1ms were applied to soil samples placed in a coaxial electrode arrangement. Several simplifications were considered to facilitate the model, such as, assuming that the discharge would be in a single cylindrical channel, hence, ignoring the interconnected current paths among the soil particles. It was also assumed that the thermal properties of the medium were uniform. A heat flow equation was applied to predict the temperature of the current path; for longer periods, the soil thermal diffusion controlled the rise in temperature. Then, the solution of the equation was used to study the streamer initiation. It was proposed that streamers were initiated when the water was heated up to

boiling point, but the initiation process of the streamers does not need to evaporate the whole water channel. However, Mousa [36] queried the assumptions considered in this study, and he claimed that the obtained results did not support the thermal process by water evaporation.

According to [40, 41], the thermal process could also take place in dry soil, where the process is probably due to the electrons colliding with air and soil atoms, but this type of temperature rise was observed mainly after the breakdown phenomenon had occurred. However, in [2, 40, 43], it was reported that the thermal and the electrical processes co-exist and that both could occur simultaneously during the discharge. Distinguishing between them is very difficult due to the problem of determining the amount of energy absorbed through high impulse excitation; in addition, no definite border between the dominance of both mechanisms has yet been identified. Despite all the above discussion, it is worth noting that the majority if not all the studies were investigating the resistivity drop mechanism by the thermal effect, particularly in the case of long delay time, but did not aim to explain the propagation of the low resistivity zone with the thermal process. According to the theory that states that the thermal effect is due to the resistive heating, and given the approximations that Snowden and Erler mentioned in their model [42], the heating effect would take place in and around the current channel only. This points to the possible conclusion that the generated resistive heat could be uniform throughout the current path if uniform soil grains and water distribution were assumed. Therefore, the resistivity reduction should occur along the current channel from the high voltage electrode until it reaches the ground electrode. This scenario contradicts the fact that the propagation process of

the lower resistivity zone starts around the electrode and then expands further away to a limited extent, so that, there will be one area that has a high electric field, and another area that has a low electric field. Consequently, the thermal effect may not be able to explain the growth stages of the low resistivity zone (ionisation zone) alone. Moreover, the unpredictable degree of heat yielded during the discharge may cause an increase or decrease in the soil resistivity, which supports this hypothesis. However, with the electrical process, as the electric field increases, the resistivity decreases up to the breakdown. With the thermal process, if the heating is excessive, then some of the moisture will evaporate and the soil will be dried, meaning, the soil resistivity will increase, but at this stage, various possibilities might occur. Firstly, the localised dried area may not be near the electrode. The other possibility is that the dry region could be shunted by the neighbouring wet area, otherwise a breakdown may occur at the greatest electric field [36, 42].

Moreover, regarding the thermal process, there has not been any temperature measurements or calculations made to provide fair quantities to support the thermal theory by performing electrical tests on soil, as the thermal studies were based on many assumptions which might not be practical in real systems [36]. For high wetness in the soil, the energy required to heat and evaporate the water is very high, and yet to date, no experiment has been carried out under very high impulse currents to investigate the thermal effect with high moisture contents [44]. As a result, the thermal process does not seem to be the main cause of the nonlinear behaviour of the soil under high impulse energization. However, it could participate during the discharge with the electric process to initiate the ionisation phenomenon.

2.3 Electric Field Threshold of Ionisation

One of the key parameters in studying soil ionisation is the critical electric field (E_c) that is required to initiate the ionisation phenomenon. E_c could be defined as the electric field value at which the current and voltage of the discharge start to demonstrate a nonlinear behaviour. Many studies have attempted to determine and predict the value of (E_c), and in the literature, there are many suggestions, experiments, and formulae which give estimated values and ranges of E_c [6]. Many authors have suggested several values for the critical electric field. This could be due to the lack of any standard or recommended method or procedure to determine E_c [35, 45]. For instance, Mousa [36] recommended that E_c should be equal to 3 kV/cm, while CIGRE [46] suggested that (E_c) should be considered to be 4 kV/cm. These two values are the most reasonable values used in the earthing systems [47]. Additionally, several factors may affect the value of (E_c) in the soil, such as water content, soil type, and the uniformity of the electric field. Therefore, Nor et al. [5] examined a few of the factors that influence the value of E_c. A hemispherical test cell and parallel plate configuration were utilized to determine the value of the critical electric field under different conditions. Water content in the samples was varied and both fine and medium sand grains were tested. Sodium Chloride (NaCl) was added to the water content to reduce the resistivity of the soil in some of the samples. The authors (Nor et al. [5]) found E_c was 5.5 kV/cm with the hemispherical arrangement, but with the parallel plates, E_c was 7.9 kV/cm. This higher value was thought to be caused by the lower uniform electric field in the parallel plate configuration. Regarding the grain size effect, the authors have concluded that E_c has an independent

behaviour, as 5.5 kV/cm was found with both fine and medium sand grains in the hemispherical test rig. Due to the high conductivity of the soil mixed with the (NaCl) and soil with a 15% water content, no soil ionisation was detected. Moreover, it was indicated that E_c has had higher value with the negative impulse, 6.6 kV/cm, than with the positive impulse.

Lee et al. [11] conducted a test with a hemispherical test setup. In order to investigate the effect of water content on the critical electric field, medium sand samples were tested with different water contents (2%, 4%, 6% and 8%). The critical electric field for soil ionisation was calculated for each moisture percentage. Moreover, E_c for breakdown was determined by up and down method. The authors found that the critical electric fields for soil ionisation and breakdown decrease with the increase of the water content as shown in Figure 2-3. This supports what was found in [36], as the relative permittivity of the soil increases with the increase of the water content, and this therefore, reduces the critical electric field.
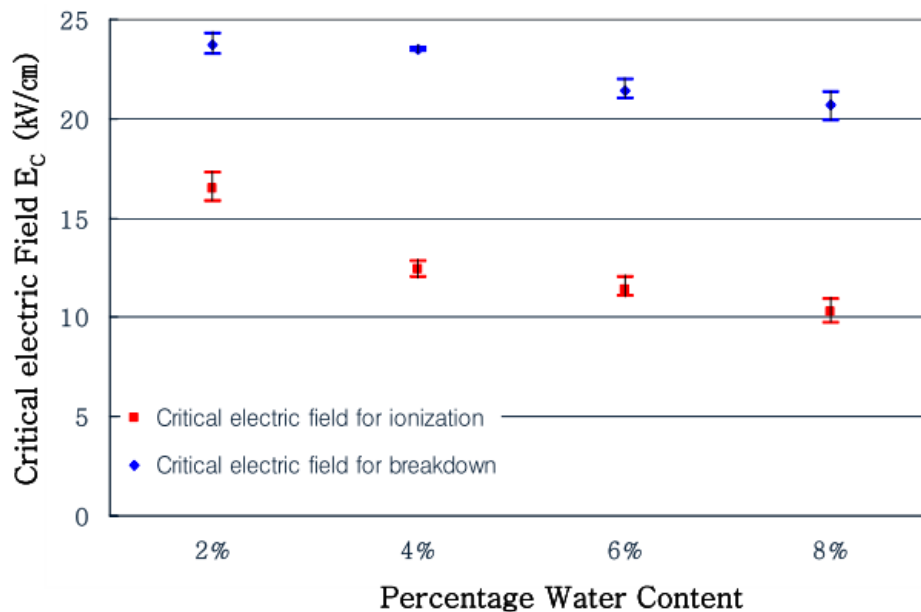
Figure 2-3 critical electric field values versus water contents[11]

Gonos and Stathopulos [6] performed some tests using coaxial cylinders. In order to estimate the critical electric field of soil ionisation, dry and wet sand samples were examined under impulse voltages. It was observed that the addition of water to the sample reduced E_c value; the (E_c) range was (3.5-13) kV/cm. Moreover, they have concluded that there is no direct link between soil resistivity and E_c, as the resistivity depends on the amount of dissolved salt as well as the water content. On the other hand, Asimakopoulou et al. [35] investigated the efficacy of using the voltage and current characterisation waveforms to determine the onset of soil ionisation and the critical electric field value. Their results demonstrated that this method could not be used with dry soil, due to the undetectable current. However, for wet soil, the I-V curves began to form loops in the shape of an inclined (8) at a certain value of the applied voltage. Hence, they concluded that using I-V curves is a suitable way to determine the critical field. In contrast, Lee et al.[11] and Nor et al. [5] adopted the emergence of the second peak in the current trace to define the start of the soil ionisation and the critical electric field. Loboda and Scuka [48] observed that at the onset of soil ionisation, the current rise time increased while the voltage rise time remained constant . Thus, the authors used this criterion to calculate the critical field.

2.4 Soil Breakdown

In some areas, under poor conditions, unsatisfactory earthing systems could be found; that is because of the high resistivity of the soil. Dry soil under high impulse voltages forms streamers leading to the breakdown of the soil. The streamer initiation may be due to the drop in the high resistivity of the soil to a much lower value [16, 40, 49, 50]. Once the streamer is initiated, it will

propagate away from the electrode. The distance of the streamer propagation and the velocity of the streamer depend mainly on the applied voltage and the sample resistivity. The streamer creates a low resistivity channel, which allows the high discharge current to flow and break down the sample [14].

Soil breakdown is a nonlinear phenomenon that occurs in the soil neighbouring the earthing electrode, reducing the resistivity to a very low value, and forcing the current to flow with a much higher magnitude. The initiation of the soil breakdown is also probably due to either the electrical process, the thermal process, or both. The first possibility considers the ionisation process in air voids among the soil grains. When the breakdown voltage is applied, the electric field in the air in the cavities will be significantly higher due to the field enhancement process. Hence, these air voids will have lower resistivity because of the air ionisation, and then streamers forming tracking in the soil will proceed to break down the soil. The other possibility focuses on the conduction through water channels in the soil. Part of the water is evaporated by the current and that leads to breakdown. According to [43], both processes could occur at the same time, but one of them could dominate the other depending on the soil conductivity and voltage level [43].

An improved dynamic version of Liew's model was introduced in [51], to enable the model to describe the soil impulse behaviour with breakdown channels. A new region was added to the model, that is, a sparking region just around the electrode (region 4) , where the highest current density occurs, as can be seen in Figure 2-4. Hence, tracking will be initiated in this area and it will then expand outwards. The authors also reported that in this zone, tracking punctures could be seen, and the resistivity may fall to zero.

The area of the sparking zone depends mostly on the injected current, so the greater the impulse current is, the wider the sparking regions will be, as the streamers will propagate further away from the electrode. The authors suggested that the breakdown under high impulse current has three stages, the first is (no breakdown), it occurs when the current density is less that the critical value ($J < J_c$). The second stage is (breakdown by the soil ionisation), it occurs when ($J_c \leq J < J_s$). The third stage is (breakdown by sparking), which occurs when ($J \geq J_s$), and this stage is represented by region 4 in the model.
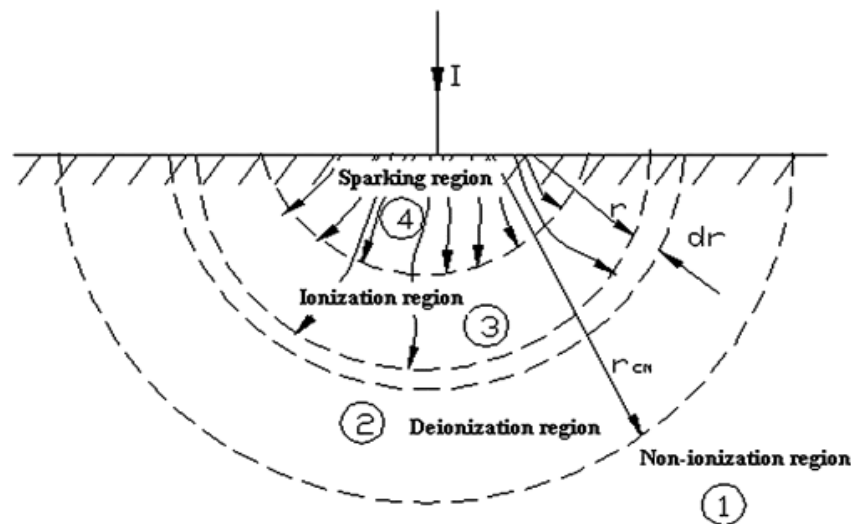
Figure 2-4 Liew's improved model [51]

In another study implemented by Flanagan et al. [16], fast and slow impulse voltages were applied to a small scale of soil samples. The wet soil was located in a plastic tube, and the electrodes, which were parallel plates, were installed at both tube terminals. The thickness of the sample was varied from 0.5 to 3 cm, and the diameter of the tube was also varied from 5 to 10 cm. The breakdown was observed once the current increased sharply with an instantaneous drop in the voltage. Moreover, different delay times were detected between the application of the voltage and the sample breakdown.

The authors believed that the time lag is a combination between a statistical delay time, which represents the initiation of the soil ionisation, and a formative delay time, which indicates the propagation of the streamer through the entire sample. Both of these times are primarily dependent on the applied voltage. However, they found the statistical delay time to be independent of the sample thickness, whereas the formative delay time tend to be proportional to the sample thickness. Furthermore, the electric field for breakdown was found to decrease with the increase of the water content which supports what Lee et al. found in [11].

Van Lint and Erler [14] conducted investigations using two different test cells, a cylindrical 90 ^{o} sector and a complete cylindrical electrode configuration. Voltage transducers were utilised to measure the voltage at various locations in the sample. Hence, the propagation of the streamers could be traced and monitored. Different sand samples were prepared by adding tap water to a dry sand. A breakdown between the high voltage electrode and the probes occurred when the streamers passed these probes. The authors observed that the initiation time of the streamers decreased with increases in the applied voltage, electrode size and decreasing the soil resistivity. Moreover, the velocity of the streamer might be controlled by the decreasing rate of resistivity of the streamer channel. However, He and Zhang reported in [22] that the streamer velocity and the final propagation distance is governed by the applied voltage, the soil resistivity and the uniformity of the soil.

The breakdown delay time is a significant factor produced by the breakdown process in soil. For that reason, He et al. [52] performed an investigation studying the breakdown delay time. Two different test rigs were used, sphere-

sphere and rod-plane arrangements. Impulse voltage and impulse current were applied to sand, yellow clay, and grey clay samples. The authors noted that the time factor is essential for the soil breakdown as well as the high voltage. The breakdown time lag relies on the impulse wave, in terms of the magnitude and time characteristics, on soil characteristics, such as resistivity, moisture and temperature; and finally, on the electrode properties, like the shape and size. The findings of this study demonstrate that the delay time decreases with increases in the applied voltage. However, the time lag of the breakdown increases with decrease in the moisture content, and the soil density and with reductions in the soil temperature.

Zeqing et al. [53] revealed from their experiments that the breakdown voltage decreases as the soil resistivity decreases. Furthermore, the water content and the compaction of soil have a significant influence on the breakdown voltage level, in that the higher the moisture percentage and the compaction of the soil, the lower the soil resistivity, which then reduces the breakdown voltage. As the breakdown voltage was 25kV for sand sample with 5% wc, and 9kV with 9% wc. Moreover, when the sample was compacted to 1.073 g/cm^3, the breakdown voltage was 23kV, but when the compaction was increase to 1.307 g/cm^3 the breakdown voltage level was reduced to 20kV. The soil resistivity affects the delay time as well, hence the lesser the resistivity is, the faster the breakdown will be (shorter delay time). Finally, the discharge channel of the breakdown current tends to propagate either along or near the previous discharge channel. This occurs if the sample is left without change or remix. Victor et al. [54] found results similar to those of the previous study, and they also found that in the case of soil with high resistivity, the smaller the

grain size, the lower the breakdown voltage level. However, this was not clear in the case of soil with low resistivity.

2.5 Impulse Impedance

The impulse impedance for the earthing system is a central factor to evaluate the performance of the system under high impulse currents, and to compare the transient behaviour with the steady state and DC performance. The transient impedance is influenced by the occurrence of soil ionisation and the self-inductance of the earthing electrode [55]. In the literature, there are several ways to define the impulse impedance. However, the most commonly used definition is to consider the ratio between the impulse voltage and the impulse current, as in Equation (2-1) (instantaneous impulse impedance).

$$Z(t) = \frac{V(t)}{I(t)} \tag{2-1}$$

In addition, the impulse impedance could also be defined as follows: [56-60]

$$Z_1 = \max (Z(t)) \tag{2-2}$$

$$Z_2 = \frac{V(t_1)}{I(t_1)} \tag{2-3}$$

$$Z_3 = \frac{V(t_1)}{I(t_2)} \tag{2-4}$$

$$Z_4 = \frac{V(t_2)}{I(t_2)} \tag{2-5}$$

where:

Z_1 is the maximum value of the impulse impedance.

Z_2 is the ratio of the peak voltage to the current value at the voltage peak time.

Z_3 is the ratio of the peak voltage to the peak current.

Z_4 is the ratio of the voltage at the time of the current peak to the current peak.

(t_1 and t_2) are the times of voltage peak and current peak respectively.

$Z(t)$ does not produce a single value as do the rest of the impedances, but rather it provides a curve describing the whole behaviour of the impulse impedance during the discharge, so that the increase and decrease of the impedance can be seen. Moreover, some of the other impedances are included in that curve, as illustrated in Figure 2-5, which makes this expression a wider and more comprehensive definition. However, according to [11, 20, 61, 62], (Z_4) in Equation (2-5) is termed as the impulse resistance. The peak current value was considered to eliminate the inductive effect in the behaviour of the sample. If the peaks of both the voltage and the current occur at the same instant ($t_1 = t_2$), which also means no inductance, then the impulse resistance will be the ratio of the peak voltage to the peak current as in Equation (2-4).
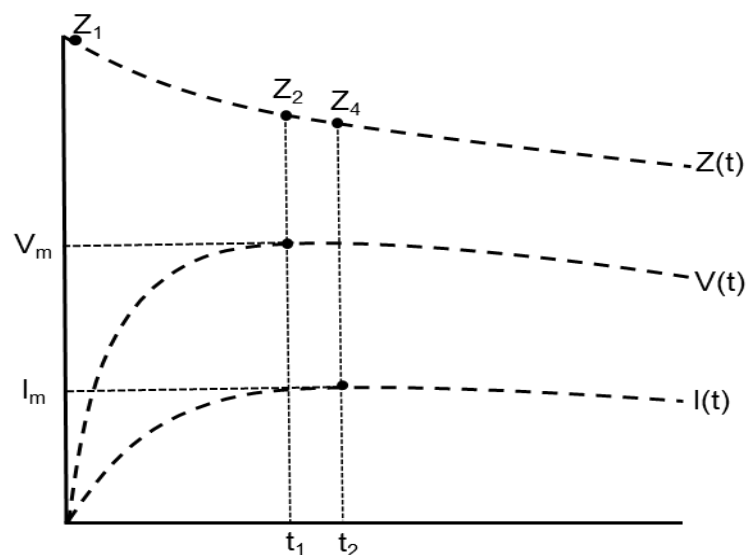
Figure 2-5 definitions of dynamic impedances (modified from[58])

Lee et al. [63] used the conventional impulse impedance as in Equation (2-1), but the authors refer to (Z_2) as the effective impedance, as shown in

Figure 2-6. They thought that the ground impedance should be reduced at the instant of the peak of the potential rise. Furthermore, it was found that this impedance is primarily dependent on the rise time of the applied current and the earthing electrode type.
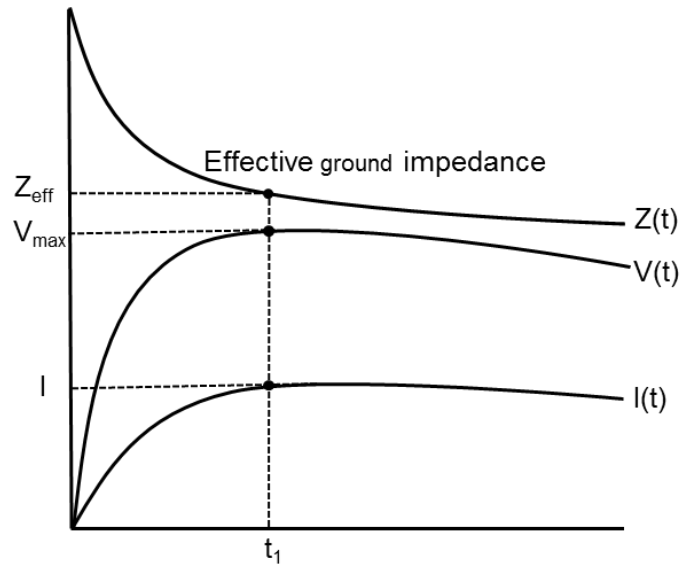
Figure 2-6 definition of effective impulse impedance (modified from [63])

Oettle [64] thought that the dynamic impedance in Equation (2-5) cannot always represent the impedance in the early stages of the lightning discharge, when the front time of the lightning current is between 4 and 8 μs. Hence, he suggested that the impulse impedance should be calculated after 6 μs from the onset of the lightning current. Then, he observed that the impulse impedance depends not only on the current value, but also on the considered time of the calculation. However, while the author agreed that choosing (6) μs could be arbitrary, he claimed that it provides more factual dynamic values than the impedance in Equation (2-5).

With regard to the electric field, when increased to the critical value, the impedance began to decrease due to the initiation of soil ionisation in the soil

around the electrode. However, under the high lightning currents, the impulse impedance became greater due to the increase of the inductance of the earthing wire by the high frequency range presented in the lightning wave. This high frequency spectrum and the high impedance shortened the effective length of the earthing wire [56, 57]

Nor and Rajab [61], carried out tests with different earthing electrodes, to demonstrate that the impulse resistance as calculated with Equation (2-5) is smaller than that under DC conditions for high DC resistance. However, in the case of a small DC resistance, no significant differences were seen between them. Therefore, they concluded that there is a correlation between the impulse resistance and the DC resistance.

Gupta and Thapar [65], in a study regarding the effective area of the earthing grid, observed that once the grid size increases, the impulse impedance decreases, up to a limit; if the size keeps increasing, then slight impedance decrease will occur. At this size, the area of the grid is called the effective area, which produces the lowest impedance. In addition, they also found that the impulse impedance is influenced by several factors, such as the shape, and size of the electrodes, the distance between the electrodes, and the wave shape and magnitude of the applied current.

2.6   Soil Circuit Models

In order to support the experimental work, various circuit models of the soil have been proposed and simulated to validate and predict the behaviour of the discharge under specific conditions and arrangements. These circuits have also helped to understand the performance of the test media under

various applied voltages. With regard to the soil ionisation phenomenon in earthing systems, several equivalent circuits have been proposed. However, including the ionisation phenomenon in the proposed circuits is considered very difficult, though it provides a better and more accurate representation of the behaviour.

Nor et al. [7, 20] employed a hemispherical electrode arrangement, in which impulse currents were applied to wet sand with a 10% moisture content. The second peak was observed on the current trace, indicating the initiation of the soil ionisation. The soil ionisation is assumed to propagate uniformly as a shell shape corresponding to the equipotential lines. The authors represented the sand sample with parallel branches. They found that pre-ionisation resistance (R_1) and capacitance control the pre-ionisation period, whereas the post-ionisation period is controlled by the post-ionisation resistance (R_2). The propagation delay time is simulated by an inductor connected in series with (R_2), as can be seen in Figure 2-7. Finally, a switch was used to initiate the soil ionisation phenomenon. From the simulation, good agreement was observed between the real discharge waveforms and the waveforms produced from the simulated equivalent circuit.
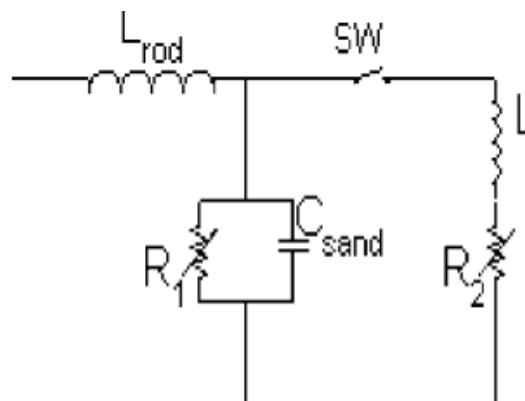
Figure 2-7 equivalent circuit including soil ionisation [20]

Zeng et al. [66] and Chen et al. [18] considered a long horizontal earthing electrode. They found that due to the inductive effect, high impedance resisted the flow of the impulse current to the far end of the electrode. Thus, the maximum current density was at the feeding point, and decreased as the current flowed further along the electrode (non-uniform distribution of the current density along the electrode). Therefore, the authors represented the ionisation zone with a pyramidal shape, but because of the complexity of the model, they represented the ionisation zone with cylindrical segments around the electrode with decreasing diameters as the current approaches the far terminal. Hence, the distributed network was considered to simulate this model of the ionisation zone. The authors found from the study that the impulse resistance is influenced by the area of the electrode and the injected current magnitudes.

Geri et al. [21] simulated a vertical rod electrode under lightning current. The soil ionisation zone was presumed to be uniformly distributed around the electrode. Various radii were considered for different layers in the discharge area, starting from the high voltage electrode up to the point where the potential is equal to zero. The equivalent circuit contains four parts. The first part is for the rod electrode. The second part represents the soil ionisation zone, and this layer has a variable radius according to the electric field and soil resistivity. The third part belongs to the layer between the ionisation zone and the measurement electrode. The last part is for the earth parameters after the measurement electrode as can be seen in Figure 2-8. This circuit could be simplified by removing the inductances and capacitances from the circuit, because they are much smaller compared with the resistors. The authors have

found good agreement between the real performance of a steel rod electrode and the simulation results.
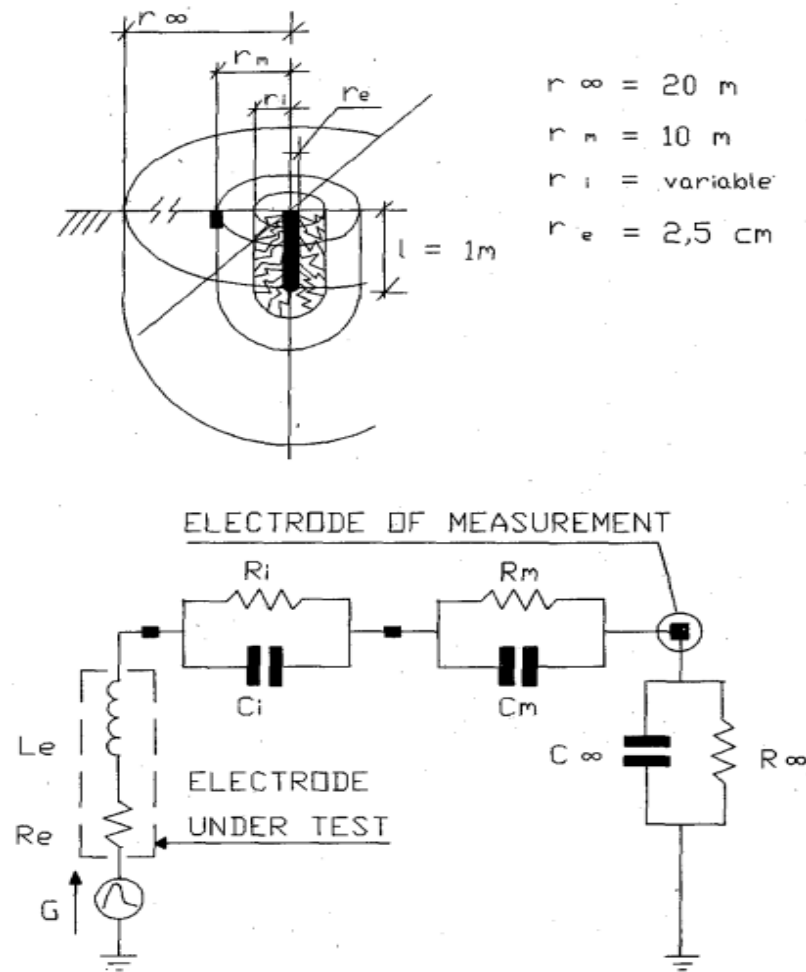
Figure 2-8 vertical rod electrode and its equivalent circuit [21]

A sand sample compacted in a cylindrical coaxial electrode configuration under high impulse currents was modelled by Kalat et al. [67]. I-V characteristics in their results formed loops indicating the initiation of the ionisation phenomenon. These loops were studied to calculate some of the parameters in the proposed circuit. The equivalent circuit of the sample consists of parallel branches including the soil ionisation. EMTP software was used to simulate the circuit model. As a result, the modelled circuit showed a

satisfactory agreement with the real discharge results of sand with resistivity 800 Ω.m and for clay sample with resistivity 100 Ω.m, where the I-V curves showed comparable results.

Nicolopoulou et al. [68], performed a comparison study between Nor's circuit model and Kalat's circuit model. Both circuits were simulated by EMTP software for 5% and 10% water content sand samples in a cylindrical electrode arrangement. They noted that the results of Nor's model are very similar to the actual discharge waveforms, especially in the case of two current peaks. However, Kalat's model gives satisfactory results in the case of one current peak only, because it cannot represent the current behaviour with two crests. Thus, it was concluded that Nor's circuit model offers a more general pattern, which could be modified and applied to different types of soil samples.

2.7 Imaging of Electric Discharge in Soil

It was found that studying the electric discharge visually in the soil offers a better understanding of the phenomenon and provides significant information on the development and the shapes of the discharge inside the soil. However, only a few techniques have been utilised to visualise soil ionisation and electric discharge phenomena in soils. The imaging process of the electric discharge in porous materials like soil is extremely difficult due to the opacity of the soil, and the complexity of the discharge phenomenon. Therefore, instead of capturing the discharge from outside the sample, there are some techniques in the literature, such as photographic films, x-ray films, and conducting paper, that have been used to record the electric discharge and the ionisation phenomenon from inside the soil, by placing those films near the earthing

electrodes within the soil. Therefore, when the discharge occurs, the produced elements, such as light, x-rays, and heat, help to reflect and copy the discharge on these films. However, recently, authors have started to investigate more effective and sophisticated techniques to obtain more details and information from the recorded images [69, 70].

In 1947, Petropoulos performed a test using hemispherical electrode configurations with sand. The glow of a spark generated by the discharge just below the soil surface could be seen at a small distance from the discharge. He concluded from the discharge shapes that the current density on the electrode surface is not uniform, but rather, there may be points that will have higher densities, which create a distortion in the ionisation zone. Thus, as the current increases, the current density at these points increases too, producing what is called Petropoulos's concept of the ionisation zone [71].

2.7.1 Sensitive Films

The sensitive films and in particular X-ray films have been frequently used to capture the discharge development around a wide range of electrode configurations in a small-scale laboratory tests. Moreover, different grain sizes of soil with different water contents were tested to investigate the conditions affecting the discharge process. He et al. [70] explained the principles of using the sensitive films. The photographic films can image the ionisation zone by capturing only the discharge light. However, the x-ray films have the ability to record the propagating streamers, as the rays generated by the ionisation process, which could be x-ray, ɣ-ray, ultraviolet, or a mixture of the three rays; can easily penetrate the cassette to copy the discharge onto the film.

36

A significant visual investigation of the electric discharge in soil was carried out in 1967 by Hayashi [26], who used x-ray sensitive films to image the electric discharge in the soil. The soil was placed in a hemispherical test rig with a spherical high voltage electrode. The x-ray film was buried vertically parallel with the electrode to image the discharge. A tree-like model was clearly observed on the film under the applied impulse voltage. The branches initiated from the active electrode propagating towards the ground.

In Hayashi and Higuchi's (1987) study, sensitive films were employed to image the discharge with two electrode bars; one has sharp needles, and the other had no needles. These two electrodes were horizontally buried under the ground over the sensitive film. Impulse voltages were applied with positive and negative polarities. A tree-like streamer model was captured on the sensitive film in the case of the electrode with needles, as shown in Figure 2-9. The development of the streamers was greater at the tip of the needle. Moreover, the streamers were produced more quickly when the needles were installed in the electrode, as the electric field at the tip of the needle was higher [72].
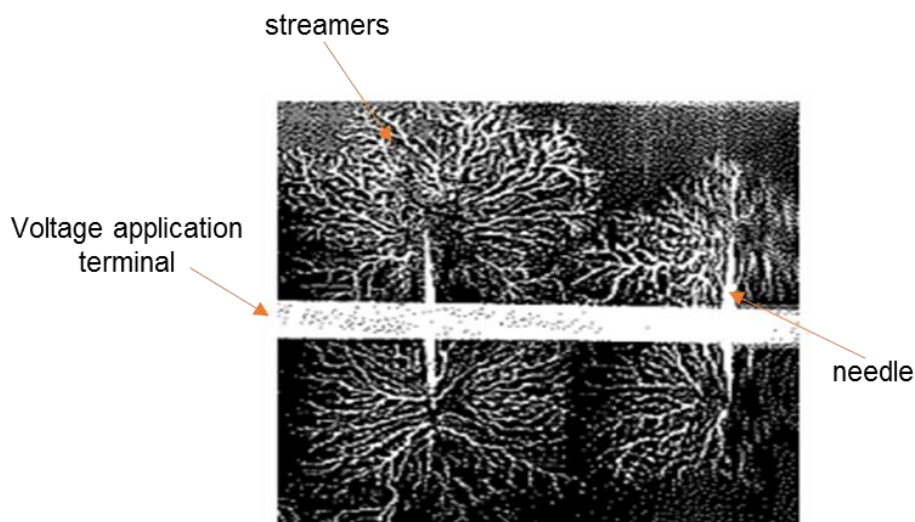
Figure 2-9 tree-like model at the tip of the needles [72]

another photographic study was conducted in 1993 [25]. Cabrera set up three tests on the discharge in sandy media. Two different test configurations were utilised in these tests. The first one consisted of a glass tube (13 mm diameter) with two electrodes at both ends of the tube. The second arrangement was a cylindrical coaxial test rig with a central conductor. A photographic camera was operated to capture the discharge in very coarse dry sand inside the glass tube under positive and negative DC and impulse voltages. For both voltages and polarities, bright discharges were observed propagating between the two electrodes. However, an x-ray sensitive film was positioned in parallel with the conductor in the cylindrical coaxial cell to image the discharge under lightning voltage. Dry and wet very coarse, coarse, and fine sand samples were tested separately. In dry very coarse and coarse sands, the streamers had a brush-like shape with large number of thin streamer. In the case of fine sand, increased number of strong streamer were seen, but the weak streamers did not appear. Thus, the smaller the size of the grains the larger number of strong steamers and the less number of weak streamers. For wet sands, stronger discharges were observed, which was attributed to the high currents flowed through these channels. Consequently, from this study, it can be concluded that the discharge shape and the streamer propagation depend primarily on grain size, moisture conditions, and impulse polarity.

In 1998, He et al. [49] employed sensitive films to visualize the shape of the breakdown region around a horizontal electrode. After the impulse current was applied, the sensitive film recorded punctures with different lengths in the soil around the electrode. The shape of the discharge along the electrode starting from the injection point had a cone shape. The area of the breakdown at the

injection point was the largest, and it decreased as it moved away. This shape was formed because of the higher leakage current at the front terminal of the electrode, and they found that due to the great inductance of the electrode under the high frequencies of the impulse current, the leakage current would decrease as the current flowed further towards the far end. Therefore, they concluded that there is an effective length for the electrode under the impulse currents.

A discontinuous soil ionisation phenomenon was observed in a study carried out by Zhang et al. in 2010 [73]. A strong ionisation effect around the electrodes and a weaker zone between them was captured on an x-ray film, as exhibited in Figure 2-10. A lightning impulse voltage was applied to dry sand and wet clay, using rod-rod and rod-plane electrode configurations. In order to investigate the discontinuous ionisation phenomenon, the authors performed a simulation work. The dielectric non-uniformity of the soil, and the size and shape of the soil grains were found to contribute in this phenomenon by changing the electric field distribution in the soil.
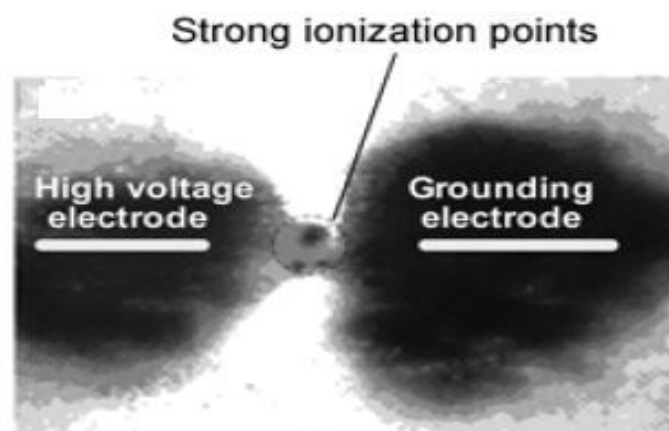
Figure 2-10 x-ray image of soil ionisation in dry soil [73]

In another major investigation, Han et al. 2011 [24] conducted a visual study on the electric discharge in soil, using three different electrode configurations (needle-plate, rod-plate, and semi-circular cylindrical-plate) and two different sensitive films (x-ray film, black and white film). The medium was soil contained in a glass box. By applying impulse currents to the soil, discharge images on both sensitive films were obtained. The captured images showed there were strong and weak discharge channels; this probably was due to the non-homogeneity of the soil. Besides, the strong channels formed a branching image that could develop into electrical treeing, while the weak channels created punctate images. The different electrode arrangements illustrated that when the electric field shows a greater degree of uniformity, the spark discharge paths also have greater degree of uniformity. The authors of this study also reported that the black and white film captured better and clearer images than the x-ray film. However, this finding contradicted the findings of the majority of the visual studies, that the x-ray films are better and more suitable to this type of imaging.

In a detailed examination by He et al. 2013 [74], the authors claimed that when soil ionisation occurs in the soil, x-rays can be generated from the ionisation process. Due to this, x-ray sensitive film was used to capture the region of the ionisation phenomenon. A Plexiglass cubic box with sides 40 cm in length was utilised in the test. Two-rod electrodes were horizontally buried in the medium inside the box in a rod-rod configuration. One of them was connected to an impulse generator, and the other was grounded. The x-ray film was employed under the electrodes and in parallel with them. Two particle-sized categories of glass beads have been tested, large beads of 0.25 mm diameter, and small

beads of 0.05 mm diameter. Both types of beads were wetted with salt water. Dry sand and wet clay were also considered in this study. The images produced from the lightning voltage discharges showed the ionisation effects and channels on the x-ray films. A tree-like model could also be observed, as demonstrated in Figure 2-11 . By studying these images, it can be seen that the ionisation in the big beads is stronger than in the small beads; this could be due to the bigger air voids in the big beads. Furthermore, the ionisation in the wet clay was also stronger than in the dry sand, and this could be attributed to the non-uniformity of the wet clay. In this study, the use of glass beads was introduced as a method to investigate the soil ionisation. However, the authors did not provide any details of the description or specifications of these beads.

0.5 cm
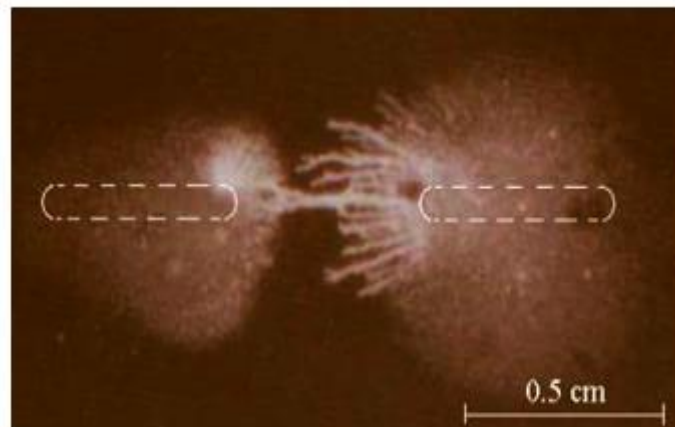
Figure 2-11 tree like model x-ray image of rod-rod in dry sand [74]

In [22], 2015, dry sand and wet clay were used as test media to examine the electric discharge under lightning currents. The horizontal electrode was buried in a tank below an x-ray film. The captured discharge images showed the soil ionisation zone surrounding the electrode with a tree-like model. The ionisation zone was found to be conical in shape, whereby the large area was at the connection between the electrode with the impulse generator and the

41

small area at the other terminal. This shape was, perhaps, due to the reduction in the leakage current along the rod. In addition, it was observed that with the non-homogenous clay, the soil ionisation was stronger than with the fine sand grains; such grains tend to have a greater degree of uniformity than clay.

2.7.2 Conducting Paper

Zeqing et al. 2000 [75] used conducting paper in both indoor and outdoor experiments. For the indoor test, current impulses were applied to a soil sample, which was placed in an insulating box. This box was earthed via conducting paper laid at the bottom to image the end of the current propagation. Wet cultivated soil, dry red soil, and wet red soil were considered in this study. Once the discharge current reached the conducting paper, it removed the top layer of the paper at the point where the current touched the paper, leaving traces on the surface of the conducting paper and holes in the case of breakdown due to high current. Single channel, multi channels, and large area channels were observed from the discharge images on the surface of the conducting paper. It was observed that the higher the soil resistivity is, the higher the tendency of the discharge to form a single channel, and as the lower the soil resistivity the higher the tendency of the discharge to form several channels. This could indicate that the breakdown mechanism could be different in both dry and wet soils. In the case of high current, the paper was completely punctured, especially with the single channel. For the outdoor test, the conducting paper was placed at the bottom of a hole that had been dug in the ground to image the discharge in real conditions. The tested soil was the same soil that was taken from the pit itself. Dry and wet samples were tested with impulse currents. The produced images exhibited three different

discharge paths; the first was a diffused channel with a 10 cm distance between the electrodes in wet and dry soils; the second was, diffused with a partial breakdown channel with a 5 cm distance between the electrodes with wet soil; and the third was an obvious breakdown channel with a 5 cm distance between the electrodes but with dry soil. The results showed that the discharge current has the propensity to form a single propagating path with dry inhomogeneous soil, and the single channel breakdown mechanism in wet soil is different from that in dry soil.

2.7.3   Thermal Imaging

In a study which set out to thermally image the change of the soil temperature during the test, Idris et al. 2005 [41] utilised an infrared camera. Lightning surges were applied to a dry soil sample in a cylindrical electrode arrangement. In addition, the thermal imager was used to record the temperature of the topsoil of the sample. After several discharges, it was observed that the temperature was slightly raised with the increment in the applied voltage, and the maximum temperature was observed around the active electrode. The voltage was applied from 10 kV up to 75kV, and the temperature was increased with 1.9 ° C during the test. This increase of temperature was attributed to the collision of the fast moving electrons with the other molecules and atoms of the air and the soil grains during the discharge.

2.7.4   X-Ray Radiation

In 2015, a new technique was introduced in [69]. X-ray radiation was utilised to capture the soil ionisation and discharge in the soil under surge currents. An x-ray imaging system (x-ray generator and digital radiography board) was used to apply the x-ray to the sample at the instant the impulse current was

injected at the electrode. This electrode was placed in a tank full of sand. The applied x-ray penetrated the soil sample and, then, was captured on a digital radiography board behind the tank. Grayscale images were obtained for several discharges with vertical and horizontal active electrode arrangements, as can be seen in Figure 2-12. After processing the images, it as found that the areas were exposed to a higher x-ray intensity were whiter, and those of less x-ray intensity were darker. From the captured images, streamer discharge channels at the ends of both vertical and horizontal electrodes can be observed with various diameters and directions according to the excitation current and electric field distribution. Furthermore, the channel area was found to increase with the increase of the current magnitude. Therefore, the authors concluded that this method is more efficient than the sensitive films, as it can capture clearer images, and has the potential to be used in a larger scale investigation.
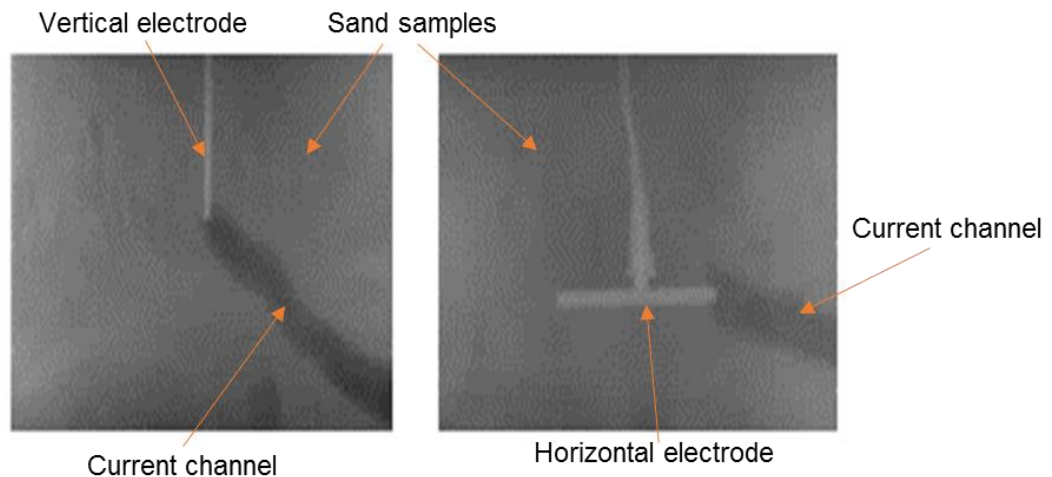
Figure 2-12 grayscale discharge images of impulse discharge in soil [69]

2.8 Soil Ionisation in Multilayer Soil

Multilayer soils with variable resistivity values are a common feature of real earthing systems, due to variations in soil composition depending on depth,

localized inhomogeneity, and numerous hydrological and geological processes. The resulting distribution of soil resistivity can, thus, be highly non-uniform. However, the high impulse current performance and the soil ionisation phenomenon have not been extensively investigated with two-layer soils, and while soil ionisation in earthing systems has been intensively studied, the majority of these investigations considered a uniform soil in the vicinity of the earthing electrode, which may not always be fully representative of soils in real conditions. Variations in weather conditions lead to changes in water content and temperature within the soil strata. This means that the upper and lower layers may have either high or low resistivity, thus, affecting soil ionisation initiation and propagation in these layers. This, in turn, affects the localized soil resistivity and the earth potential rise (EPR) due to current injection at the earth electrode [76].

Liu et al. [76] investigated a rod electrode installed in two-layer soil with a simulation study. The upper layer had high resistivity and the lower layer had low resistivity. The lower layer was only 20 cm from the 100 cm rod. A High impulse current was injected through the electrode, and the transient voltage was measured at the injection point. The findings of this test were compared with the results of the same rod injected in the high resistivity layer only. The transient voltage was observed to be 12 times less in the case of stratified soil, and the current dissipated in the lower resistivity soil at the bottom with 98% of the injected current, initiating soil ionisation only in this layer despite most of the electrode being in the upper high resistivity soil.

Nixon et al. [77] have tested a vertical rod electrode installed in three-layer soil. An impulse current was applied into the soil, and the potential was

measured at the injection point. Then, the authors used the transient impedance as in Equation (2-1). From the findings, they observed that the effect of the layers is minor, as the soil resistivity drops very quickly to the minimum value due to the effect of soil ionisation. Therefore, it can be concluded that considering the bulk of the soil resistivity instead of the individual layer resistivity could be an acceptable simplification for transient modelling. However, the water content in all soil layers was very high (more than 10% in each layer). Thus, this simplification could be acceptable in low resistivity layers, but in the case of poor soil conditions (high resistivity soil), this simplification may not be applicable. Taking advantage of the tendency of the current to flow in the soil with less resistivity will help understand the behaviour of the current in each layer. Therefore, it is better to have the low resistivity layer below the surface layer, and to have an electrode long enough to reach this layer, so that the majority of the current will be dissipated in this layer rather than in the topsoil layer. Then, the soil ionisation is guaranteed to initiate and propagate in the lower layer far deep inside the earth, thus reducing the EPR at the ground surface [76].

He et al. [78] and Unde et al. [79] suggested that using a longer vertical electrode could minimise the influence of the seasonal changes, particularly in freezing weather or hot weather, which increases the resistivity of the surface layer. Moreover, if the thickness of the freezing layer exceeds the depth of the electrode, then the impedance of the earthing electrode will be approximately 1.7-3 times higher than under normal conditions. Therefore, the thickness of the layers is also a significant factor that influences the impulse behaviour of the earthing systems in two-layer soil, because it affects the impedance value

46

of the soil, which then affects the initiation and propagation of the soil ionisation in these different layers.

2.9 Discussion

Soil ionisation is an important phenomenon that significantly helps to dissipate high impulse currents into the soil. Researchers have found several criteria to identify the initiation of this phenomenon and to calculate the critical electric field required for the initiation. Hence, several values have been suggested. The majority of the studies have indicated that the main cause of the soil ionisation and breakdown phenomena is the electrical process, due to the field enhancement in the air pockets trapped among the soil grains. In addition, the critical study of the literature revealed that the thermal process could not explain the propagation process of the ionisation zone.

It has been confirmed that soil breakdown comprises several stages, starting from the initiation of the soil ionisation until the full propagation of the ionisation through the entire sample, and different delay times have been observed for each stage. The transient impedance has been shown to have several definitions, and particular definitions have been set by different authors to serve their purposes, but the instantaneous impedance was found to describe the impedance of the soil with a curve, which includes some of the other definitions. Several circuit models have been proposed under various electrode configurations, soil sample arrangements, and considered assumptions. Furthermore, Nor's circuit model has been demonstrated to be successful, and it can be adjusted and generalized for different types of soil and electrode arrangements.

Recently, there has been renewed interest in studying the electric discharge visually in the soil, which was found to be a good auxiliary element in achieving better understanding of the phenomenon. It can be seen from the studies mentioned previously that the imaging process of the electric discharge in soil is extremely difficult, due to various reasons. These include firstly, the physical properties in terms of colour, size, and shape of the grains, and moisture content; secondly, the chemical and electrical nature of the material in terms of the chemical composition, permittivity, and conductivity; thirdly the discharge mechanism in the porous material where the soil ionisation phenomenon could occur; and fourthly, the type, shape, and polarity of the applied voltage.

From the reviewed studies, sensitive films (mostly x-ray film) are considered the most commonly used technique in this field. However, there are certain drawbacks associated with the use of these techniques, such as the restricted view they give of the discharge. Moreover, they cannot capture the dynamic change of the discharge over time. Besides, in the case of strong discharges, the film will suffer from punctures and colour distortion due to the thermal and light sensitivities. However, the current techniques are simple, cheap, and easy to use, and they have given very useful images, which have helped in understanding the phenomenon. Therefore, new techniques need to be found and developed that are able to record the dynamics of the discharge, since imaging the discharge in the soil is becoming a powerful tool to acquire considerable data for the discharge phenomenon in soil.

The existence of several layers in the ground with different water contents could lead to a significant change in the impedance value of the earthing

electrode and in the initiation and propagation of the soil ionisation processes in all layers. It is well known that the current flows in the soil with less resistivity, so this will force the current to dissipate in a specific layer rather than being uniformly distributed around the electrode. Besides, the thickness of each layer could be a vital element for the earthing impedance and the ionisation initiation. Nonetheless, few high voltage tests have been published to investigate the ionisation phenomenon in layered soil. Therefore, more research is required to address the issues related to the initiation and propagation processes in two-layer soils.

Chapter Three

Methodology and Test Arrangements

3.1   Introduction

The objective of this study is to investigate visually and electrically the soil ionisation phenomenon in porous materials under high impulse voltages. In order to accomplish this and assist with the experimental work, the high voltage laboratory at Cardiff School of Engineering has advanced pieces of apparatus for the visual investigation, such as sophisticated high-speed cameras, and advanced microscope machines. Many different equipment and devices were also provided to facilitate the practical tests including the impulse generators, the measurement devices, test cells and the discharge media used in all the test samples. Moreover, a finite element software program

(COMSOL Multiphysics) and a transient software program (EMTP) were also used throughout the research to study different aspects of the discharge. Therefore, this chapter aims to explain the methodology and discuss the test circuit including the test rig, the impulse generation and data acquisition, the test media, and the other devices that have been used during this study.

3.2   Methodology

To achieve the objectives of this thesis, many laboratory experiments in the high voltage laboratory in Cardiff School of Engineering and many software simulations were performed. The laboratory work involved high voltage tests investigating the soil ionisation phenomenon in two different media: glass bubble material and sand. Visual and electrical techniques were utilised to study the phenomenon; the visual techniques included high-speed cameras to record the discharge phenomenon in the glass bubble material under lightning and switching impulse voltages and microscopic imaging to investigate the filaments produced by the current flow in the glass bubble material.

A correlation between the recorded videos of the discharge and the waveforms of the measured signals was implemented to deliver a better analysis and understanding of the dynamic changes of the discharge under impulse voltages. A new sample configuration for the glass bubble material was specially prepared for this study in order to obtain better and clearer captured videos of the discharge. The sample had an upper part with only dry material and a lower part with wet and dry sections. The electrical techniques included voltage and current measurements. The voltage measurements consisted of three voltage measurements at different positions in the sample at the same

time throughout the discharge. The applied voltage was measured on the active electrode, and two other voltages were measured via potential transducers installed at different positions along the sample. The current detection was carried out with a current transformer to measure the current flowing in the sample during the impulse. These potential and current measurements made it possible to observe and track the ionisation initiation and propagation in the media under investigation.

The instantaneous impulse impedances were calculated to examine the effect of the soil ionisation on the total sample impedance and the impedances between the probes. The sand samples also consisted of two layers; these layers contained different moisture percentages to examine the ionisation phenomenon in two-layer soil under lightning impulses. Finite element software (COMSOL) was used to study the behaviour of the electric field in the sample during the discharge. The test rig was built using a 2D model, and was meshed with a finer mesh. Electrostatic physic toolbox was selected to study the electric field behaviour and measure the maximum electric field at the electrode surface under lightning impulse voltage. Furthermore, an electromagnetic transient program (EMTP) was also used to simulate the proposed equivalent circuit of the glass bubble material sample. The proposed circuit was based on the performance of the sample under lightning voltage. There were different components, and the values of these components were derived from the voltage and current waveforms of the discharge.

3.3 Impulse Voltage Generators

Investigating the soil ionisation phenomenon in this thesis requires the use of

different high impulse voltages. Thus, two different impulse generators were utilised to generate standard high lightning and switching impulse voltages.

(i) Haefely Impulse Generator

The Haefely impulse generator (SGSA 400-20) with four stages was utilised to generate the standard lightning impulse voltage (1.2/50 µs). Each stage has a capacitance of 2 µF, which can deliver up to 100 kV, and the maximum generated output voltage from the generator is 400 kV. The four capacitors of the generator are charged with a charging rectifier LGR 100-20 unit. An AC voltage is fed to this charging unit from a power point in the laboratory.

A (GC 223) digital control unit was connected to the generator and the charging unit to control the generator, charging voltage and triggering circuit. The spherical gap distance is adjusted automatically according to the charging voltage required for the test based on the calibration settings of the generator. Figure 3-1 shows an example of the generated lightning impulse voltage, which conforms to the standard lightning impulse. $T_1 = 1.67(T_{90\%} - T_{30\%})$. $T_1 = 1.67(0.8-0.2) = 1$ µs. $T_2 = 55$ µs.
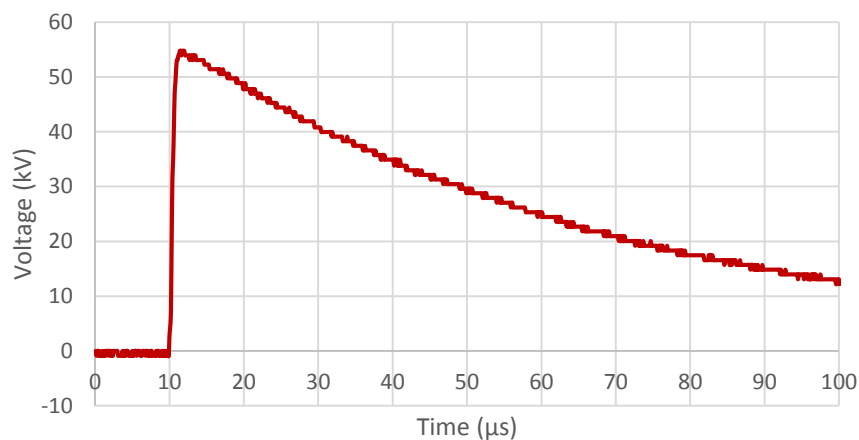
Figure 3-1 generated lightning impulse voltage

(ii) Ferranti Impulse Generator

A Ferranti impulse voltage with six stages was modified to generate the switching impulse voltage; the new arrangement of the generator used only four capacitors, 0.14 µF each. The maximum yielded output voltage was 200 kV. New sets of front and tail resistors were connected with the existing four capacitors in the generator to produce the switching voltage. A different charging unit from that used with the Haefely generator was charging this generator. The control unit of this generator was an analog unit controlling the functions of the generator, such as the charging voltage, spherical gap distance and the triggering circuit. The generated switching impulse voltage is shown in Figure 3-2 was 216/2150 µs. This impulse shape was found to be within the standard range for the switching voltage as described in 60060-1[80]. $T_1 = 2.4(T_{90\%} - T_{30\%})$. $T_1 = 2.4(160-70) = 216$ µs. $T_2 = 2150$ µs.

Figure 3-2 generated switching impulse voltage

3.4 ABEM SAS 1000

This device is a complete system that provides a DC current, measures the voltage, and then calculates the resistance. This device was used to measure

the resistivity of the glass bubble material. This system can deliver different current values up to 1000 mA with a maximum measured voltage of -/+ 400 V. It has a chargeable battery and an LCD screen.
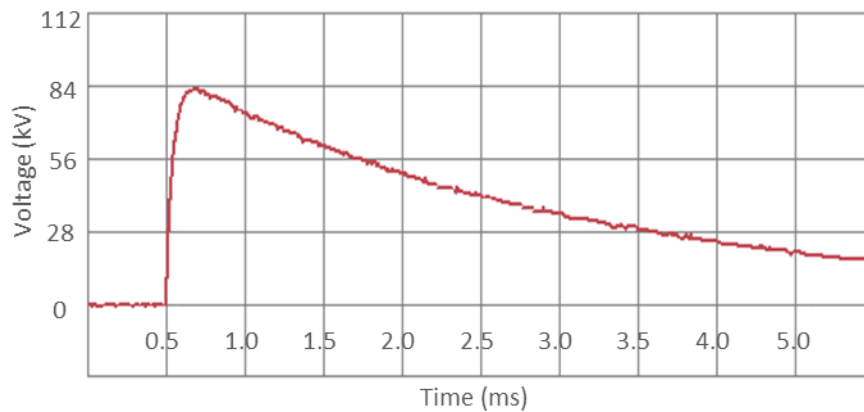
3.5   Measurement Systems

The measuring devices employed in this project include three voltage dividers to measure the applied voltage and two other voltages at different positions through voltage probes installed in the sample, and two current transformers to measure the current flowing through the samples.

3.5.1   Voltage Dividers

Due to the need to measure several voltages at different positions in the sample at the same time during the discharge, three various potential dividers were utilised and were connected with the test circuit. These dividers were calibrated according to IEC 60 standard. The different voltage ratios for these dividers were as follows:

(i)   Haefely Voltage Divider

This investigation used a large Haefely capacitive voltage divider with maximum voltage 700 kV. This divider was mainly used to measure the applied voltage on the high voltage electrode in the test rig. Its ratio is 27931 to 1 and its response time is 49 ns.

(ii)   Ross Voltage Dividers

The VD-45 and VD-150 voltage dividers are RC divider with a 150 kV and 45kV maximum voltage respectively. The voltage ratio for VD-45 is 1000 to 1,

while VD-150 has a voltage ratio of 2000 to 1.These dividers were connected to voltage probes installed along the sample to measure the potential in specific positions in the sample. This was to trace the soil ionisation propagation in different layers of the sample.

3.5.2   Current Transformers

Two commercial Stangenes current transformers with ratios 0.1 V/A and 1.0 V/A respectively and response time 20 ns for both transformers; these were employed to measure the currents flowing through the samples, depending on the expected current values. The ground electrode of the test rig was connected to the earthing point via a braid. This braid went through the current transformer to detect the current flow.

3.5.3   Digital Oscilloscopes

Two LeCroy oscilloscopes were operated to capture the fast impulse voltages and currents. The first was a LeCroy Wave jet 314 Digital Oscilloscope with four channels. The maximum sampling rate was 1- giga sample per second. The second oscilloscope was a LeCroy Wave runner 64 Xi Digital Oscilloscope also with four channels. This device is a more advanced machine than the first; it has a touch screen and runs with windows software. The maximum sampling rate is 10-giga sample per second.

3.6   Imaging Machines

(i)   FASTCAM SA5 Camera

A high-speed camera was used to record the discharge light in the glass bubble material during ionisation. The camera records images in black and white and it is controlled with a special software installed on a laptop, which

operates the camera and processes the recorded videos. The Fastcam SA5 camera is able to film with a maximum frame rate of up to one million frames per second. Moreover, the specification of 20 μm pixels improves the light sensitivity of the camera in dim light applications. It is also provided with a cooling system to protect the camera from overheating.

(ii) Lightning RDT Camera

The RDT camera was used to image the breakdown discharge occurring outside the glass bubble material. The maximum frame rate is 16000 frames per second with a reduced resolution, which is much lower than the Fastcam camera. The resolution is 1280×1024 pixels up to 500 frames per second, and then, as the frame rate increases, the resolution decreases. The advantage of this camera is the coloured frames, which can capture an image with a 7.4 μm pixel size. The camera is operated by software on a computer, which is connected to the camera via a cable with a GPIB port.

(iii) Hitachi Benchtop SEM TM3030

The Hitachi TM3030 machine is an advanced scanning electron microscope; it uses electron technology to deliver excellent microscopic images for the samples. It is a small, lightweight machine, controlled via software installed on a computer. The sample is placed in a vacuum chamber, and then a beam of electrons is applied to the sample. The Hitachi microscope offers many features and techniques to obtain much better images than those taken by conventional devices.

This machine is also capable of providing compositional elements analysis of the sample via Energy Dispersive X-ray spectroscopy (EDX), which is

essential for deeper analysis of the sample, as an X-ray sensor detects the emitted x-ray from the sample to produce the spectrum diagram of the elements as will be seen in the next chapter.

(iv)   Nikon LV100D-U Base Unit

This optical microscope has a wide range of motorized nosepieces, which has several methods for observing the samples. This microscope works with various stages to suit the variety of samples sizes, with episcopic (when the light is reflected by the sample) and diascopic (when the light traverses the sample) features together with the fluorescence imaging facility, thus providing a higher performance with a better contrast and resolution.

3.7   Tests Media

Three different materials were utilised in this thesis as test media: glass bubble material, sand, and tap water. The latter medium was mostly used as an additive to the other two substances in specific amounts to produce wetted layers.

(i)   Glass Bubble Material

Glass bubble material (S38XHS) consists of hollow low-density glass microspheres (average diameter of 30 microns) as in Figure 3-3. It is an insoluble substance, which takes the form of a white powder, and is made from soda lime-borosilicate glass. This substance is the raw material used as an additive in many industrial applications to improve the properties of various materials and compounds. However, due to its ability to transmit light, it was utilised in this study to investigate visually the ionisation phenomenon that

occurs in the soil under high impulse voltages. Since glass bubble material is not intended to be used in any electrical applications, most of the electrical properties are not known. The only electrical property that was mentioned in a common data sheet for different types of glass bubbles is the theoretically calculated relative permittivity, which is 1.2-2 at 100 MHz. In fact, this permittivity range is not specifically for the S38XHS type, but it is for all S series glass bubble types.

(ii) Sand

As can be seen in Figure 3-4, all the soil samples used for studying the initiation and propagation of the soil ionisation phenomenon were made using medium grain size sand (Garside sand No. 60), with a size range of 0.25 - 0.6 mm. Silica is the main component in this sand. The shape of the grains is sub angular to rounded. This sand, which is usually used in the construction industry, is pure sand without any added minerals or salts.
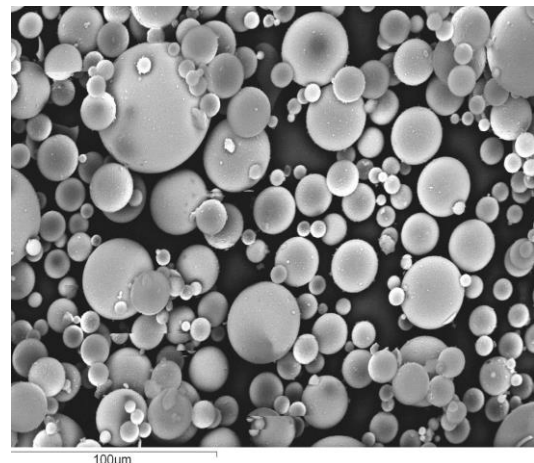
(a) glass bubble material   **(b) glass bubbles under Nikon microscope**

Figure 3-3 glass bubble material

Figure 3-4 sand used in the tests

(iii) Tap Water

The water used during this research was normal tap water that had not undergone filtering or the addition of any salts. The average conductivity of the water was (0.28 mS/cm). This water was mixed with the test porous media (glass bubble material and sand) to prepare the wetted layers. The water content (wc) mass is calculated as a percentage of the dry material mass as stated in BS1377-1 [29].

3.8   Samples Preparation Equipment

Several pieces of equipment were used to prepare the samples for all the tests, whether it was glass-bubble material samples or sand samples; these included an oven, scale, and graduated cylinders. According to BS1377-1 standard [29], soil should be dried at a temperature of between 105-110 °C. However, because the glass bubble material has a low softening temperature (600 °C), it was dried at 50 °C. The time required to dry the samples varied depending mainly on the amount of moisture in the sample. Throughout the drying period, the sample was remixed to ensure complete dryness in the

whole material. The laboratory conditions (temperature, humidity) were also monitored in the laboratory during the practical tests using the temperature and humidity sensor.

3.9 Laboratory Test Arrangements

3.9.1 Test Cell and Test Circuit

Figure 3-5 shows the special test rig with a rod-plane electrode configuration that was implemented to facilitate the practical laboratory tests. This rig consisted of a clear tube made from dielectric acrylic material 50 cm high, and 8 cm in diameter. The tube was attached to a sealed earthed aluminium plate with an aluminium base to prevent any water leakage from the tube that may occur due to the settling of water in the samples. The earthing plate was connected to the ground via an earthing braid, around which a current transformer is set to measure the current. The high voltage electrode was an aluminium rod that had a tapered shape to provide a stronger electric field at the tip of the electrode which was inserted into the sample. The HV terminal was connected to the voltage divider and to the impulse generator. The high voltage electrode was held vertically in such a way that it could be adjusted to change the height from the ground plate according to the height of the test sample in the tube. The test cell frame was made from dielectric substances to prevent any induced voltages near the tube. Figure 3-6 shows the main equipment of the test circuit and illustrates how these pieces of equipment were connected to each other. The test circuit consisted of a high impulse voltage generator with its control and charging units. A Haefely voltage divider is used to measure the applied voltage on the HV terminal of the test cell. The

current flowing in the sample is measured with a current transformer. Both voltage and current signals are captured and recorded on a digital oscilloscope. When the high-speed camera was involved in the test, it was placed near the test rig in an aluminium box for its safety, and was connected to the computer by an optic cable. A computer is used to control the camera and save the data of the experiments.
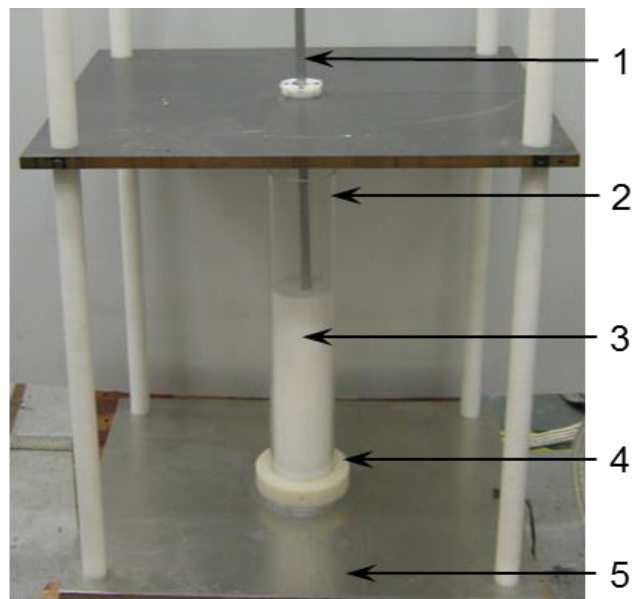
1. HV electrode, 2. Clear tube, 3. Glass microspheres, 4. Tube base. 5- Earth plate

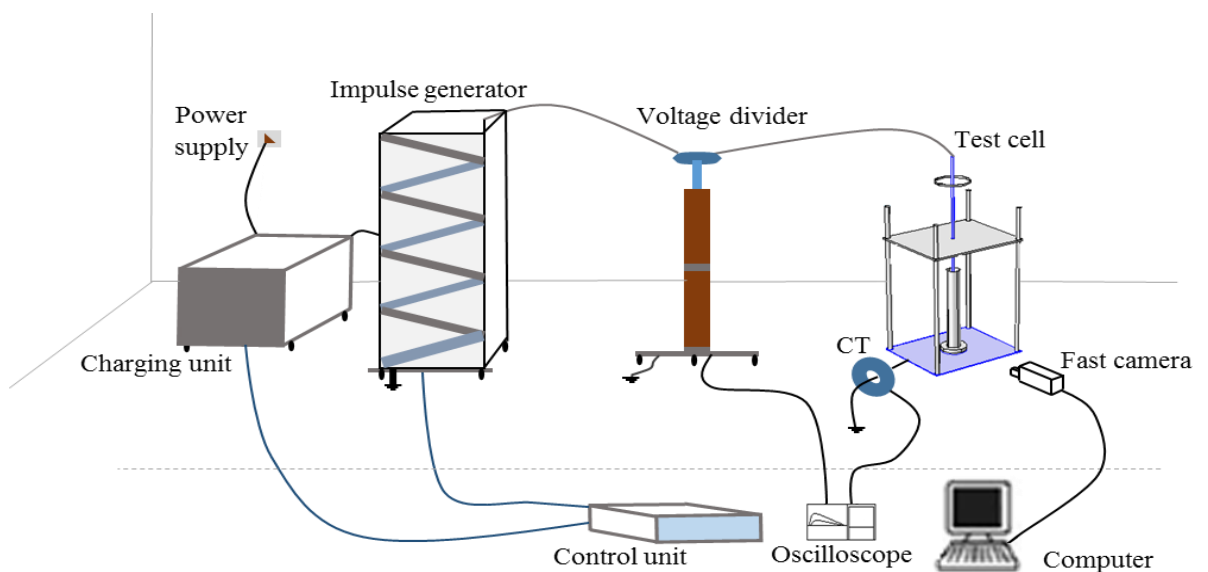**Figure 3-5 test cell**

Figure 3-6 test circuit configuration

3.9.2   Simulation of the Test Cell

The purpose of simulating the test rig was to examine the behaviour and determine the electric field when the impulse voltage is applied to the sample, and to see how the field is distributed between the electrodes. Rod-plane and spherical-plane electrode configurations were considered. The simulation was implemented with COMSOL software (version 3.4a). The two models consisted of the test cell with a 30 cm gap between the active electrode and the ground plate, as shown in Figure 3-7. The used physics was electrostatic; the materials and their properties were selected from the built-in materials in the software, and the test medium of the simulation was air. Then, the models were meshed with finer meshing. The applied voltage was a double exponential impulse voltage with a 40 kV peak value. The time characteristic of the impulse voltage was 1.2/50 µs to simulate the standard lightning wave; the equation of the double exponential impulse voltage, as in Equation (3-1), was entered into the software as a function of time.

$$V = V_m \left[e^{-\alpha t} - e^{-\beta t} \right] \qquad\qquad (3\text{-}1)$$

where :

V_m is the peak value.

α is 1/68.2 µs.

β is 1/0.405 µs. [81]

In order to study the electric field distribution between the two electrodes, the lightning surge was applied at the high voltage electrode; then the equipotential lines (contour), the electric field (streamlines) were plotted. The maximum electric field was determined by plotting the profile of the electric

field from the tip of the HV electrode to the ground electrode at the voltage peak value, as shown in Figure 3-8 and Figure 3-9. The simulation showed clearly that the electric field distribution was extremely non-uniform, and the highest electric field value, which was at the tip of the rod electrode, was 13.83 kV/cm, and it decreased as it moved down towards the grounded plate. (See Figure 3-8).
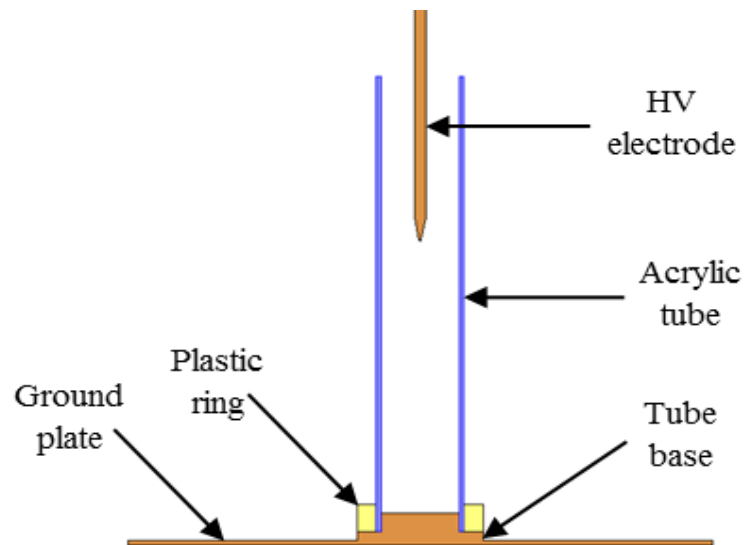
(a) rod electrode
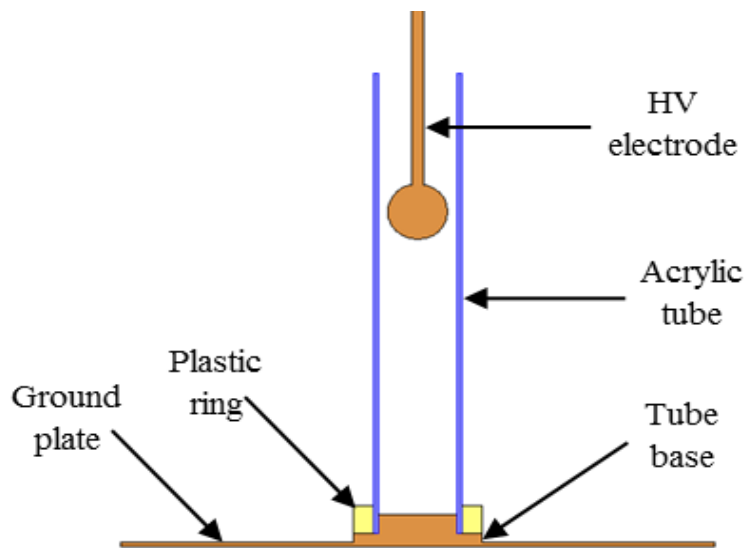
(b) spherical electrode

Figure 3-7 test cell configurations in COMSOL software
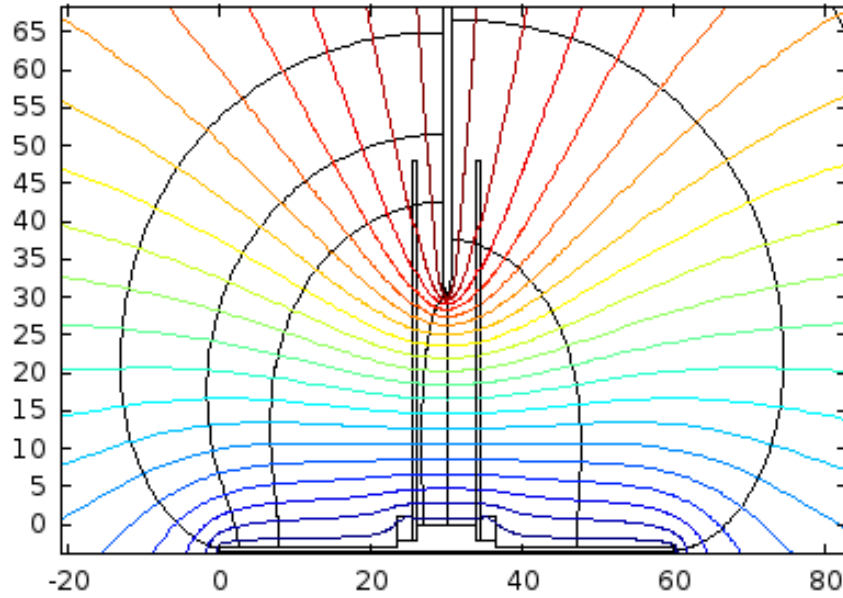
(a) equipotential lines (contour) and electric field (streamlines) for rod electrode
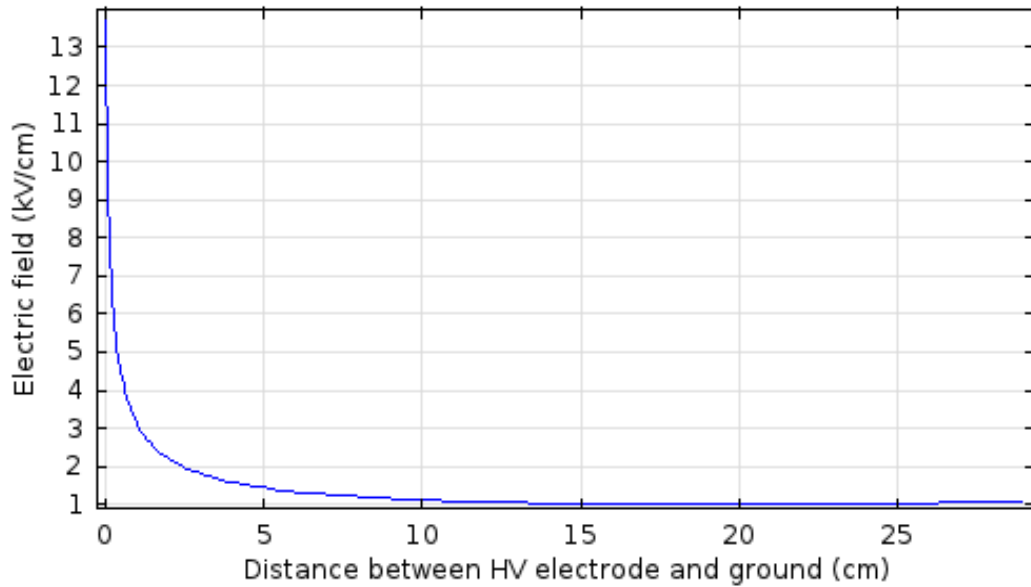
(b) electric field profile along the gap between the electrodes for rod electrode

Figure 3-8 equipotential and electric field plotting for rod electrode

(a) equipotential lines (contour) and electric field (streamlines) for spherical electrode

(b) electric field profile along the gap between the electrodes for spherical electrode

Figure 3-9 equipotential and electric field plotting for spherical electrode

However, the electric field at the surface of the spherical electrode was 3.59 kV/cm, which was almost 4 times lower than that of the rod electrode, as can be seen in Figure 3-9. Given the two e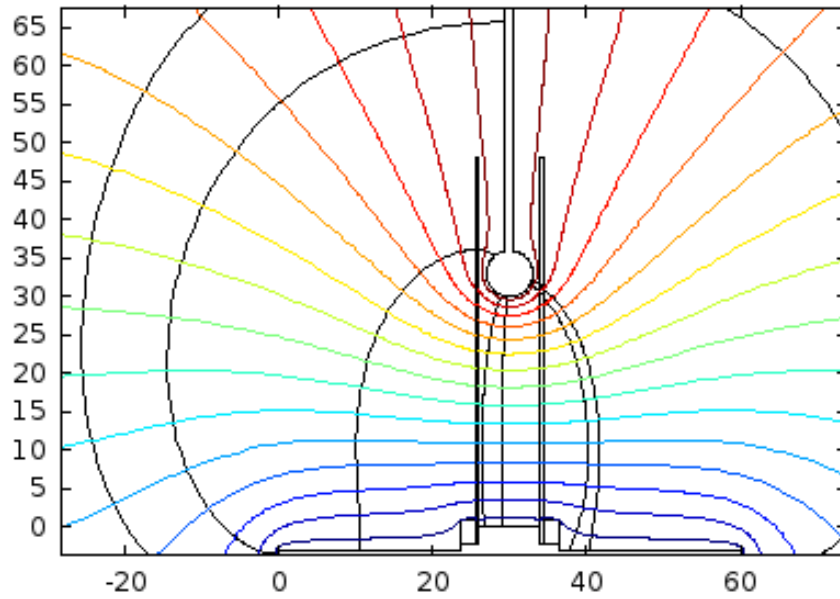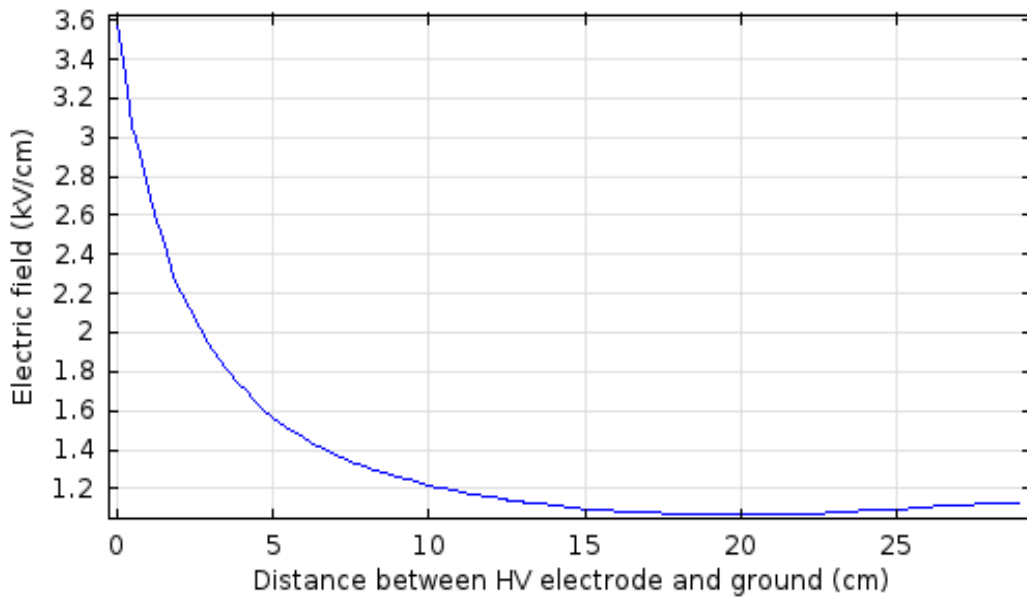lectrode types, it seemed that using the rod electrode would be more suitable for the study conducted in this thesis, where the rod electrode would provide a higher electric field intensity than the spherical electrode with the same applied voltage. Thus, a lower applied voltage was required for approaching the critical electric field needed for the test. The other advantage was the greater possibility of obtaining a single streamer from the rod electrode tip. However, with the spherical electrode with a larger surface area, there was a possibility that several streamers might initiate from different points on that wider surface, which would make it very difficult to control the propagation channels of the streamers, and this could disrupt the visual observation with the high-speed camera, as will be discussed later in Chapter 4.

3.10 Examination of the Test Cell

In this experiment, salt water, which is thought to have a resistive conduction, was tested to assess and examine how the test rig would behave under impulse voltages. Sodium chloride (NaCl) was added to tap water to decrease the conductivity of the water. The tap water conductivity was 0.26 mS/cm. The volume of the tested salted water was 1.21×10^{-3} m^3 with a conductivity of 4.98 mS/cm (water height in the tube was 24 cm). Then, the high voltage rod electrode was inserted into the water. Lightning impulse voltage was applied to the solution; the applied voltage and the flowing current were measured. From the analysis of the voltage and current traces in Figure 3-10, it was clear that the current had a similar behaviour as the voltage, which confirmed the

resistive behaviour of the salt water. Therefore, this could indicate that the test cell would have no impact on the substances placed in the tube during the discharge.
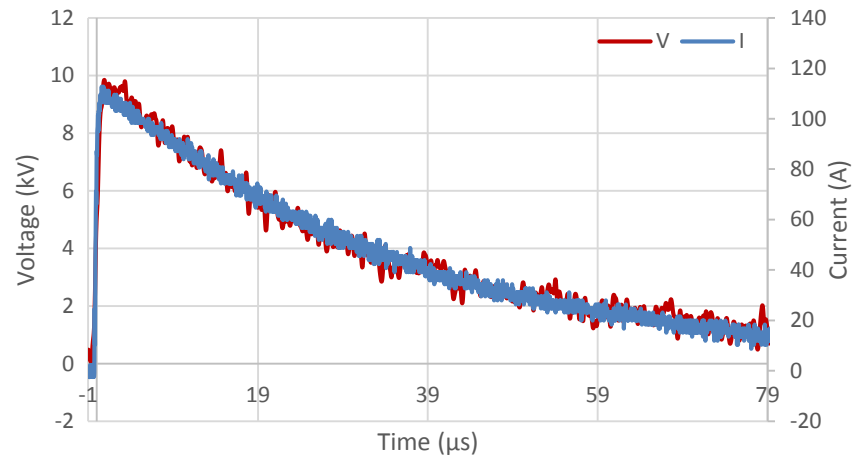
Figure 3-10 discharge traces in salted water

The resistance of the water was determined by two methods. The first was using the reading of the conductivity meter and the water volume in the tube, as in the Equation (3-2):

$$R = \rho \, \frac{L}{A} \tag{3-2}$$

The conductivity of the salted water was 4.98 mS/cm as measured by the conductivity meter.

The resistivity of the salted water was $\rho = \dfrac{1}{\sigma} = 2 \; \Omega.m$

The height of the sample was   L= 24 cm = 0.24 m,

 The radius of the tube was   r = 4 cm = 0.04 m

The cross area of the tube was   A= $\pi \times r^2$ = $\pi \times 0.04^2$ = 5×10^{-3} m²

Then, by substituting the above values into Equation (3-2), R = 96 Ω was found.

The second approach was by using the voltage and current waveforms. By dividing the voltage peak on the current peak, these two peaks occur at the same time. The resistance values are plotted in Figure 3-11. The average resistance of these resistances was 93.8 Ω ± 2.8. The differences between the measured resistances could be due to noise in the voltage and current waveforms. As a result, both methods presented very close values, which could indicate that carrying out discharge experiments in this test rig with this electrode configuration would provide the real performance of the test medium under the applied impulse voltages. Hence, any different behaviours may occur during the discharge would probably be due to the test material's actual behaviour under the test conditions.
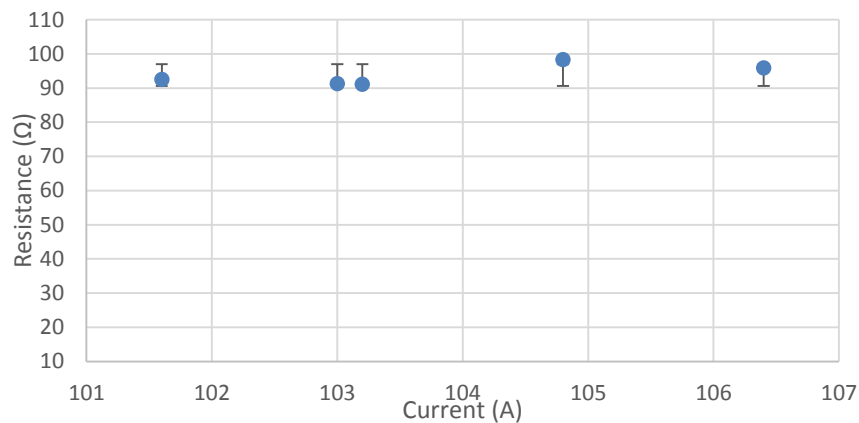

Figure 3-11 resistance versus current for salted water

3.11 Comparison between Discharges in Glass Bubble Material and Sand

The glass bubble material is a relatively new material, and it was not manufactured to be used in high voltage applications. However, due to the

advantages of it transmitting the light, and of being a porous material, it was chosen for this study to simulate soil ionisation in the earthing systems. The soil ionisation phenomenon is initiated in the soil under high impulse currents because of the field enhancement in the air voids among the grains. Despite the differences in the electrical properties between the sand grains and the glass bubble microspheres, when used in volumes both substances exhibit the ability to hold water and contain air. Therefore, the mechanism of the field enhancement in the air voids among the microspheres of the glass bubble material and the grains of the sand should follow a similar process.

Hence, to investigate the discharge in the glass bubble material and sand, a sand test similar to that of the glass bubble material was performed. The sand sample consisted of a 10 cm dry layer at the top and a 20 cm 1% wet layer at the bottom. Figure 3-12 exhibits the impulse discharge waveforms in the glass bubble material with similar sample configuration as that used in Chapter 4 (Figure 4-14) except 10 cm dry glass bubbles, while the discharge voltage and current traces in the sand sample are shown in Figure 3-13. It can be seen that the ionisation phenomenon initiated in both dry porous matrials around the electrode, and then propagated away towards the ground. Both had a capacitive effect before the ionisation, and there were time delays for the initiation and propagation of the ionisation in the dry layers in both materails.

Therefore, it can be said that both materials have a similar mechanism for the field enhancement process among the particles of both materials, as the relative permittivity of both materials plays a vital role in the field intensity in the air pockets inside these porous substances. Hence, the field enhancement is considered the main reason for the soil ionisation phenomenon under high

70

impulse voltages particularly in dry porous materials where the heat produced by the current flow in the moisture content is eliminated.
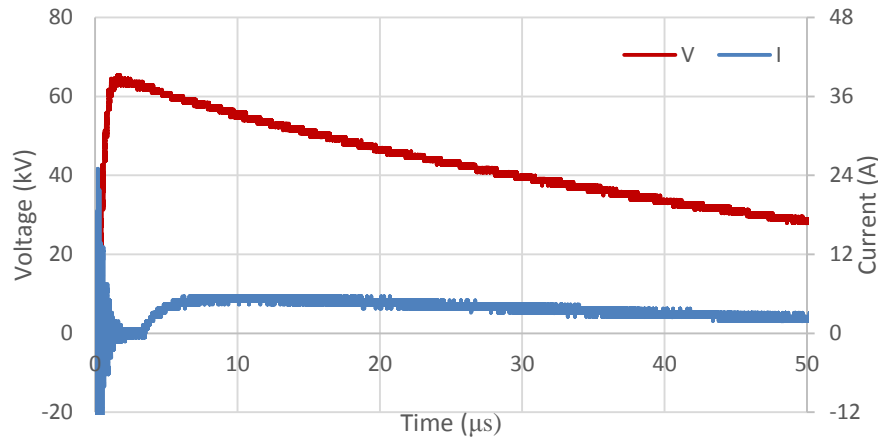
Figure 3-12 discharge traces in glass bubble sample (64kV)
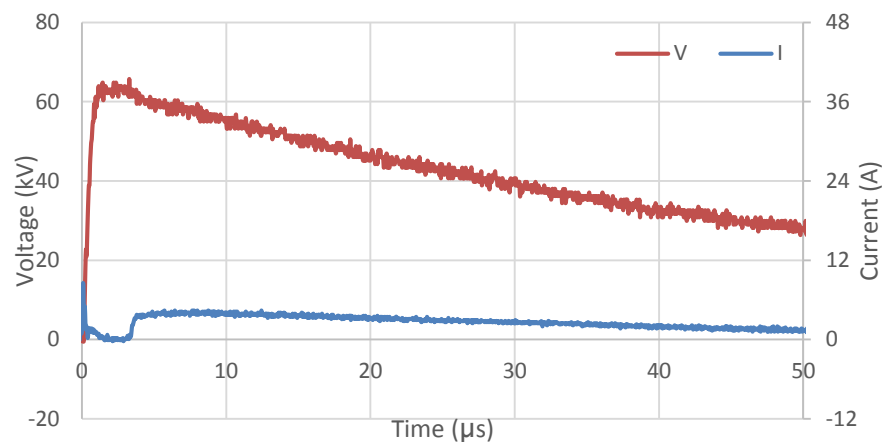
Figure 3-13 discharge traces in two-layer sand sample (64kV)

3.12 Conclusion

This chapter delivered a brief description of the facilities utilized in the experimental work; that is the visual and electrical examinations. The impulse generators, imaging machines, test media, and the test circuit were described. A special test cell was designed and built to investigate the soil ionisation phenomenon visually with high-speed cameras. The rig was constructed with

a rod-plane electrode configuration and was provided with a transparent tube. All these aspects were implemented to allow the discharge light to be transmitted from the sample to the high-speed camera placed near the cell. A new dielectric glass bubble material, which has the ability to transmit the discharge light through its particles, was placed in that vertical tube in the test rig, so that the discharge light could be captured for the visual study. Furthermore, the soil ionisation was also examined electrically by the installation of voltage probes in the tube to measure the potential in the ionisation zone, as will be seen in Figure 5-14 in Chapter 5.

Therefore, these voltages could trace the propagation of the ionisation phenomenon during the discharge. Using a rod-plane electrode configuration is not a common electrode arrangement when electrically investigating the discharge in soil and soil ionisation. However, this arrangement was most suitable for the visual study even with the sensitive films, as reported in [73]. Additionally, this arrangement provides a high electric field intensity with a relatively low applied voltage, and offers a single tip where the current is expected to initiate and flow from the active electrode. This is very helpful with the filming process, so that the camera will record one streamer propagating from the electrode through the material towards the ground. The hemispherical or the cylindrical arrangements would not be appropriate in the investigation conducted in this thesis, due to the difficulty of using a transparent container to transmit the discharge light.

The test rig was simulated with COMSOL software to study the electric field between the electrodes. From the simulation results, the electric field produced by the rod electrode is much higher than that of the spherical electrode under

the same applied voltage; also, the electric field was found to be concentrated in the area under the active electrode where the sample was placed. The examination of the rig with the Sodium Chloride solution showed a resistive behaviour of the liquid as was expected.

Therefore, it can be concluded that the rig is able to deliver the real behaviour of the test medium under the applied impulse voltages and has no influence on the discharge process. The glass bubble material and sand were tested under different conditions to investigate the initiation and propagation of soil ionisation and the breakdown phenomena in two layer samples. This study was facilitated by utilizing high-speed cameras and microscopic imaging machines, while the electrical investigation in both dielectric porous media was facilitated by voltage dividers; these were coupled with the potential probes to measure the voltage across the ionised zone below the rod electrode, and with a current transformer to detect the current flowing through the samples.

Chapter Four

Visualisation of Ionisation and Electric Discharge in Glass Bubble Material

4.1   Introduction

The soil ionisation phenomenon is considered one of the main causes of the nonlinear behaviour observed in the impedance of earthing systems under high currents such as those generated by lightning surges. Despite the attention that soil ionisation has attracted and the large number of experiments that have been published, some aspects of the ionisation phenomenon are still unclear and not fully understood and explained. Most of the research investigations have examined this phenomenon in terms of the electrical

74

aspect, such as electric field, current density, and resistivity, and by measuring and recording the voltage and the current waveforms. However, there is a growing body of literature that recognises the importance of studying the electric discharge visually in the soil to obtain a better understanding of the phenomenon, and to find better explanations for the developments and the shapes of the discharge inside the soil. The imaging process of the electric discharge in porous materials like soils is extremely difficult. In the literature, techniques such as x-ray films [23-25], photographic films [24] and conducting paper [75], have been used to record the electric discharge and the ionisation phenomena from inside the soil. However, these methods suffer from several disadvantages as discussed in Chapter 2. The key purpose of this chapter is to discuss the process of imaging the electric discharge in a new dielectric porous material (glass bubbles), using a different technique from those in the literature, i.e. using a high-speed camera, so that the discharge process can be recorded and analysed in conjunction with the voltage and current waveforms. Thus, the recorded videos displayed the dynamic developments of the discharge process with time.

4.2 Test Circuit

The circuit of the test consists of the Haefely four stages impulse voltage generator (1) to generate a standard lightning impulse. This generator was connected to the capacitive voltage divider (2) to measure the voltage. The voltage divider was connected to the high voltage electrode (3) at the test cell. The ground plate in the rig was connected to an earthing point via a braid through a current transformer (7) to measure the current. The voltage divider and the current transformer were connected to a LeCroy digital oscilloscope

(9) via coaxial cables. The high-speed camera (6) was also set up and connected with the computer (8). Figure 4-1 shows the test circuit.
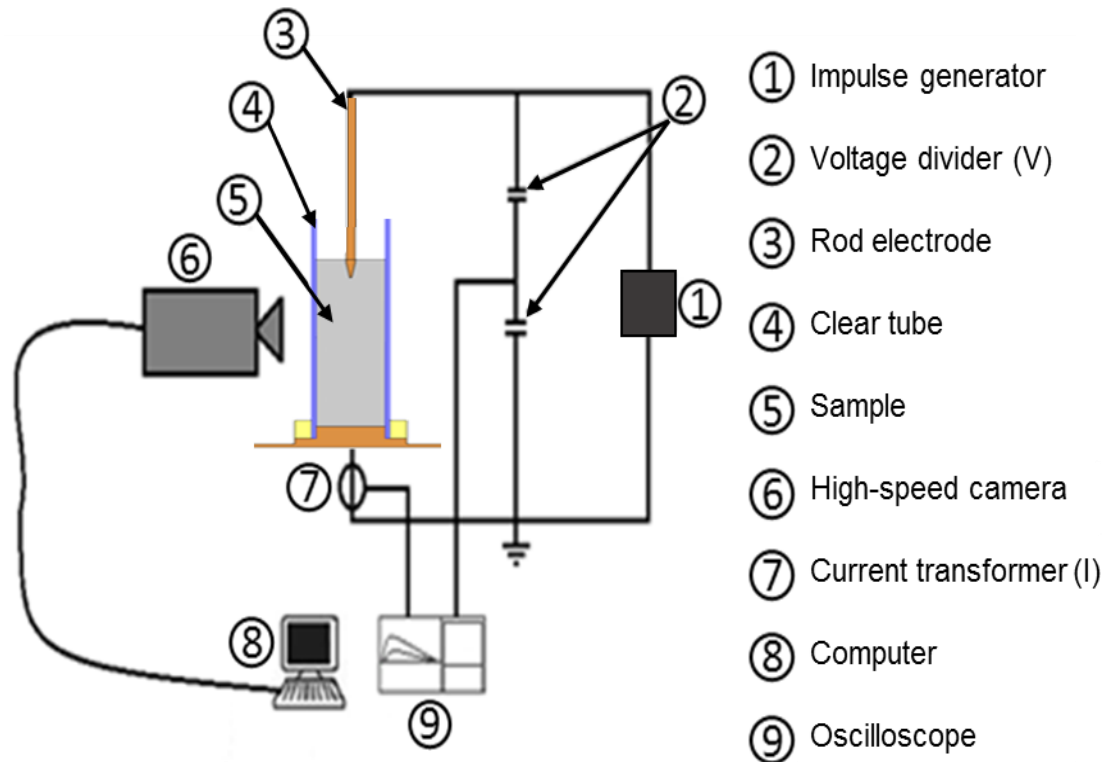

①	Impulse generator
②	Voltage divider (V)
③	Rod electrode
④	Clear tube
⑤	Sample
⑥	High-speed camera
⑦	Current transformer (I)
⑧	Computer
⑨	Oscilloscope

Figure 4-1 test circuit for the visual investigation

4.3   Soil Test

The aim of this test was to observe whether the discharge inside the sand could be seen from outside through the transparent tube or not, and to examine the electric field provided by the electrode arrangement in the test cell to initiate the ionisation phenomenon in wet soil to obtain a second current peak.

4.3.1   Soil Sample Preparation

The wetted sand test was carried out to examine the test rig. Medium grain pure sand was used. The sand was wetted with tap water. The amount of water was calculated by adding water as a percentage of the dry sand mass

according to BS 1377 standard. In order to ensure a good moisture distribution among the grains, the sand and water were mixed thoroughly, and then, the mixture was poured into the tube. At this point, some pressure was manually applied to the sample to make sure that the mixture was distributed uniformly in the tube, and to prevent there being any gaps inside the sample. This process was repeated until the desired height was achieved.

4.3.2   Test Procedure

In this test, a 10% water content was used with sand, and the sample height in the tube was 9 cm. The high voltage electrode was inserted into the sample to a depth of 3 cm in the centre of the tube. A high impulse voltage test was conducted to examine the ionisation phenomenon in the wetted sand, as was described in the literature. The impulse voltage was applied to the sample with gradual increase in magnitude. The voltage and current waveforms were captured by the oscilloscope. When the voltage approached (18kV), a second current peak started to appear. As the voltage increased further, the current peaks increased accordingly. Figure 4-2 is an example of the voltage and current traces for the soil ionisation and full breakdown. As was expected, the ionisation phenomenon appeared very clearly with the presence of the second current peak, which could be attributed to either thermal or electrical processes. The thermal process could be due to the heating by the current conduction through the water channels, while the electric process could be due to the field enhancement in the air voids inside the sand. These two processes could explain why the phenomenon of soil ionisation would occur. From this test, it can be concluded that the test rig produces measurement results as predicted, as the electric field distribution could initiate the soil

ionisation. However, from the visual observation of the discharge through the clear tube, the discharge could not be seen visually, and that could be due to the opacity of the soil, so that the light produced by the discharge could not be transmitted through the sand. Consequently, another porous material was required that could emulate the soil, but through which light could be transmitted, and glass bubble test medium was what was used to visualize the discharge under the impulse voltages.
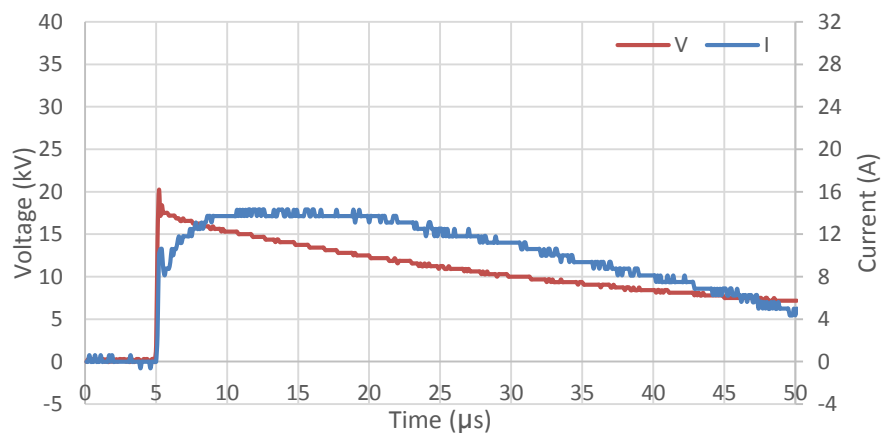
(a) discharge traces for soil ionisation without a breakdown
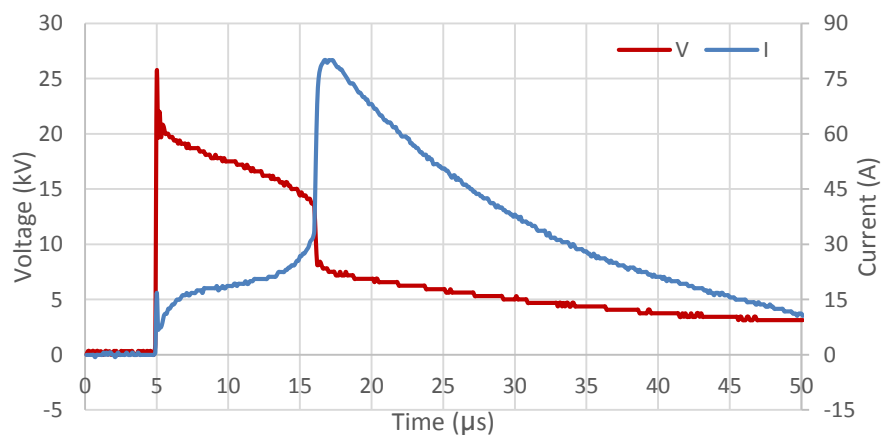
(b) discharge traces for soil ionisation and breakdown phenomena

Figure 4-2 discharge traces for soil ionisation in wet sand

4.4 Glass Bubbles Resistivity Measurement Test

This experiment was conducted in order to acquire a rough estimation of the resistivity of this material for the first time. As was reported earlier in Chapter 3, the electrical properties of this material are not known. The circuit of the investigation included an ABEM SA1000 tester, and the test cell comprised two parallel square aluminium plates (20 cm × 20 cm), as shown in Figure 4-3. These two electrodes were fixed inside a special dielectric container. The material was dried in the oven at 50°C, then when the material is dry and at the room temperature, it was poured between the two electrodes to fill the gap between them completely. The tester was connected with the electrodes to inject a DC current into the material in order to measure the resistance of the glass bubbles. Therefore, when the tester was adjusted to output a 1 mA DC current, it automatically calculated and displayed on its screen the value of the measured resistance of the sample between the plates.
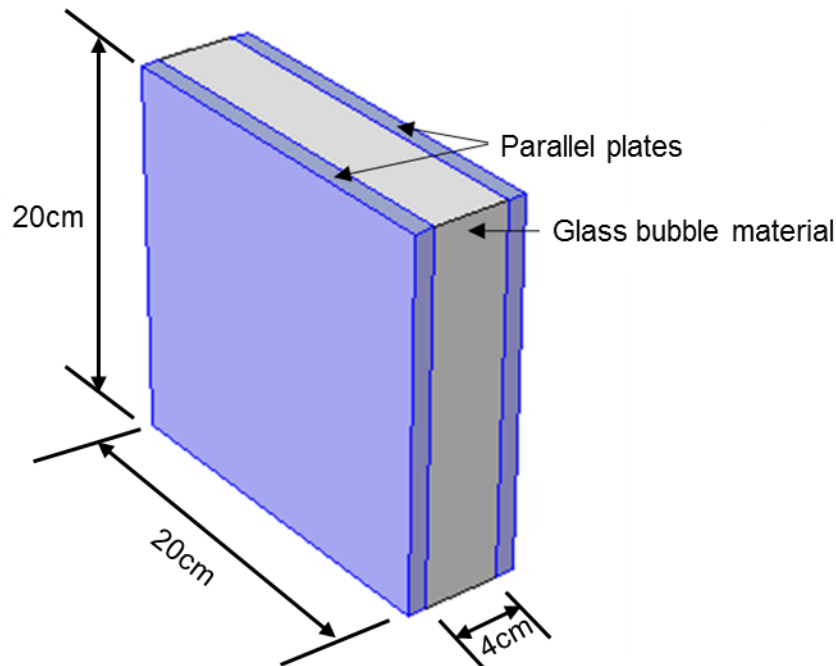
Figure 4-3 parallel electrodes arrangement for dry material resistivity test

Then, by using the dimension of the plates and the distance between them, the resistivity could be calculated as follows:

Plate area (A) = 0.2 m × 0.2 m = 0.04 m^2

The distance between the plates (L) = 0.04 m

The measured value of (R) = 325 kΩ

$$\rho = \frac{R \times A}{L} = 325 \text{ k}\Omega.\text{m} \tag{4-1}$$

By repeating this test six times to obtain several readings, it can be concluded that the DC resistivity of glass bubble material is 325 kΩ.m ±2.4.

4.5   Discharge in Dry Glass Bubbles Only

4.5.1   Dry Glass Bubbles under Lightning Impulse Voltage

The first step was to fill the tube with dry glass bubble material up to a height of 28 cm. Then, the electrode was inserted into the material making the distance between the two electrodes 25 cm, as shown in Figure 3-5. By connecting the test circuit and arranging the Lightning RDT camera with 1600 frames per second to record the discharge, lightning impulse voltages were applied to the sample. When the generator was fully charged, the camera was triggered first and then the generator. This process ensured that the entire discharge was filmed. It was clear from the resistivity test that this material has a large resistivity and that the breakdown would be at a high voltage level. Therefore, when increased impulse voltages were applied, the camera did not capture any light, until a certain voltage level where the breakdown occurred; a very bright light was captured by the camera. The voltage and current traces

illustrated that the voltage collapsed to a lower value at almost the peak value, and the current soared suddenly to a very high value, as in Figure 4-4. The camera was able to record the discharge with just one frame representing the breakdown moment. However, the light emission from the breakdown was initiated around the electrode on top of the material, and then propagated down towards the ground, outside the material on the inner surface of the tube wall. The current channel trace can be seen clearly in Figure 4-5.
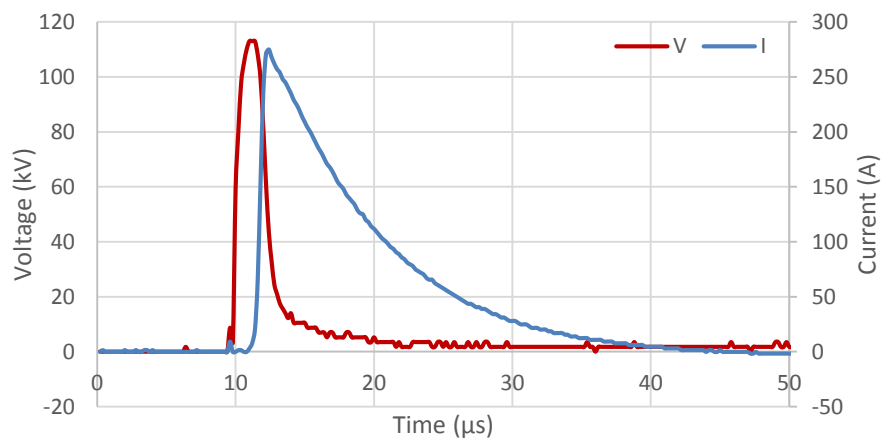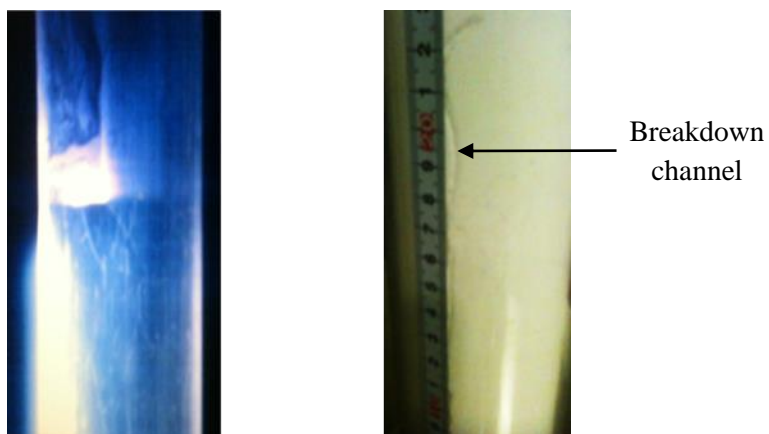

Figure 4-4 discharge traces in dry material at 25 cm gap

(a) breakdown light emission   (b) breakdown channel

Figure 4-5 breakdown discharge in dry material at 25 cm gap

The gap was reduced to 20 cm, and then, when the breakdown voltage level was applied, as in Figure 4-6, the breakdown current flowed down from the tip of the electrode through a few centimetres of the material and then to the inner tube's wall toward the ground. On checking the tube, a groove on the inner wall of the tube could be clearly observed, which indicated the breakdown current channel, and Figure 4-7 shows an example. As can be seen, these grooves did not have any branches as would a tree-like model, but they mostly had curvy lines as the breakdown occurs. The distortion in the electric field of the streamer during the propagation could have an effect on the streamer path. The applied voltage had a longer rise time than the standard time; this possibly due to an accumulation of charges around the electrode before the breakdown occurred. This accumulation prevented the voltage from decaying as the standard lighting impulse after the voltage peak.
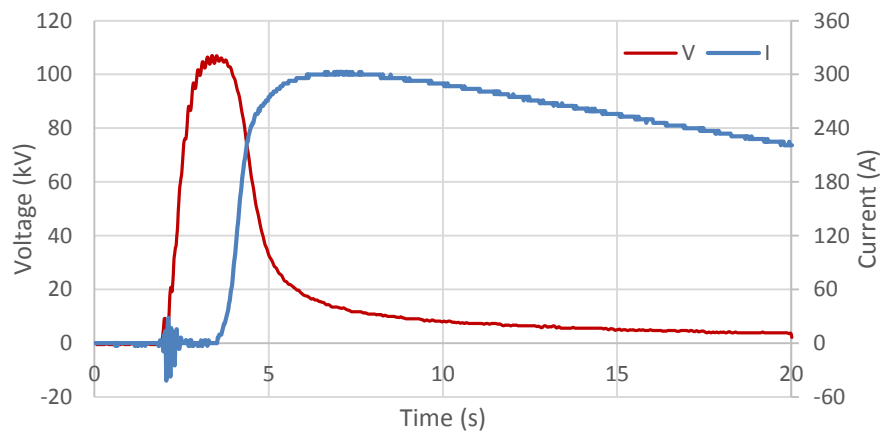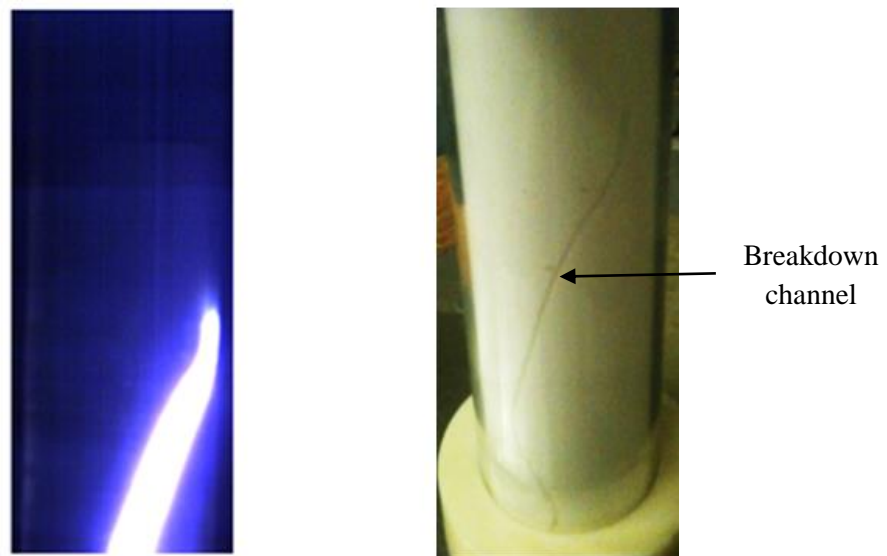

Figure 4-6 discharge traces in dry material at 20 cm gap

Due to the high resistance of this material, negligible or no current was detected before breakdown. Hence, the gap between the electrodes was

further reduced to 15 cm and then to 10 cm. The material presented the same performance, which was that the current was undetectable until the full collapse occurred. The measured voltage had a longer rise time up to the delay time before the current conduction, so the injected charges may have accumulated around the electrode building up a potential, which would have maintained the voltage on the sample until the breakdown. Then these charges drained in the current channel to the ground, as in Figure 4-10. As the applied voltage increased, the current delay time and the rise time of the voltage decreased as well. The reason for the breakdown current flow on the internal surface of the tube could be controlled by the electric field, which is concentrated at the sharp edge of the tube base on the ground plate, as in Figure 4-11.

(a) breakdown light emission   (b) breakdown channel

Figure 4-7   breakdown discharge in dry material at 20 cm gap
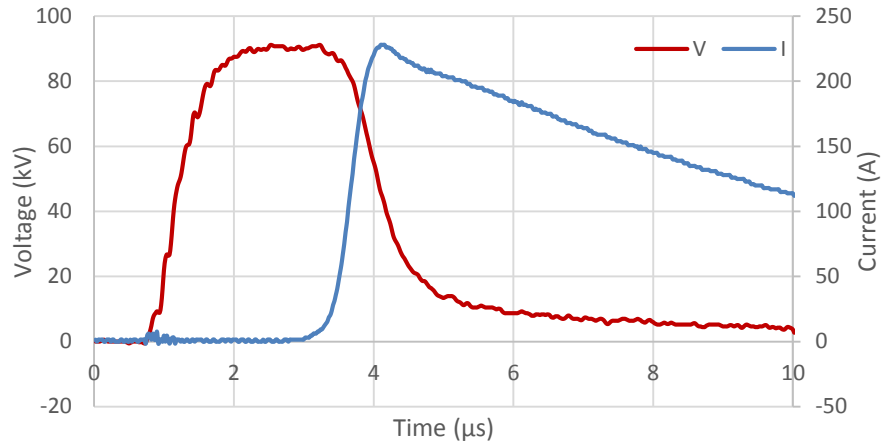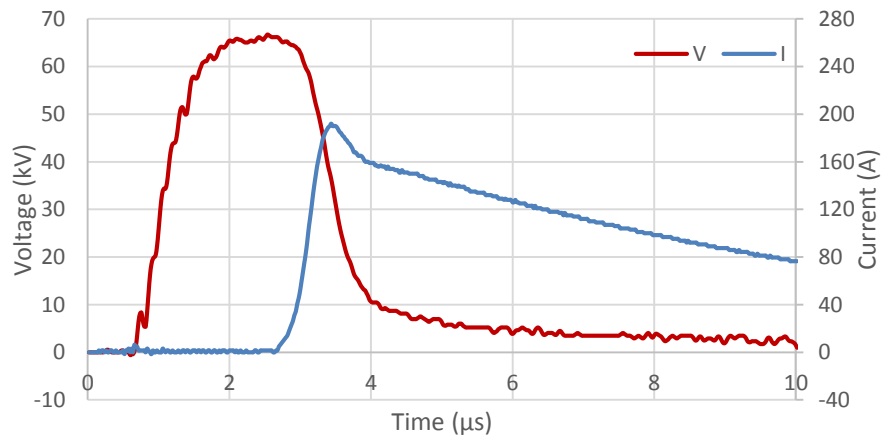
Figure 4-8 discharge traces in dry material at 15 cm gap
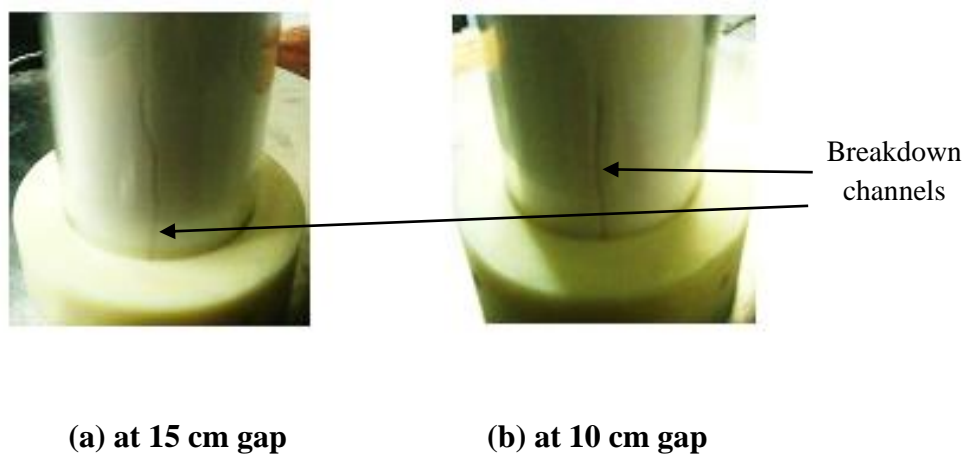

Figure 4-9 discharge traces in dry material at 10 cm gap

(a) at 15 cm gap   **(b) at 10 cm gap**

Figure 4-10 breakdown channels
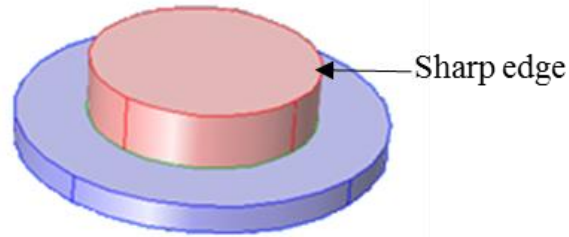
Figure 4-11 aluminium base of the tube that has sharp edge

4.5.2 Dry Glass Bubbles under Switching Impulse Voltage

When the same procedure was repeated as for under the lightning voltage with a 20 cm dry layer, it was found that the material demonstrated a similar behaviour, i.e., no current was detected until the breakdown occurred, whereupon the voltage broke down at a certain voltage level to a low value, and the current rose sharply to a high value for just a short time. Then due to the generator's high front resistance, the current collapsed, which meant the voltage recovered for some time until the current rose again for short time, also to a high value. Then, when the current dropped to a low value, the voltage fell down again to a low magnitude until the end of the wave, as shown in Figure 4-12. However, even with the switching voltage, the current was still flowing outside the material, as seen in Figure 4-13.

Figure 4-12 discharge traces in dry material under switching voltage

| (a) breakdown light emission | (b) breakdown channel |
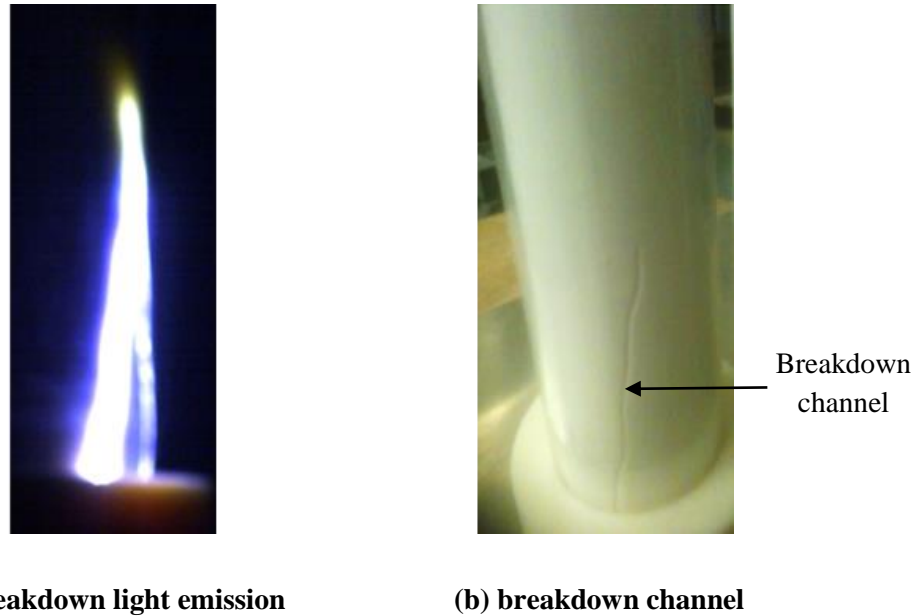
Figure 4-13 breakdown discharge in dry material under switching voltage

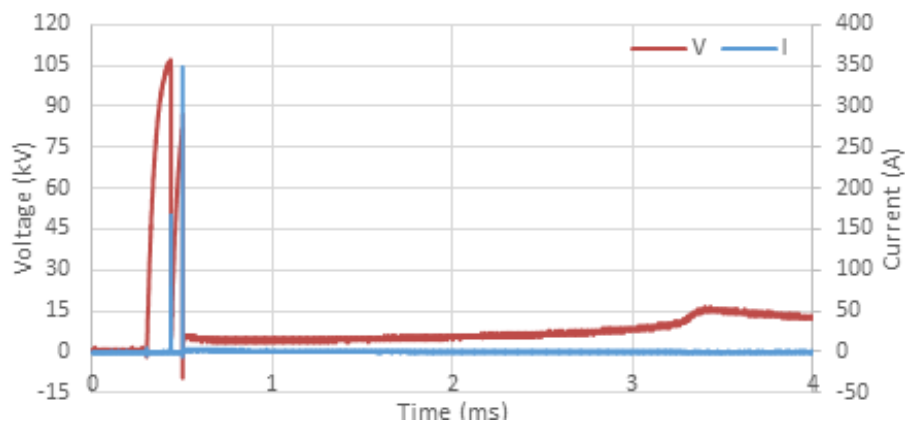## 4.6   Discharge in Dry and Wet Glass Bubbles

Standard impulse voltages were applied to the sample. An instantaneous triggering between the impulse generator and the high-speed camera was arranged to record the entire discharge process in the dry glass bubbles. The FASTCAM SA5 high-speed camera was setup to operate at 175000 frames per second. Setting the camera at this frame rate will produce frames representing 5.5 µs duration each, with an exposure time range of 1-5 µs.

4.6.1   Glass Bubbles Sample Preparation

The measured resistivity of the material was very high. Therefore, the dry glass bubble material test did not provide any useful results for the understanding of soil ionisation, i.e., there was no conduction current until the full breakdown occurred, and the breakdown current flowed along the inner wall of the tube, and not in the middle of the material. For these reasons, the filming process required a particular sample arrangement in order to achieve the following

objectly: firstly, ensuring that the whole discharge occurred inside the material; secondly, obtaining a conduction current without a breakdown (meaning the discharge would have a longer period) so that the camera could record a considerable number of frames; and finally, creating some sort of control over the current propagation path (to direct the current towards the side where the camera was placed). It was decided that the best sample to adopt for this investigation was the two-layer sample. The upper layer was just dry glass bubbles where the discharge is intended to be. The lower layer was divided into two sections. The section facing the camera was glass bubble material wetted with tap water, and the other or the back section was filled with dry material, as shown in Figure 4-14. The water content was calculated by adding water as a percentage of the dry material mass; a 20% moisture was added to the material in this series of tests. This percentage may seem high, but due to the material's high capacity for water absorption, this percentage was sufficient to obtain an acceptable homogeneous and uniform mixture with an appropriate resistance value of the wet section.

To ensure a good moisture distribution among the grains, the material and water were totally mixed. Then, this mixture was poured into the lower part of the tube. At this point, some pressure was manually applied to the sample to ensure that the mixture was distributed uniformly in the tube, and to prevent the gaps from forming inside the sample. The process was repeated until the height of the wet section was (15 cm). The dry material was then poured over the wet material up to a certain height. This new configuration presented significant improvements to the discharge results, as it meant the current would now flow inside the material towards the section with less resistance,

87

which was facing the camera (wetted part), thus increasing the possibility of the camera being able to capture the discharge with a brighter discharge light.

| (a) sample configuration | (b) wet section |
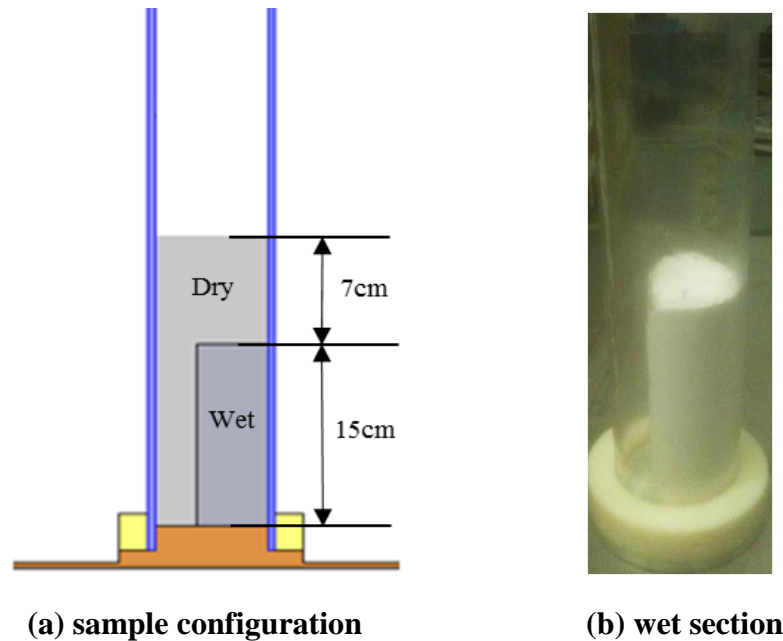
Figure 4-14 glass bubble sample in the tube

4.6.2 Lightning Impulse Test without a Breakdown

At a certain lightning voltage level (49 kV), both the current transformer and the camera detected a current flow from the active electrode to the ground; this current was attributed to the ionisation phenomenon in the air pockets among the microspheres. Based on the analysis of the recorded videos, it was found that the intensity of the emitted discharge light depends on the current magnitude. Hence, the brightest light occurs at the current peak, and as the current decays the light intensity decreases as well. On the other hand, close examination of the current waveform showed there was a time delay before the current rise, which could indicate the time required for the streamer to cross the high resistivity dry material. With the increase of the applied voltage, this delay time was reduced. In order to understand the dynamic developments of the discharge behaviour, the recorded video was correlated with the voltage

and current waveforms. Thus, video frames from the high-speed camera were associated with specific instants on the voltage and current impulse curves, where each frame represents the discharge at a 5.5 µs time range. Figure 4-15 displays an example of correlating current and voltage waveforms with particular frames. Each horizontal division in the figure is 5.5 µs, and each video frame is also 5.5 µs. At this point, associating each frame with the corresponding division. The height of the frame represents the dry material part, and the frame width represents the tube diameter. Furthermore, the location of the electrode tip is at the top of each frame.
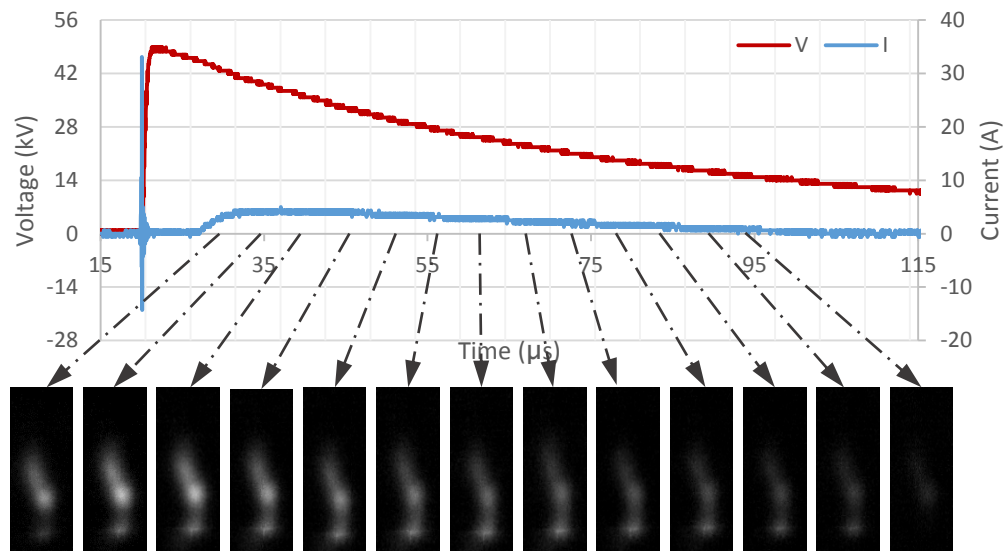
Figure 4-15 correlated frames with discharge traces with no breakdown

Recording the discharge in a porous material under a lightning impulse with this extremely fast frame rate is considered a very significant outcome, especially with no breakdown case. Therefore, seeing the light of the discharge may support the claim that the ionisation phenomenon is perhaps produced by the localized discharges in the air cavities under the field enhancement process. In terms of the impulse impedance, dividing the

impulse voltage by the current from the instant when the current began its rise, showed the impedance was declining dramatically to reach a minimum value at around the current peak. This was probably due to the ionisation effect in the upper dry layer. When the resistance of the wet section was measured, as will be seen in the next chapter, the resistance value was around 10 kΩ, which is close to the minimum value of the total impedance fall. Then, the impedance recovered its value slowly because of the deionisation process, as can be seen in Figure 4-16. This figure shows also that the glass bubble material's behaviour is similar to the soil's behaviour under high impulse voltages, as was described in Liew's dynamic model [34]. At the current peak, the ionisation process causes a drop in the sample impedance to reach a minimum value, and then the deionisation process takes place to recover the resistivity of the dry material on the wave tail of the applied voltage.

4.6.3   Lightning Impulse Test with a Breakdown

Under a higher applied voltage level, a conduction current was also observed. The current started with a low magnitude and then developed to full breakdown with a higher current magnitude. The occurrence of the breakdown may be due to the collapse of the wet layer, as will be explained in the next chapter. At the onset of the current, a very faint light could be seen from the current channel. This then, developed to form a full sample breakdown with higher current and a much brighter light representing the breakdown process. As the voltage and current decayed, the ionisation was gradually extinguished before it disappeared completely at very a low current. Figure 4-17 exhibits the correlation between the captured video frames and the waveforms of the voltage and current signals. The delay time was less than that in the previous

case, as the ionisation phenomenon initiated faster under a higher applied voltage.

(a) impulse impedance versus time
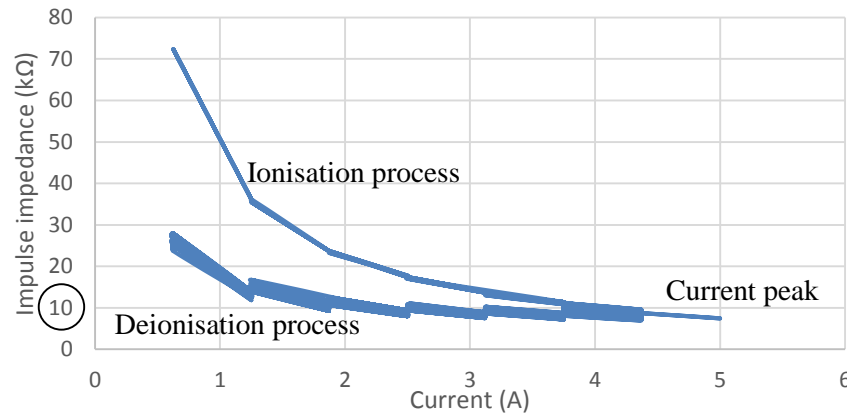
(b) impulse impedance versus current

Figure 4-16 impulse impedances of the discharge in figure 4-15
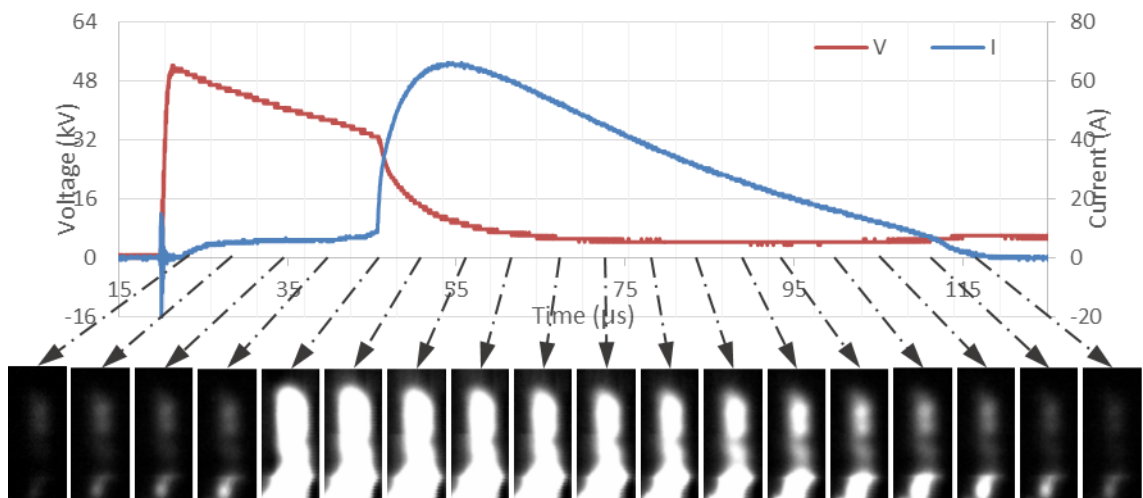
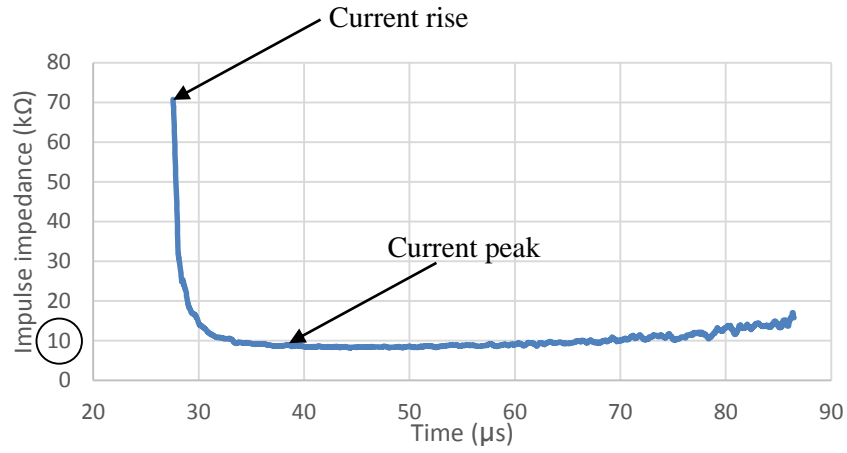**Figure 4-17 correlated frames with discharge traces with full breakdown**

91

In this case, there were two impedance reductions; the first was at the current rise, which was mostly in the upper dry material until about 10 kΩ. Then, the drop continued as the current increased, but probably in the wet section this time, leading eventually to the breakdown of the whole sample as is clearly seen in Figure 4-18 (a). The second reduction was probably in both the dry and wet parts due to the full collapse, but was mainly in the wet section, where the total impedance of the current path had fallen even lower, before the deionisation process took place, as shown in Figure 4-18.

(a) impulse impedance versus time

(b) impulse impedance versus current

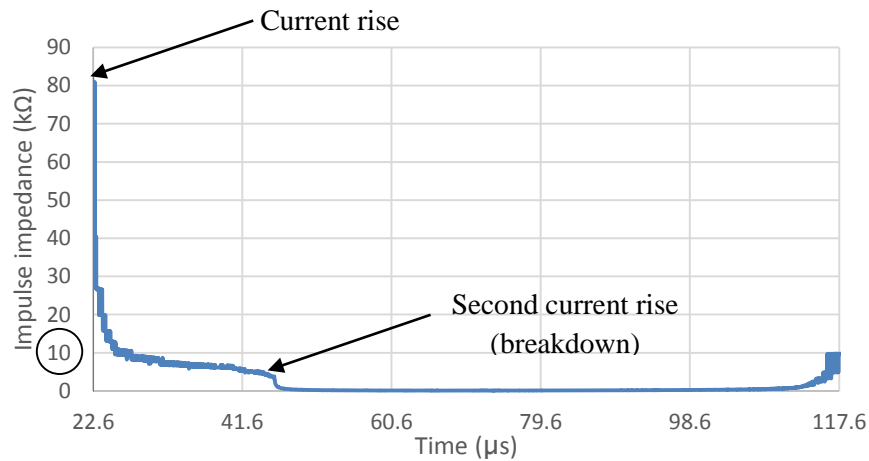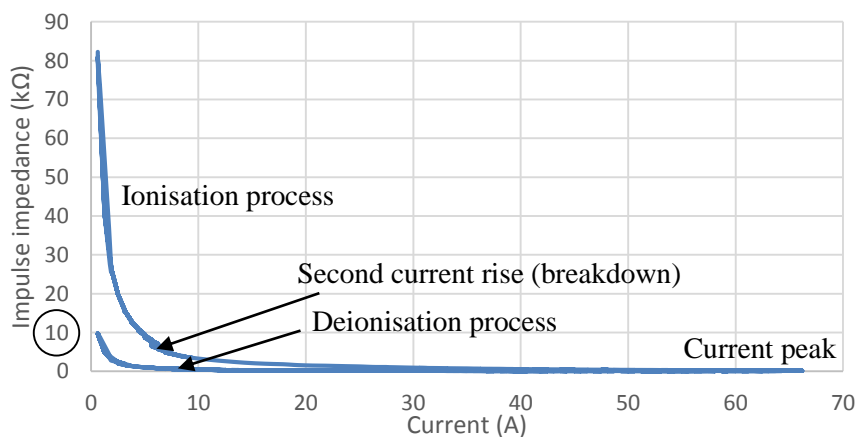**Figure 4-18 impulse impedances of the discharge in figure 4-17**

In both previous cases, the high-speed camera did not capture the developments of the streamer through the dry material before the current rise during the delay time. This might have been due to either the fast rise time of the lightning voltage, which caused the initiation of the streamer to be faster than the frame rate settings of the camera, or to the streamer light being very dim, which may be due to the low current flowing in the streamer, as the light intensity depends on the current value. Therefore, a longer rise time lightning impulse and switching impulse voltages were employed with the same sample configuration in an attempt to delay the initiation of the streamer, so that the high-speed camera could detect the streamer propagation.

4.6.4   Long Rise Time Lightning Impulse Voltage Test

In order to examine the possibility that the lightning impulse voltage was too fast for the camera to record the initiation and propagation of the streamer before the current rise; the lightning surge was slowed down by increasing the front resistor of the Haefely impulse generator. A 9.7 kΩ resistance was connected in series with the generator; this resistor was added to the front resistor of the impulse generator to increase the rise time of the lighting impulse wave from 1.2 to 22 µs, as can be seen in Figure 4-19. A sample configuration similar to that of the previous tests was used in this test; the frame rate of the camera was also set to 175000 frame per second.

The voltage was applied until the current conduction was detected by the current transformer and the camera. The recorded frames, the voltage, and the current waveforms are shown in Figure 4-20. The behaviour of the discharge was found to be comparable to previous behaviour: the light intensity tended to change according to the current magnitude. However,

despite the long-time delay before the current rise, the camera did not capture the instant of the streamer initiation and propagation in the dry layer.
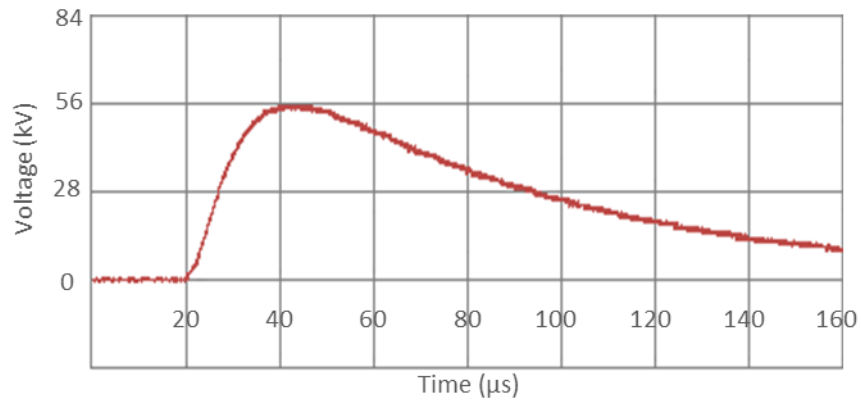
Figure 4-19 long rise time lightning impulse voltage
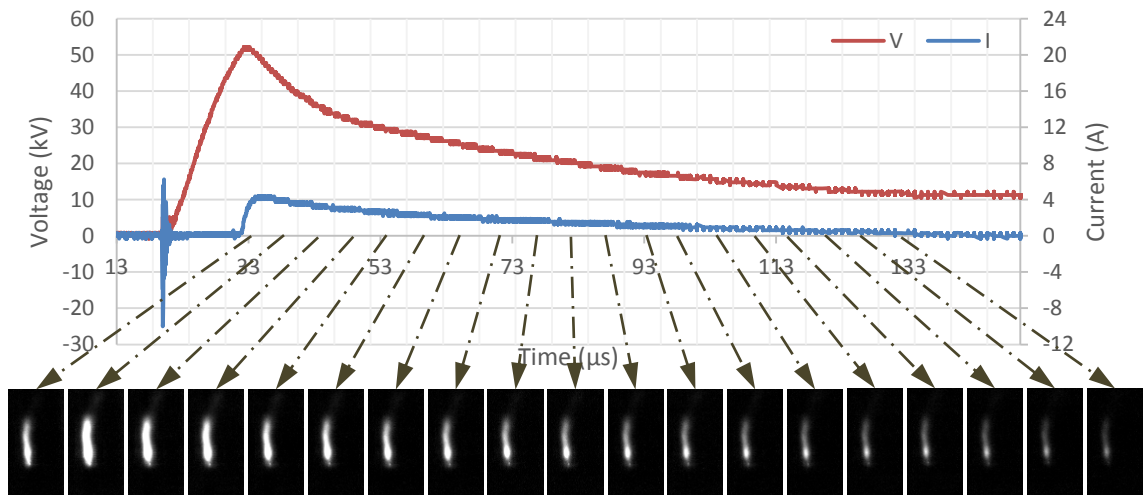
Figure 4-20 correlated frames with discharge traces under long rise time lighting wave

4.6.5 Switching Impulse Voltage Tests

Using the same procedures as in the lightning tests, switching impulse voltages were applied onto the same sample settings. The high-speed camera was set-up to operate at 100000 frames per second; the camera at this frame rate will yield frames with 9.8 µs each, with an exposure time range of 1-9 µs.

The switching voltage generator was triggered up to a level where the current was forced through the material. The conduction period lasted for an extended time due to the longer impulse voltage duration; this led to longer recorded videos, meaning many more frames. As can be seen from the discharge traces when the current rose, the voltage dropped to a certain value until the current approached zero; then voltage recovery took place. An example of the switching discharge is shown in Figure 4-21, where there is a similar trend of behaviour to the lightning discharge. Figure 4-22 presents the correlated video frames with the voltage and current waveforms of Figure 4-21. Due to the large number of frames, only the important frames were considered as numbered in the figure to demonstrate the different stages of the discharge.

Each time division in the figure and frames is 9.8 µs. The video of this discharge exhibited tendencies comparable to those in the previous tests only at the beginning of the current flow. Therefore, the brightness of the discharge light corresponded to the current value, until about 215 µs (frame number 22). After that, while the current was decaying, an increase in the brightness of the light was observed. This behaviour was completely opposite to the lightning discharge scenarios, as the period of the current flow did not exceed 200 µs even in the breakdown case.

In order to explain this new observation, more tests need to be conducted and new parameters may also be considered, such as the electron density and the temperature, which is, however, outside the scope of this thesis. An initial conclusion can be drawn based on the investigation carried out in [82], where an electron density measurement was performed for a discharge in an air gap. The authors found that the areas that have a brighter light tend to have a higher

electron density. Therefore, in this case, the increase in the brightness of the light might also have been due to the increase in the electron density, which may have led to an increase in the light emitted, as the current was flowing in the ionised air pockets trapped inside the dry material.
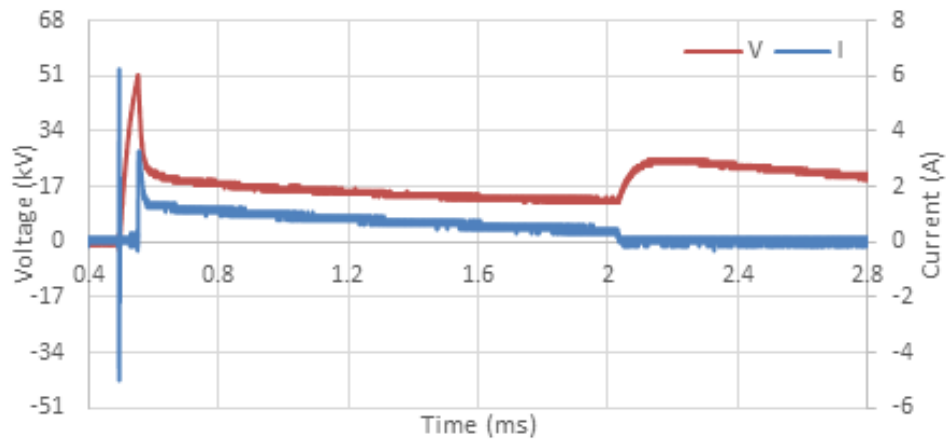
Figure 4-21 discharge traces under switching impulse voltage
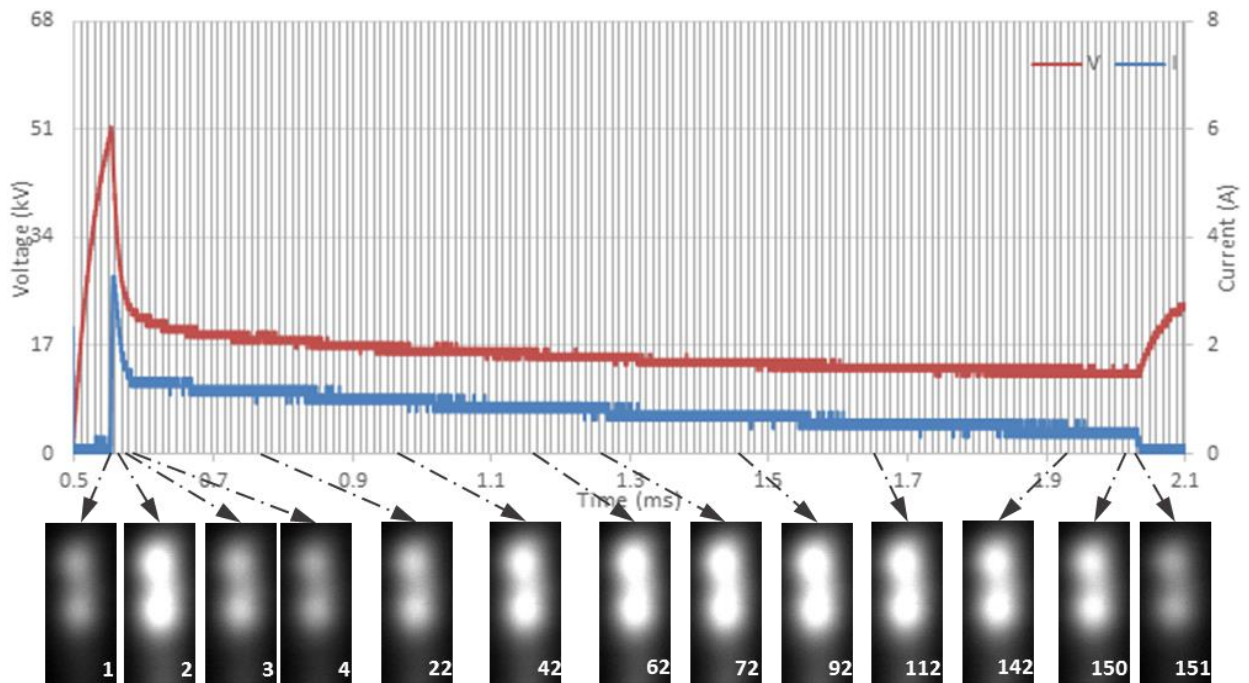
Figure 4-22 correlated frames with discharge traces under switching impulse voltage

96

A reduction in the impedance occurred at the current rise until its minimum at the current peak, which was almost 10 kΩ (the wet resistance value), and then the impedance recovered its pre-ionisation value, but slowly, as seen in Figure 4-23. Liew's model [34] seems to work even with a very slow impulse voltage. Despite the long front time, the impedance drop was so rapid, but the recovery process was very slow. On the other hand, the new phenomenon did not affect the impedance behaviour; the impedance continued to recover with the deionisation phenomenon but for a longer time because of the longer switching impulse tail time.
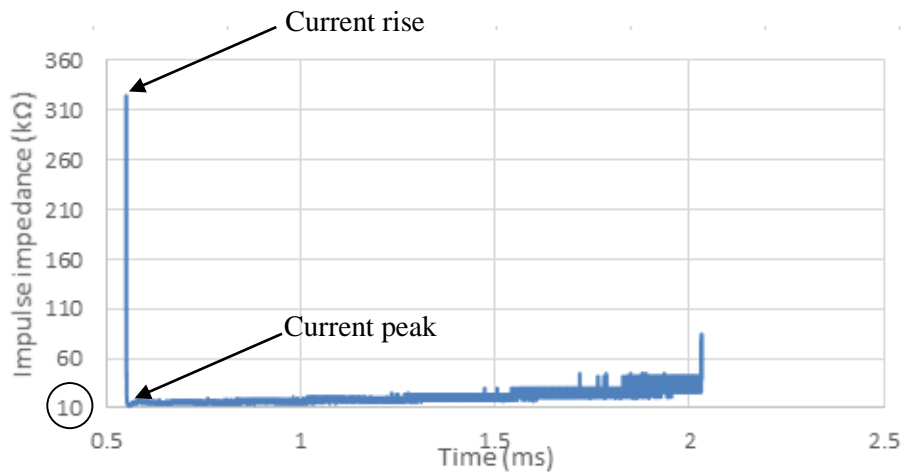
(a) impulse impedance versus time
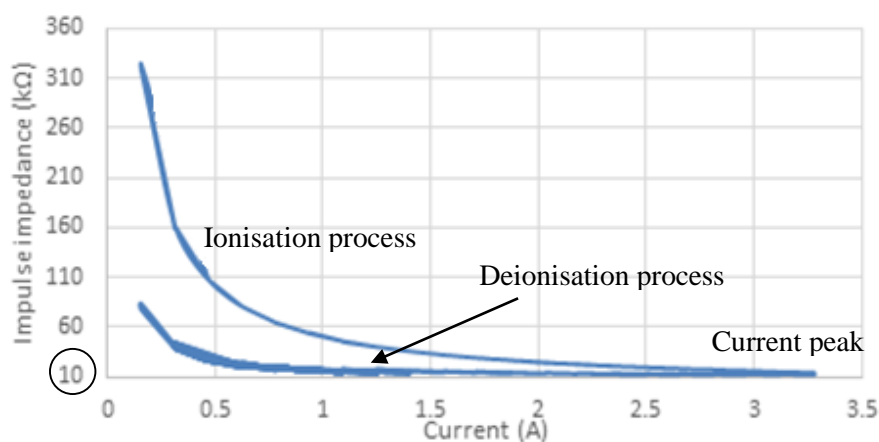
(b) impulse impedance versus current

Figure 4-23 impulse impedance of the discharge in figure 4-21

With the switching impulse, the high-speed camera could not detect the streamer propagation as well, which is probably due to the streamer having a very dim light during the propagation, as the first frame captured by the camera at the current rise had an observable light intensity. Based on the correlation between the current value and the light intensity, this could indicate that the streamer had very low current magnitude during the propagation, which is similar to what was reported in [43]. Then, when the streamer reached the wet layer, the current flowed with an increased value; at this instant, the light started to appear, and the camera began to detect and record the discharge.

4.7   Microscopic Imaging of Glass Bubble Material

When the dry glass bubble material was evacuated from the tube, pieces of white threads were found inside the dry material. They were very fragile and had different diameters, as can be seen in Figure 4-24. These filaments may have been formed due to the heat generated by the passage of the current through the ionised air voids in the dry material, especially the breakdown currents, which had higher current values for a longer time. This process was thought to be very similar to what is called fulgurite in soil under lightning strikes. Thus, the diameter of these threads could represent the current channel through the dry material. The diameter range of these threads is very small less than 3 mm, which may be due to the fine grains (very small air voids). However, the examined filaments had a cylindrical shape without any tree-like branches, as was seen in [71], and they appeared to make curves with a single channel. The temperature needed to melt sand is extremely high (possibly reaching up to $1400°$C), and the temperature that may be produced by the lightning strike could reach more than $1800°$C [83], but according to the

data sheet of the glass bubble, the softening point is 600 °C. Therefore, the heat generated by the current channel may have reached this temperature, so the microspheres did not completely melt. A scanning electron microscope (SEM) technique was utilised to examine and image these threads using a Hitachi Analytical Benchtop SEM TM3030 and a Nikon LV100D-U base unit. Figure 4-25 and Figure 4-26 show the microscopic images of these threads. It is obvious from the images that despite the thermal effect of the current flow, the microspheres had not completely melted, which could be due to either the flow time of the current being short or to insufficient heat being generated to melt the particles. The Hitachi system TM3030 has the ability to analyse the glass bubble microspheres in terms of the chemical elements as follows. An electron beam excites the atoms of the different elements of the filament. Various values of x-ray are emitted, and then an x-ray sensor detects the different x-ray values for each element that makes up the microspheres. This process is called Energy Dispersive X-ray spectroscopy (EDX). One microsphere from the sample was selected to undergo the elemental analysis using EDX with Hitachi machine as exhibited in Figure 4-27. In Figure 4-28 an EDX spectrum diagram is shown. It can be seen that the microspheres are composed of four elements. It should be noted that the carbon element is actually not an element from the sample, but is only from the background layer. This carbon layer was used to stick and fix the filament onto the machine's sample stage in the vacuum chamber. The main element is Silicon with the highest value, and the other elements are Sodium, Calcium, and Oxygen. The Energy dispersive X-ray spectroscopy was also performed using Nikon LV100D-V microscope, and the same elements were found as in Figure 4-29.
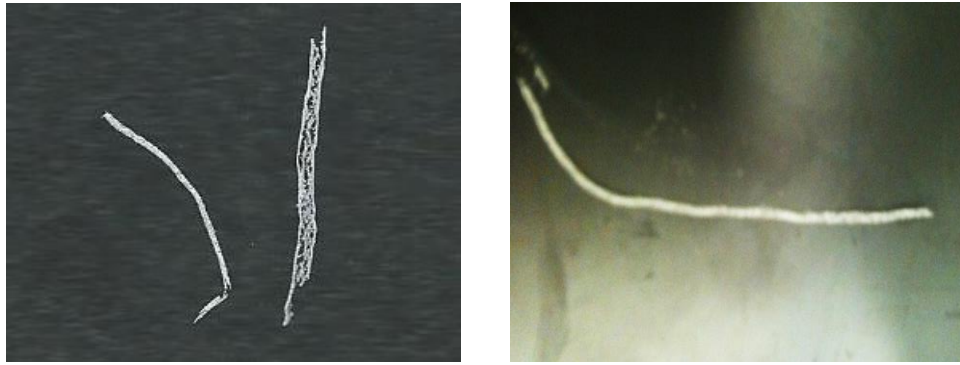
Figure 4-24 glass bubble filaments
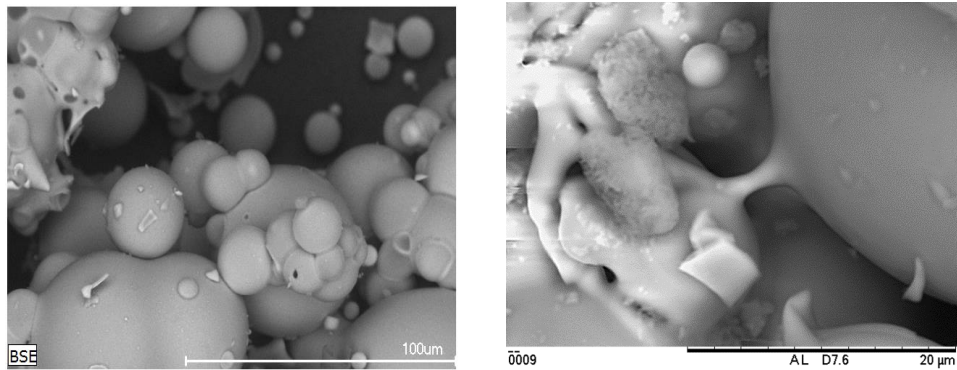
Figure 4-25 microscopic images of a filament with Hitachi TM3030
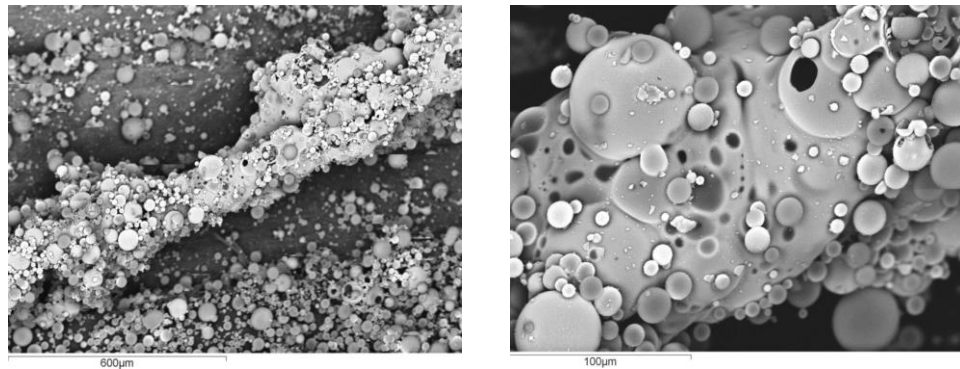
Figure 4-26 microscopic images of a filament with Nikon LV100D-U base unit

In the wet layer, the current flow created holes on the wet layer surface and grooves or channels inside the wet material along the height of the wet section. Figure 4-30 shows an example of these holes and channels; they had variable diameters, which probably corresponded to the current value. From the current grooves, it seems that the current did not tend to flow in a straight line through

the wet layer, where these channels had twisted lines and without any tree-like branches similar to the dry layer.
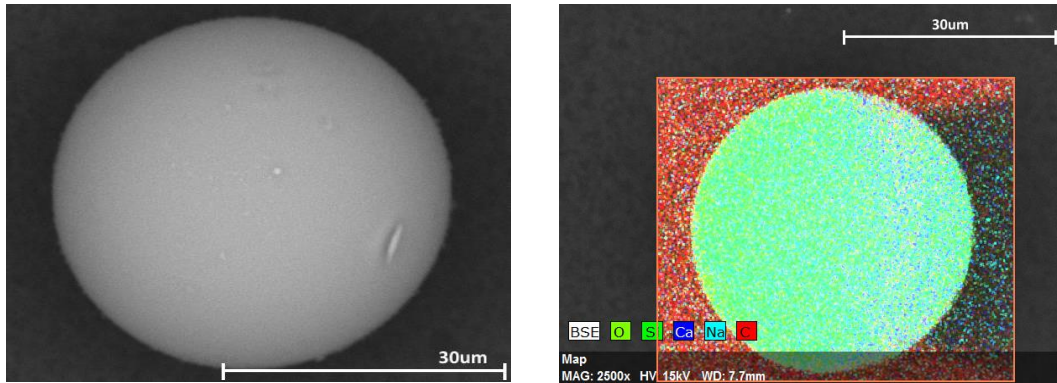
Figure 4-27 single microsphere components analysis
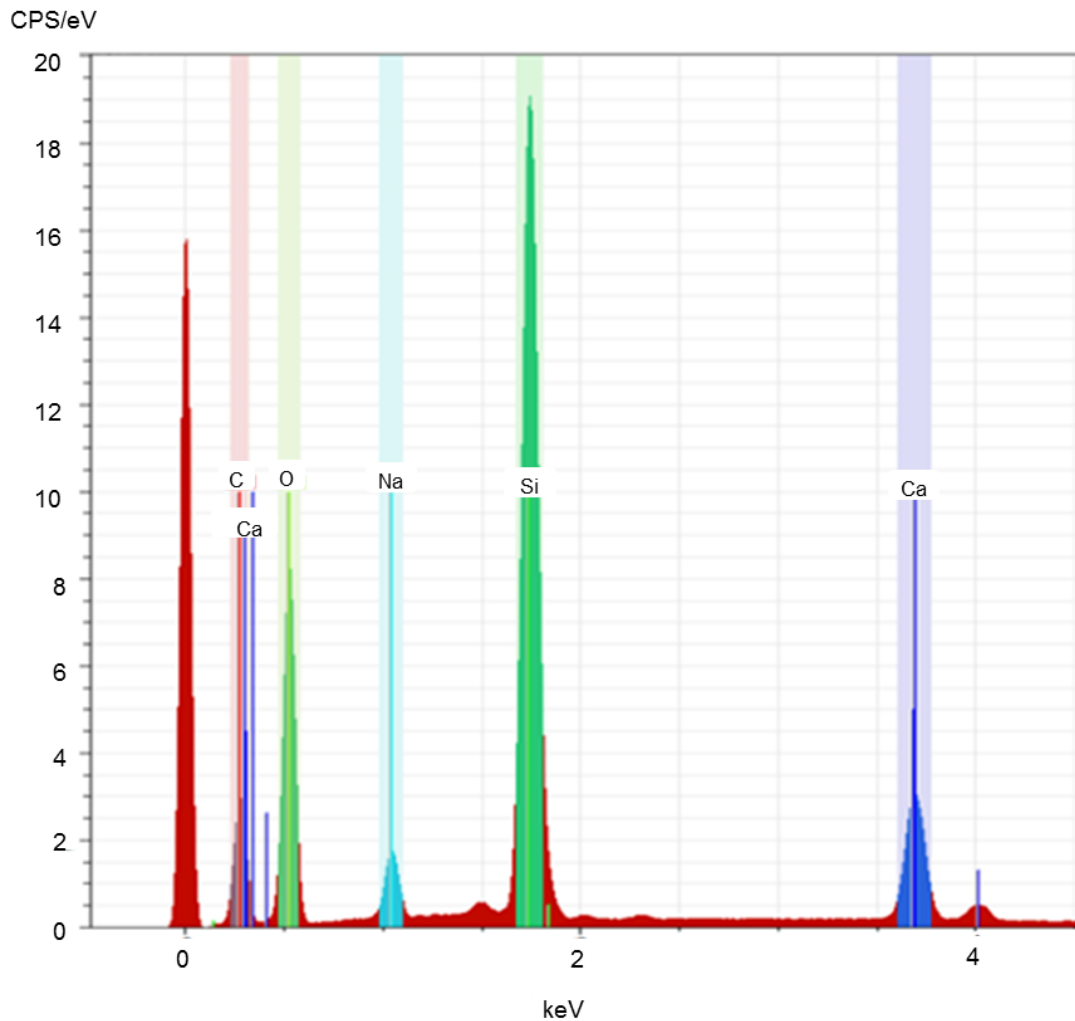
Figure 4-28 energy dispersive X-ray spectroscopy for a filament with Hitachi machine
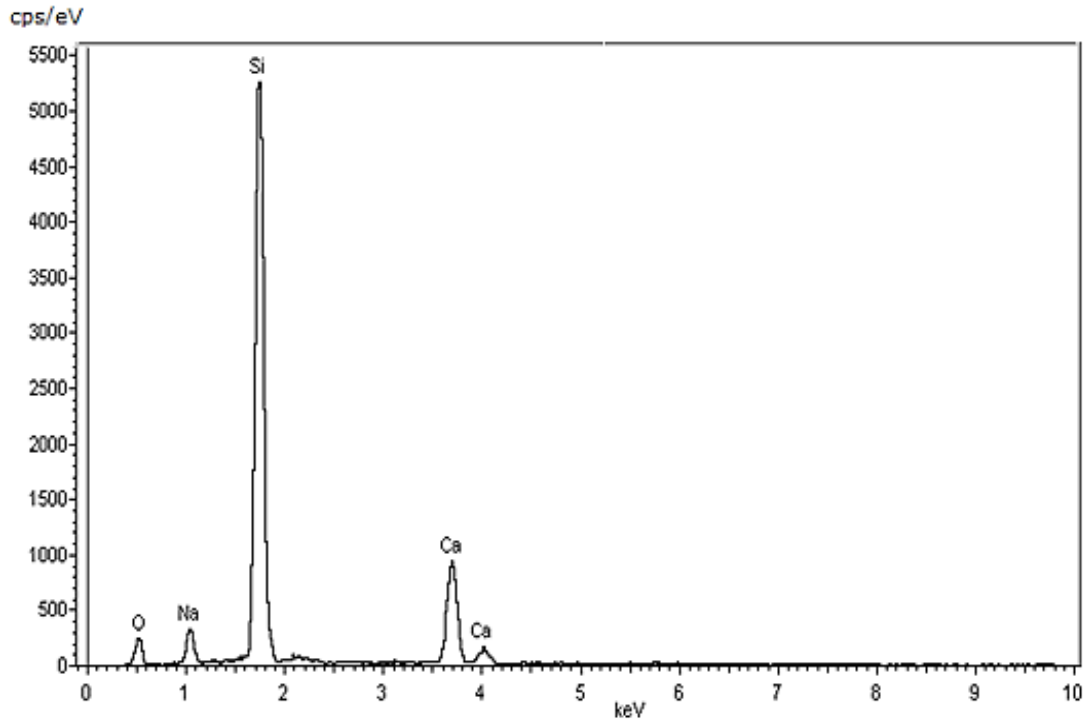
Figure 4-29 energy dispersive X-ray spectroscopy for a filament with Nikon machine

| **(a) holes on the wet layer surface** | **(b) channnels inside the wet layer** |

Figure 4-30 current holes and channels in the wet layer

4.8   Discussion

The ionisation phenomenon in dry material occurs when the electric field is sufficiently high to ionise the air voids between the grains. Then, if the electric field can sustain the ionisation process, the ionisation will expand towards the

ground electrode until the wetted section, generating a lower resistance channel, which allows the current to flow through the dry layer. Examination of the propagation channels in the acquired videos shows that the current propagates in the direction of the electric field lines, which moves from the surface of the active electrode towards the ground plate, in a vertical manner with only a single channel. Due to the dependence of the camera on the emitted light, it was not possible to record every discharge with the high-speed camera. This could be due to the uncontrollable discharge behaviour and the discharge propagation path. The light is possibly produced by the flow of the current through an ionised path i.e. ionised air voids among the glass bubbles. Therefore, when the ionisation phenomenon initiates around the active electrode, and then extends towards the ground, if the ionisation zone reaches the wet part, current will flow. This development process causes the delay time at the onset of the current curve. Hence, the ionisation reaches its maximum at about the current peak, after which the current starts to decrease; and the deionisation process takes place until the current approaches zero. However, in the case of the breakdown, due to the higher electric field, the ionisation process will occur more rapidly. Thus, the impedance of the dry material will dramatically drop to allow the current to flow, as in the previous case. The impedance of the wet material may drop as well due to either thermal or electrical effects, which might cause a decrease in the impedance of the current path, leading to a full breakdown of the whole sample. The discharge under switching voltage has a similar behaviour, with a longer time delay compared with the lightning discharge due to the slower rise time. Compared to how they appear in the videos, the discharge channels have very small

diameters according to the filaments and holes diameters found in the sample. This confusion is possibly due to the reflection of the light among the glass microspheres. Furthermore, it is worth noting that as the rise time of the impulse wave increases, the delay time, which represents the initiation and propagation, increases as well.

4.9 Conclusions

A visual study of soil ionisation phenomenon was implemented. The investigation considered a new glass bubble porous material, which was used for the first time in this kind of experiment. Due to the unknown resistivity of this material, a resistivity measurement test was carried out using a parallel plate configuration under direct current energisation. The resistivity test of the dry glass bubble material revealed a high resistivity value of this new material. Due to this high resistivity, no current was detected until the breakdown occurred under the applied voltages. The other issue was that the breakdown occurred outside the material on the inner wall of the tube. In order to overcome these concerns, the sample was divided into two layers: a dry layer was at the top where the discharge occurs, and a wet layer at the bottom of the tube. This sample configuration significantly improved the results through different conduction scenarios. Standard lightning impulse, longer rise time impulse, and switching impulse voltages were applied to this material to examine the behaviour of the discharge phenomenon using a high-speed camera. The recorded videos were then correlated with the captured voltage and current signals. Different cases were distinguished through these series of experiments, such as the current conduction with no full breakdown of the sample, full breakdown, and long conduction period under the switching

impulse voltage. Soil ionisation and breakdown phenomena were visualised by a high-speed camera for the first time in a porous material under extremely fast impulse voltage. Recording the discharge developments under lightning surges with 5.5 µs per frame was a significant achievement; frames were obtained representing the dynamic changes of the discharge behaviour. In addition, current conduction without a breakdown in the high resistivity dry material was clearly observed and recorded. Under switching voltage, many more frames were recorded, thus, identifying a new observation, which could be caused by the long current conduction. The high-speed camera recorded the current propagating channel. Despite the frame's time being incredibly small and the slow impulse voltages, but the camera could not capture the propagation of the streamer before the current rise. The correlated frames of the recorded video with voltage and current waveforms allow visualisation and monitoring of the discharge phenomenon at various times during the impulse. Using the glass bubble material could be successful in terms of transmitting the discharge light, so that a high-speed camera could capture it, instead of using the conventional sensitive films, which offer a limited view of the discharge. Microscopic examination of the test samples revealed the effect of the discharge current on the material.

Chapter Five

Multi-Point Measurement Technique for the Characterisation of Soil Ionisation Propagation

5.1 Introduction

In light of the recent successful results of the new sample configuration in the previous chapter in preventing the discharge current from flowing outside the material onto the inner tube wall, and due to three discharge scenarios (conduction without full breakdown of the sample, full breakdown of the sample and long conduction period under switching voltage) have been obtained using the new sample arrangement; the next step of the research investigation was the electrical examination of the two-layer sample. Therefore, this chapter

investigates the electrical properties of this new sample construction and explores the effect of the ionisation phenomenon on the dry layer, especially in the case of no full breakdown so that the recorded videos obtained by the high-speed camera can be complemented by a wider understanding of the discharge behaviour in this type of sample.

This study was carried out through series of tests and analyses of the discharge waveforms. More voltage measurements were performed using voltage probes installed in the sample to measure the dynamic propagation in the ionisation zone during the discharge. The aim was that these transducers would also help explain the delay time before the current rise, and the propagation velocity of the streamer, and hence could provide some insight into defining the limits for recording the discharge using the high-speed camera. This sample configuration was also represented by an equivalent circuit to investigate the different stages of the discharge behaviour before and after the ionisation under lightning voltage.

5.2   Wet Section Resistance Measurement Test

In order to begin the analysis of the discharge mechanism in this sample configuration, a resistance measurement test of the wetted material section was performed to obtain the value of the resistance and to give an indication of what kind of behaviour the wet material might display during the impulse voltage. The wetted material was prepared and placed in the tube, as shown in Figure 4-14 (b). Then, the high voltage electrode was inserted in the material. A standard lightning impulse voltage was applied in increasing steps, and the resulting impulse current was measured for each step. Figure 5-1

shows an example of the voltage and current traces, where the current had a faster rise time to its peak than had the voltage, which may indicate the capacitive effect of the material. However, both the voltage and the current signals have a similar decay rate, indicating the prevailing resistive conduction. Thus, it can be seen that the linear resistive behaviour dominates the discharge in the material. At voltage magnitudes higher than 40 kV, the resistance of the material began to decrease with the increase of the voltage, which could indicate a nonlinear resistance. This change to the nonlinearity may be due to the thermal effect caused by the ($I^2 \times R$), which led to the increase in the ionic conduction and then a reduction in the resistivity. On the other hand, the nonlinearity could also be due to the ionisation phenomenon in the small air voids trapped inside the material, because this medium is porous. This phenomenon could occur easily if suitable conditions were available.
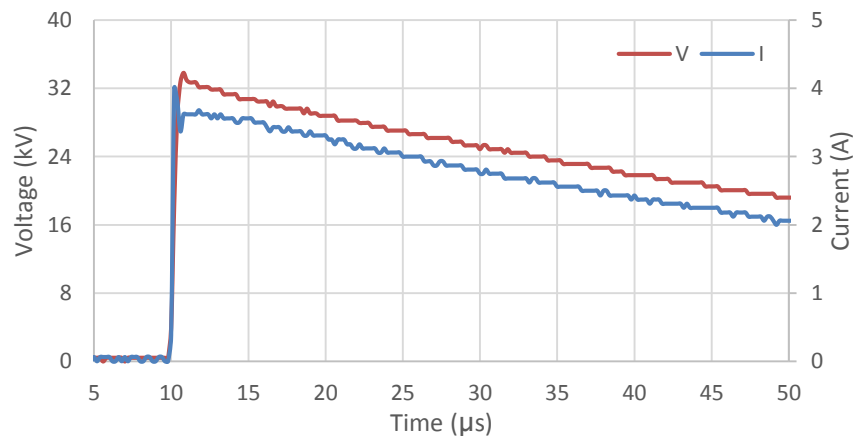

Figure 5-1 discharge traces in wet section only

As can be seen in the Figure 5-2, the resistance values were at around 10 kΩ, and then the resistance started to decrease until the breakdown of the sample occurred. These resistance values were calculated by dividing the voltage by

the current at the instant of current peak, where (di/dt) is zero, so that the inductive effect was eliminated. The test results show the obtained resistance value of the wet layer was about 10.3 kΩ; this value depends mainly on the water content and the volume of the wet section. The behaviour of the wetted glass bubble material could be either a linear resistance or a nonlinear resistance. This finding was expected, because the glass bubble material is a porous material similar to soils found in earthing systems and so could support the occurrence of the nonlinear behaviour in the soil. Overall, the nonlinearity of the wetted section before the breakdown is very limited, so the dry layer presents the main nonlinearity of the discharge in the dry and wet layers sample.
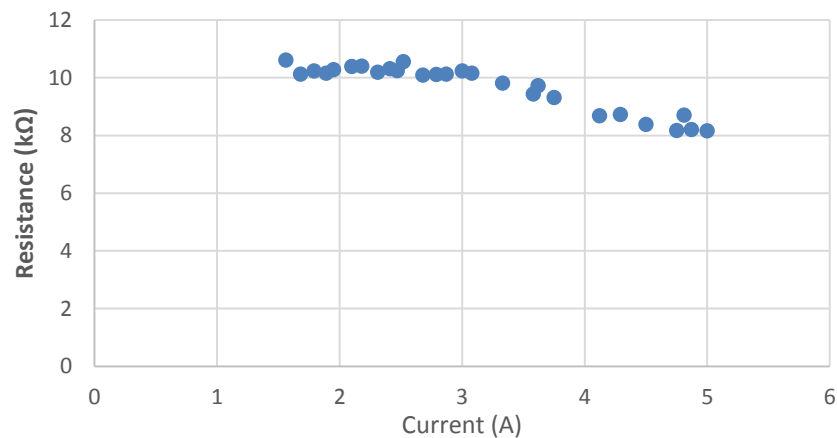

Figure 5-2 resistance versus the current (wet section only) ($V_{I\ peak}$ /I_{peak})

5.3 Wet Layer Voltage Measurement

For the purpose of understanding the current flow in the dry layer prior to breakdown of the sample material, a voltage transducer was installed in the tube at the interface between the upper dry section and the lower wetted

section to measure the voltage across the wet material section, as shown in Figure 5-3. Obtaining this voltage makes it possible to calculate the voltage across the dry layer, and so helps explain the delay time before the current rise. The procedures and sample configuration were those used previously, except the dry layer thickness was 10 cm and no high-speed camera was involved in this test. Lightning impulse voltage was applied to the sample in steps until a current conduction was detected. With regard to the analyses of the waveforms of the applied voltage (V_t), the voltage of the wet part (V_w) and the current (I), (V_w) rose at the instant of the current rise, which means the current flows from the active electrode through the dry material until reaching the wet layer. This confirms that the ionisation process took the time to initiate and propagate from the active electrode until the wet part.
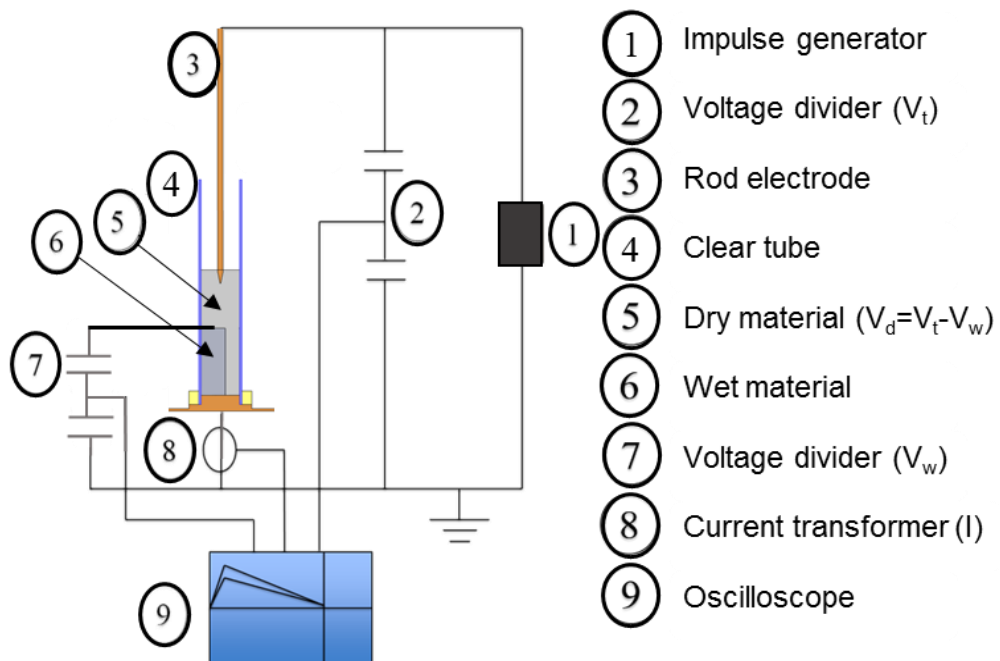

Figure 5-3 test configuration for wet layer voltage measurement

In addition, when the voltage across the dry material ($V_d = V_t - V_w$) was calculated and plotted with the rest of the parameters, it could be seen that the

dry material breaks down once the ionisation reaches the wet part and the current rises, as summarized in Figure 5-4. Therefore, the ionisation initiates around the high voltage electrode where the electric field is at its highest magnitude, and then expands through the material. This expansion creates a low resistivity path for the current to flow and break the dry section. As soon as the dry material section breaks down, the majority of the applied voltage will appear across the wet part, which explains why the applied voltage did not exhibit any sign of breakdown during the discharge.
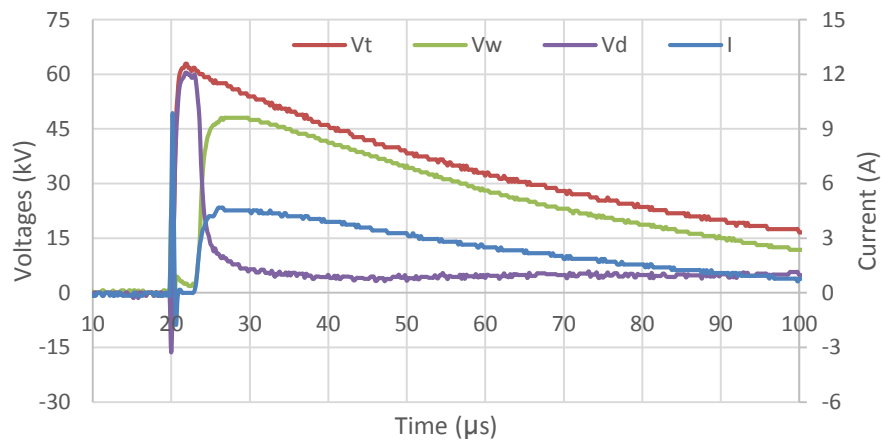
Figure 5-4 waveforms of the measured parameters with no full breakdown

The applied voltage level influences a number of parameters of the discharge behaviour in this sample configuration, which are the voltage across the dry layer (V_d), the impulse impedance of the dry layer ($Z_d = V_d/I$), the voltage across the wet section (V_w), the current (I), and the current delay time. 68 kV, 65 kV and 64 kV applied voltages were considered to analyse the above parameters. When the applied voltage increases, this results in a higher electric field that is able to initiate the ionisation more quickly, i.e., there is a shorter delay time in current increase.

This leads to an increase in the voltage across the dry layer before the ionisation, and a breakdown after the ionisation takes place (see Figure 5-5). There is also a decrease in the impulse impedance of the dry section. This impedance was affected by the ionisation phenomenon, which sometimes in the literature was assumed to be zero, [18, 22, 84] but in this experiment, it retained a certain residual resistivity after the significant drop as in Figure 5-6. In addition, it seems that as the applied voltage increased, the impulse impedance of the dry layer decreased, this is similar to what occurs with the wet soil. For V_w, as the dry layer broke down more rapidly with a higher applied voltage, a higher voltage was applied to the wet section, which led eventually to an increase in the current (I) (see Figure 5-7, and Figure 5-8).

Furthermore, the impulse impedance of the wet section (V_w/I) was found to decrease slightly with the increase of the voltage across the wet section, which was probably due to either electrical or thermal processes in the wet material. This result could confirm that the main nonlinearity of the sample is caused by the dry layer. See Figure 5-9.
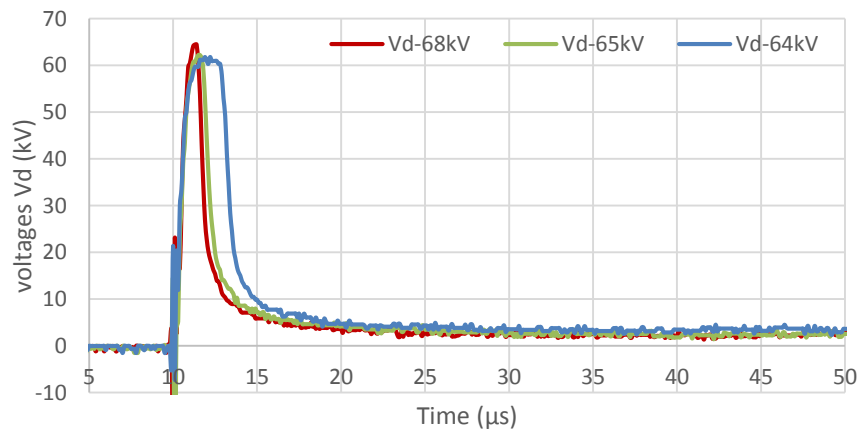
Figure 5-5 dry layer voltage (V_d) under different applied voltages
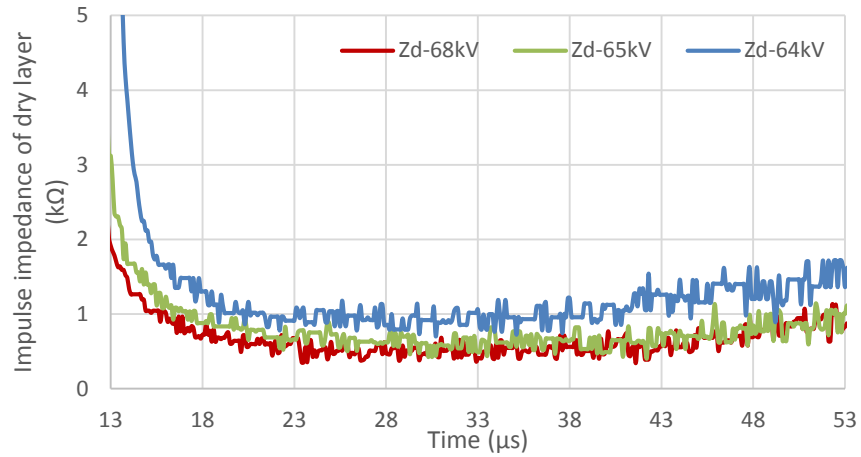
Figure 5-6 dry layer impulse impedance (Z_d) under different applied voltages
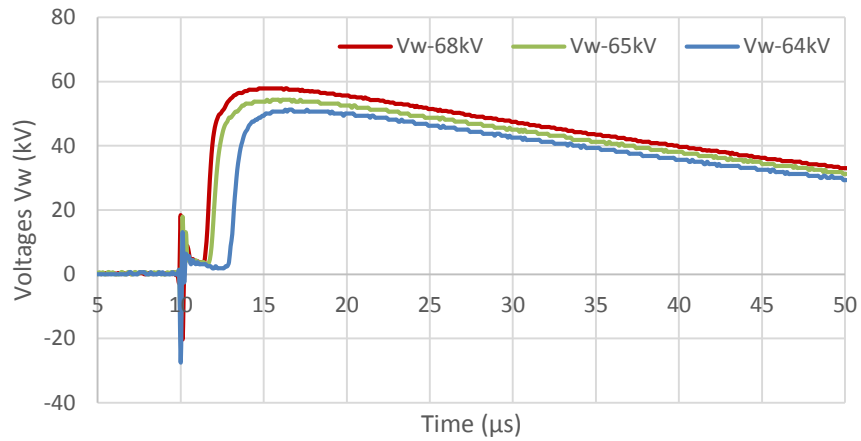
Figure 5-7 wet section voltage (V_w) under different applied voltages
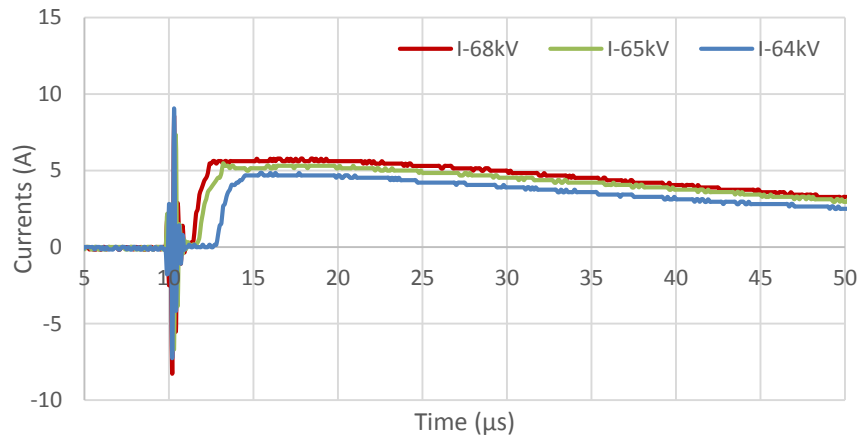
Figure 5-8 the current (I) under different applied voltages
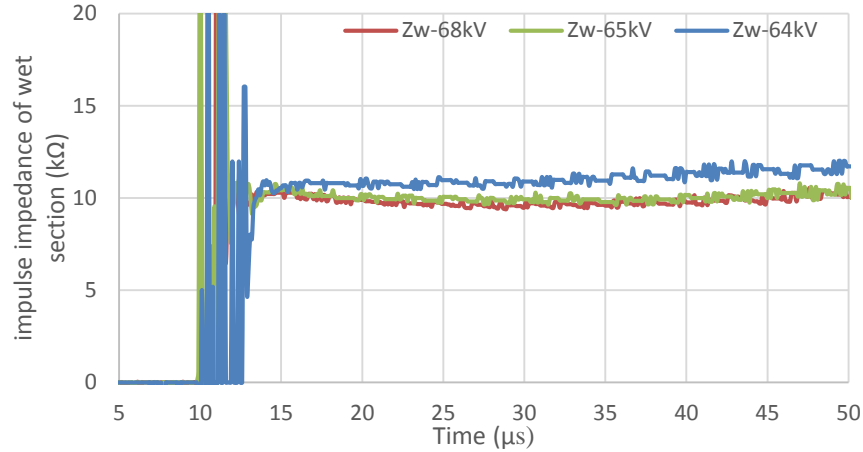
Figure 5-9 wet layer impulse impedance (Z_w) under different applied voltages

When the magnitude of the applied voltage was further increased, a full collapse of the voltage occurred at the instant of the breakdown, which was due to the breakdown of the two layers of the sample (dry and wet sections). The dry layer collapsed first due to the drop in impedance caused by the ionisation, as discussed earlier, and then the wet layer broke down probably due to electrical failure under a higher (V_w), so this voltage will be applied to the wet section, as can be seen in Figure 5-10. The voltage across the dry layer further dropped after the sample breakdown occurred, which was possibly due to the additional decrease in the impedance of the dry layer.
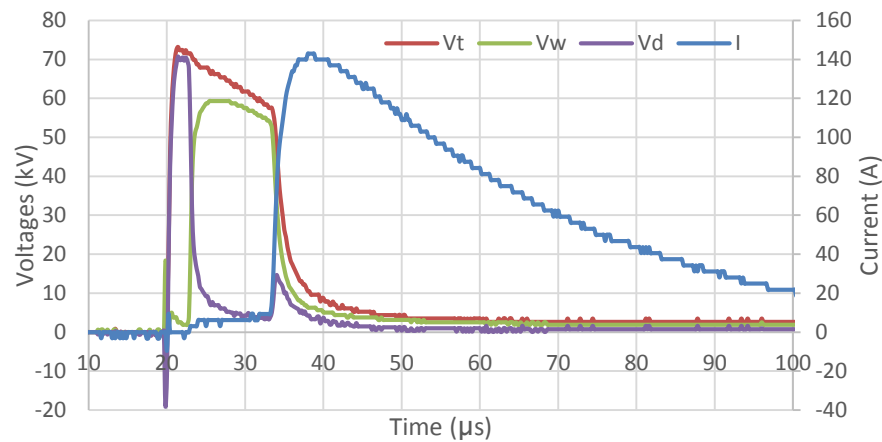
Figure 5-10 waveforms of the measured parameters with full breakdown

5.4 The Effect of the Thickness of the Dry Layer

Choosing the right thickness of the upper dry layer is critical for the discharge development and investigation of its properties. A thin layer is not beneficial, as it will break down very quickly under a low applied voltage, and thus making it difficult to observe the propagation of the streamer from the electrode. On the other hand, the very thick layer is not useful either. It needs a higher applied voltage to initiate the ionisation and maintain the propagation of the streamer for a longer distance through the entire dry layer, which then applies a higher voltage to the wet layer after the breakdown of the dry material, leading eventually to the breakdown of the wet section and the full sample.

The thicker the dry layer is, the higher the required applied voltage will be for the current to flow. In order to determine the appropriate layer thickness for the discharge without a full sample breakdown and for the ionisation propagation study, the thickness should be increased until the applied voltage is sufficiently high to cause the failure of the upper layer only, preventing the chance of breaking the wet layer. Therefore, based on this aim, the three dry layer thickness ranges were found. The first range is when the thickness is less than 11 cm, and discharge without a breakdown is easily obtained. The second range is 11-13 cm; this range is critical, where the applied voltage could cause either a full breakdown or a normal discharge.

The last range is more than 13 cm; the applied voltage will be even higher, which causes the full breakdown of the sample. The time delay is also influenced by the thickness of the dry layer; thus, the same sample arrangement was tested except for the thickness of the dry layer, which was 6 cm and 9 cm in two separate tests. Using the same applied voltage with these

two thicknesses, the delay time was around 6.1 µs for the thicker layer (9 cm) (see Figure 5-11), while the delay time was almost 1 µs with 6 cm thickness, which is obviously shorter than with 9 cm thickness (see in Figure 5-12).
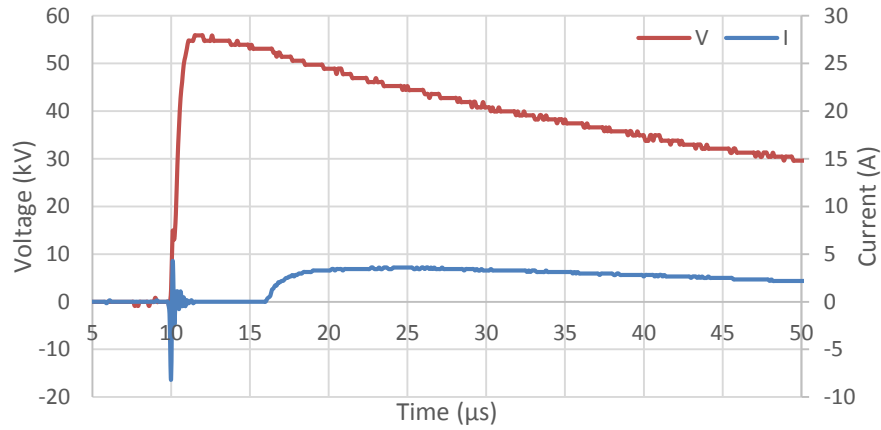

Figure 5-11 discharge in 9 cm dry layer under 54 kV
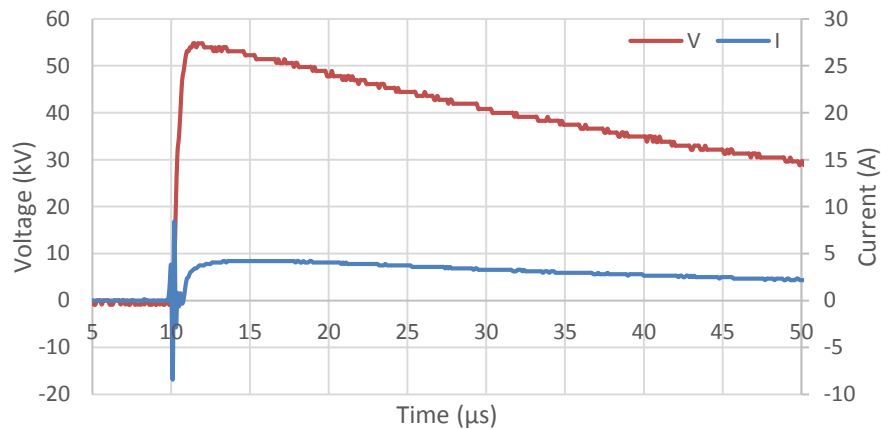
Figure 5-12 discharge in 6 cm dry layer under 54 kV

5.5 Ionisation Propagation in Dry Layer

The aim of this test was to investigate how the ionisation phenomenon expands and propagates through the dry glass bubbles to cause the breakdown of the material. To achieve this objective, a second voltage probe

was installed in the tube, as depicted in Figure 5-13, and Figure 5-14. This new probe was inserted at mid-point between the high voltage electrode and the transducer on top of the wet section. Hence, this transducer could measure the development of the ionisation activity through the dry layer, and could illustrate how quickly the ionisation zone expands away from the HV electrode. At a relatively low applied voltage 60 kV, no current was detected and neither voltage probes (V_1 and V_2) measured any voltage except the capacitive voltage at the beginning of the discharge. When the applied voltage was increased 62 kV, only transducer (V_1) detected a high voltage value, which indicates that the streamer propagated only up to this transducer in the middle of the dry layer, as shown in Figure 5-15.

The other probe (V_2) did not measure any voltage increase during the discharge. The current transformer detected two capacitive current peaks; the first peak is attributed to the voltage being applied to the top of the dry layer through the active electrode, and the second one is thought to be due to the capacitive effect produced when the first probe (V_1) was energized by the propagation of the streamer. Moreover, the measured voltage through the first transducer had a fast rise time, which is caused by the breakdown of the material between the active electrode and the first probe. After 23 μs, the measured (V_1) became bigger than the applied voltage (V_t), which was attributed to the accumulation of the charges around this transducer, which led to the build-up of a higher potential than the decaying applied voltage.

This situation is similar to what was measured in Chapter 4 in the case of only dry glass bubble material test under lightning surges, as exhibited in

Figure 4-9. However, in that case, the accumulated charges provided the applied voltage with a longer rise time until the breakdown occurred.
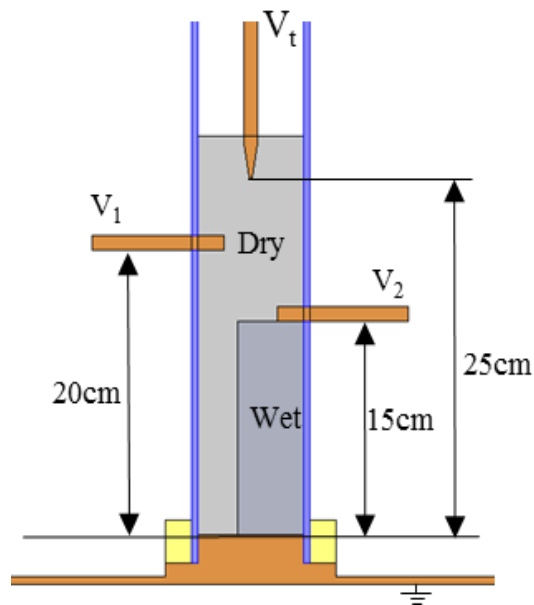
Figure 5-13 voltage probes arrangement for ionisation propagation in dry layer
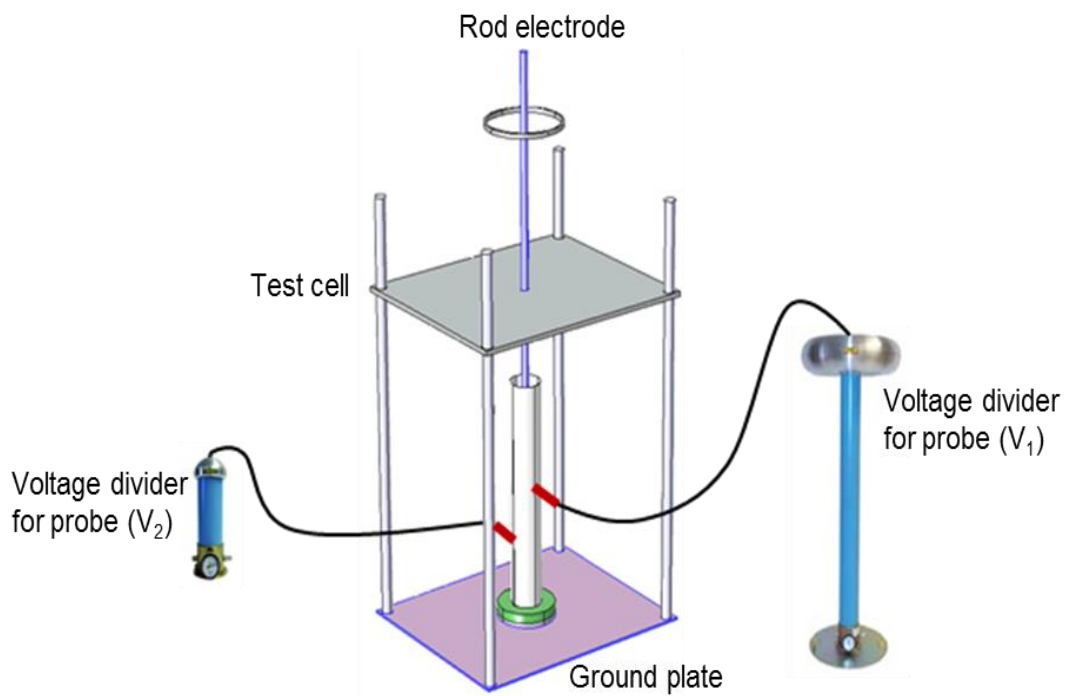
Figure 5-14 test cell and voltage probes arrangement
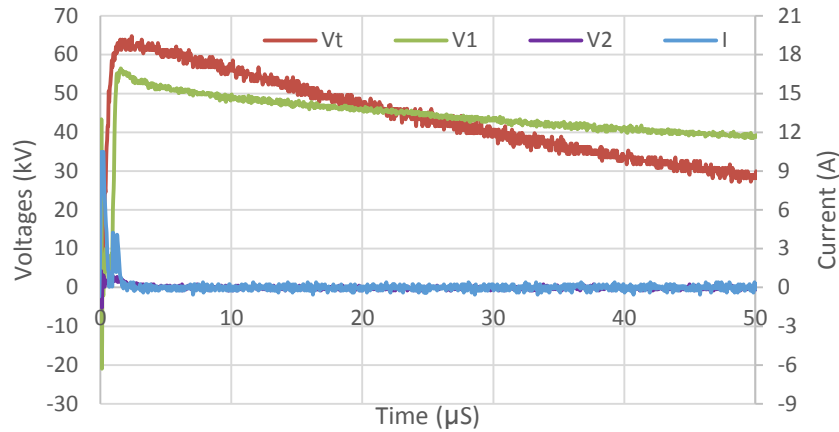
Figure 5-15 discharge traces with limited streamer propagation in dry layer

Furthermore, when the applied voltage was even higher 67 kV, the ionisation phenomenon propagated up to the wet layer, where the two transducers (V_1 and V_2) detected different potentials according to their locations in the dry layer, as shown in Figure 5-16. From Figure 5-15 and Figure 5-16, it can be concluded that in order to drive the streamer a greater distance, the applied voltage should be high enough to sustain the propagation of the ionisation zone and the streamer from around the active electrode, where the electric field is at its maximum value, until the wet layer. Figure 5-16 shows also that the ionisation phenomenon has been traced during the propagation from the active electrode up to the wet layer through the entire dry layer.

In addition, there were different delay times between the measured voltages (t_1, t_2), which indicates that the streamer may have a varying velocity at each stage of the propagation. These different speeds are thought to be caused by various factors, such as the reduction rate in the resistivity, as reported in [14] or perhaps are due to strength of the electric field at the leading edge of the ionisation discharge, the development process of the streamer, the streamer path length, and the initiation process of the streamer. It is worth noting also

119

that the time (t_1) represents not only the propagation time of the discharge up to (V_1) probe location, but also includes the time taken for the soil ionisation initiation. The initiation times of the soil ionisation and the streamer cannot be identified using the voltage transducers. Furthermore, the exact location where the ionisation process starts is not known, it may be at the HV electrode, but it can also start away from the electrode due to the field enhancement in the voids inside the material. As the streamer proceeds down toward the ground through the material, the dry layer breaks down immediately. Hence, as the streamer arrives at the first probe, the material above it has already collapsed, and then, as the streamer goes further down, it breaks the second half of the dry layer up to the wet section.

Thus, using the voltage transducers, the two breakdown steps could be seen based on the calculations of the voltages cross the two halves of the dry layer ($V_{\_up} = V_t - V_1$) and ($V_{\_down} = V_1 - V_2$), see Figure 5-17. As indicated earlier, this discharge initiation is thought to be driven mainly by the electrical process rather than the thermal process, which supports the results presented in [13, 15, 36, 39].
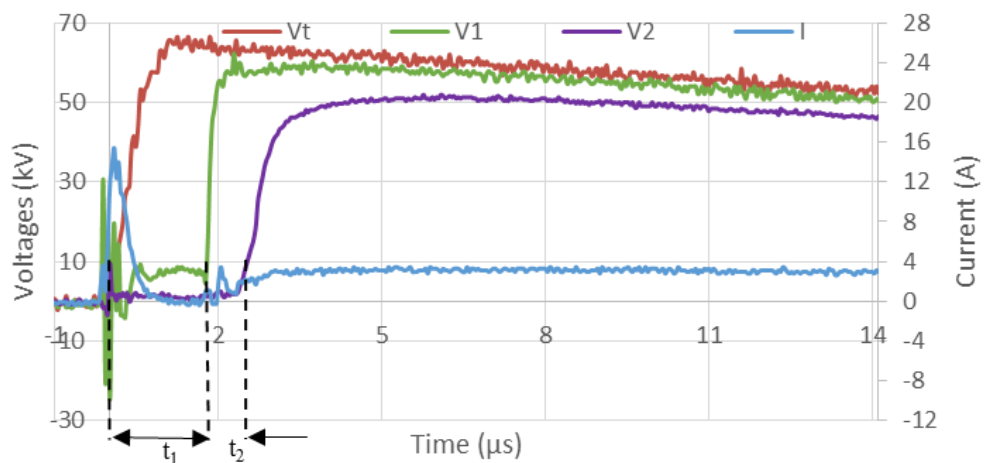
Figure 5-16 discharge with full streamer propagation (67 kV)
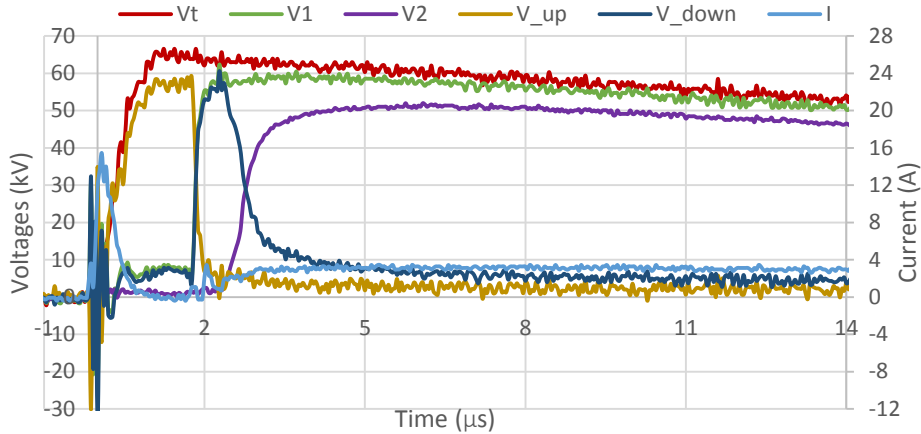
Figure 5-17 breakdown steps of the two dry layer halves (67 kV)

Moreover, the total delay time (t_1+t_2) of the current tends to decrease as the applied voltage magnitude increases and the thickness of the dry material decreases, possibly corresponding to the ionisation having a faster initiation and propagation velocity, as was found in [43]. Using the measured data for (t_2) in Figure 5-16, the estimated velocity of the streamer propagation was 6.25 cm/µs, which is an extremely fast speed. The differences between the two delay times (t_1, t_2) in Figure 5-16, Figure 5-18, and Figure 5-19 may indicate the variable velocities of the soil ionisation initiation around the electrode. Hence, it seems that the initiation depends not only on the applied voltage, but that there may be other factors that influence the speed of the initiation, such as the arrangement of the microspheres, where the air cavities in the material are not uniform, which then affects the field enhancement process during voltage application. In Figure 5-19, the delay time (t_1) is very short, which highlights the faster ionisation initiation and propagation up to the probe (V_1), but the time (t_2) is longer. This might indicate that the speed of the initiation tends not to affect the velocity of the streamer propagation. Therefore, different initiation and propagation stages can be identified, starting with the initiation

121

of the soil ionisation, and then the initiation and propagation of the streamer through the material, as was found in [14, 16], where statistical and formative delay times were recognised during the discharge. The former is thought to represent the initiation while the latter represents the propagation of the soil ionisation through the entire sample, and both delay times are dependent on the applied voltage [16]. See Table 5-1 for the comparison between the delay times (t_1, t_2) and propagation velocities (v_1, v_2). Consequently, having different initiation and propagation velocities could also be an additional factor that explains why the high-speed camera did not capture the propagation of the streamer before the current rise.
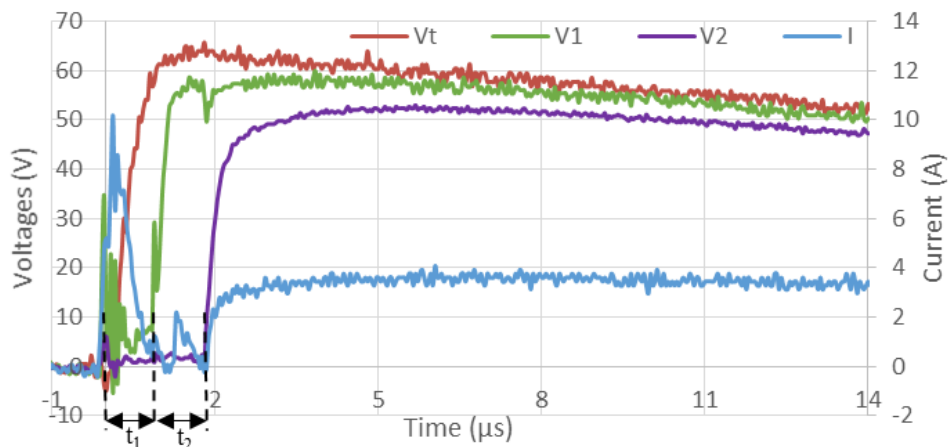
Figure 5-18 discharge with full streamer propagation (66 kV)
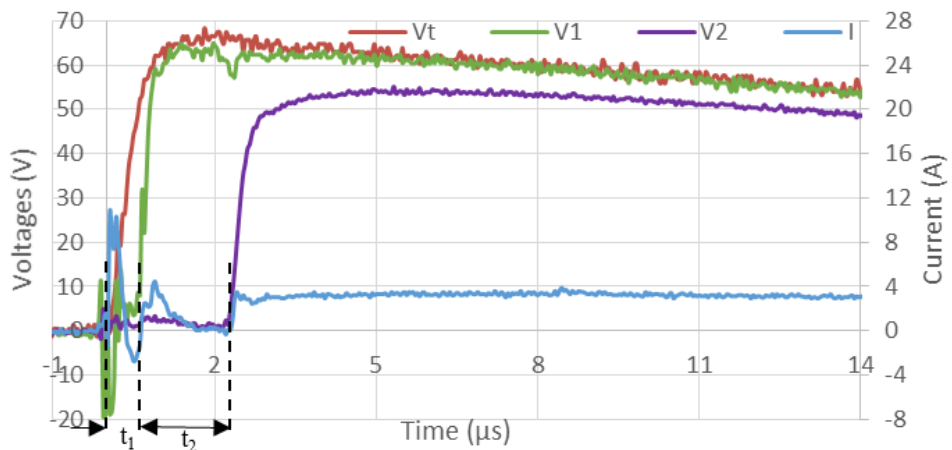
Figure 5-19 discharge with full streamer propagation (68 kV)

Table 5.1 delay times and the calculated velocities of the propagation of the discharges in Figure 5-16, Figure 5-18 and Figure 5-19.

Applied voltage (kV)	t_1 (µs)	t_2 (µs)	v_1 (cm/µs)	v_2 (cm/µs)
66	0.8	1.09	6.25	4.59
67	1.6	0.8	3.125	6.25
68	0.65	1.68	7.7	2.97

5.6   Proposed Equivalent Circuit of the Sample

When analysing the voltage and current waveforms of the discharge in the case of no breakdown, without the two voltage probes in the middle of the sample. Some initial oscillations were observed at the beginning of the current trace, indicating that the behaviour is capacitive, and then no current was detected until the breakdown of the dry part took place due to propagation of the ionisation zone. The high impedance fell significantly to change the current to resistive conduction until the current approached zero and then the impedance recovered its original value due to the deionisation process.

From the previous sections, it is known that the wet layer may have a nonlinear behaviour, but the stronger nonlinearity was found to be in the dry material. The ionisation phenomenon and then the breakdown of this layer force the material to have a much lower resistance, even lower than the wet layer. However, while the value of the dry layer resistance differs from discharge to discharge, it tends to decrease with the increase of the applied voltage. Therefore, it led to the equivalent circuit of the discharge in this sample configuration that contains a capacitor to simulate the capacitive effect at the

onset of the current trace. This capacitor is connected in parallel with a non-linear resistor to simulate the resistance of both the dry and wet parts during the ionisation, a switch to simulate the initiation of the current and an inductor to control the current rise time. The circuit was built and simulated in EMTP software.

Based on the equivalent circuit in [20], that circuit is similar to the circuit in this study except the proposed circuit did not have a pre-ionisation resistance parallel with the capacitor. The tested sample in [20] was only wetted soil. Thus, there was a conduction current at the beginning of the discharge, which was represented by a pre- ionisation resistance (R_1) parallel with a capacitor. However, in this study, due to the high resistivity of the upper dry layer, no current was detected after the initial oscillations. Subsequently, the pre-ionisation resistance was very high that it could be represented with an open circuit, i.e., a capacitor only, as in Figure 5-20. The nonlinear resistor of the sample can be estimated using the maximum current value and the corresponding voltage value for some discharges before the breakdown occurred as in Equation (5-1); the resistance values are plotted in Figure 5-21. An empirical equation can also be derived for these resistances as a function of the current, as in Equation (5-2).

$$R=\frac{V_{Ipeak}}{I\ peak} \tag{5-1}$$

$$R=19482.i^{-0.233} \tag{5-2}$$
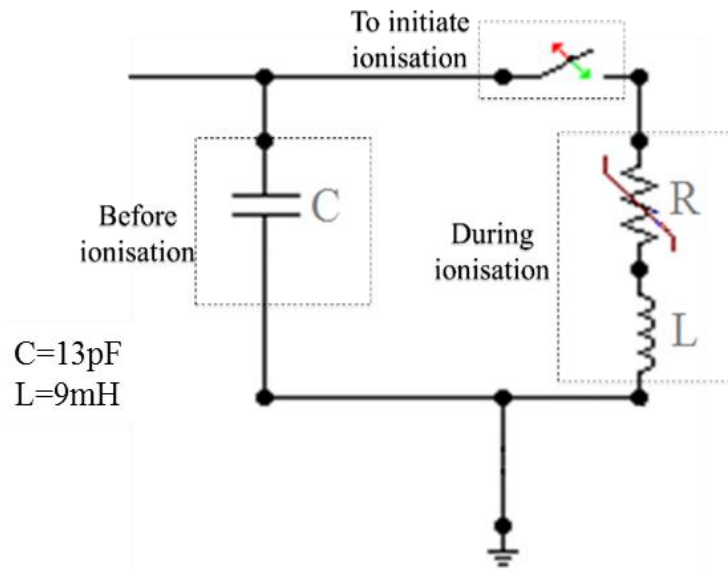
Figure 5-20 equivalent circuit in EMTP
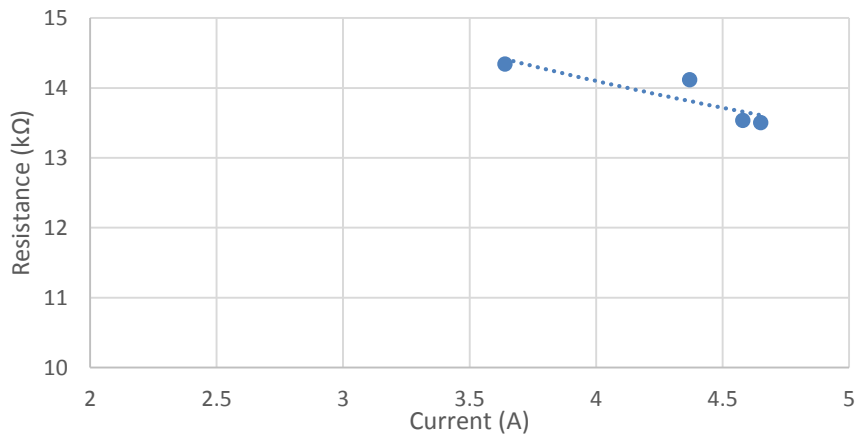
Figure 5-21 whole sample resistance values under lightning voltages

The resistance values of the sample tend to decrease with the increase in the applied voltage, which may be because of the drop in the dry layer resistivity due to the ionisation effect. Therefore, the nonlinear resistor in the equivalent circuit will be the total resistance of the current channel in both dry and wet layers. The total delay time (for the current rise) is different from one waveform to another and will be governed by a switch to initiate the soil ionisation.

Figure 5-22 presents the actual and simulated voltages and currents for a discharge. As can be seen from this figure, the proposed circuit model is able to generate similar voltage and current waveforms, offering a satisfactory agreement between the actual and simulated signals. Hence, this simulated circuit confirms that the discharge behaviour of this sample under lightning voltage can be represented with a capacitive behaviour before the ionisation and a resistive behaviour when the ionisation effect takes place in the dry layer.
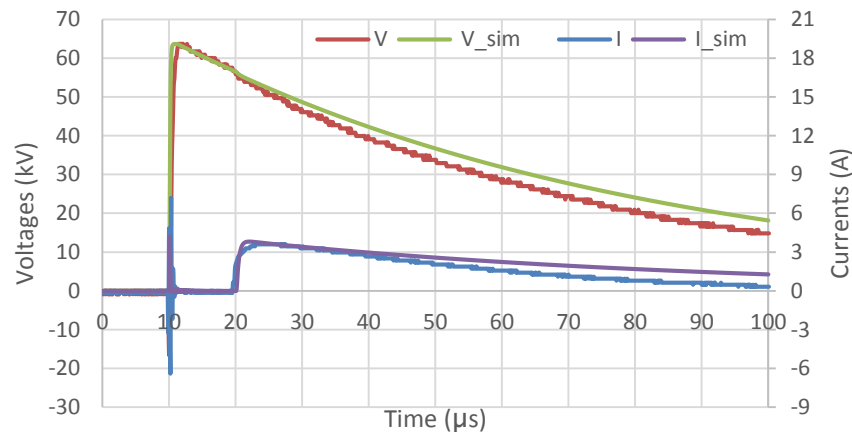
Figure 5-22 actual and simulated voltages and currents of the discharge

5.7 Comparison between Lightning and Switching Voltages Discharges

The time characteristics of the impulse voltage may have an impact on the discharge behaviour in the porous media, as the duration that the material is exposed to the electric field is another significant factor that influences the ionisation initiation time, the current delay time and the critical voltage level for the ionisation. Due to the longer rise time of the switching voltage, the material

is exposed to the electric field for a longer period, which may result in the initiation of the ionisation phenomenon and then the conduction current at lower voltage level with a longer delay time than the corresponding lightning surge. This is very clear from the switching voltage discharge. Moreover, under switching impulse voltage, once the dry layer breaks down and the current starts to flow, the applied voltage drops to a lower value. This led to the difficulty of obtaining a breakdown discharge in the case of the two-layer sample configuration under a switching voltage.

Therefore, when the switching voltage magnitude is low (less than 40kV), there will not be any considerable ionisation and current flow, but as soon as the applied voltage is sufficiently high (46kV), the ionisation is initiated and propagated throughout the dry layer, causing the collapse of the dry layer. For a higher voltage 50kV, the same mechanism will apply, except the delay time will be shorter, because the voltage reaches the critical level more quickly; as consequence the current increases and the applied voltage drops even before the voltage peak at 200 µs.

In the case of lightning impulse discharge, a higher voltage level 50kV is required to initiate the ionisation phenomenon, which is probably due to the fast rise time of the impulse to the peak value; and this leads to initiate the ionisation in a shorter time with a shorter current time delay. The deionisation process takes a very long time under the switching impulse voltage due to the longer tail time of the switching wave, while under lightning voltage it is much shorter. Table 5.2 summarizes the main differences between the fast lightning impulse and slow switching impulse in the case of the two-layer glass bubble sample configuration.

Table 5.2 Comparison between lightning and switching voltages discharges

Lighting discharge	Switching discharge
Higher voltage (50kV) to initiate the ionisation	Lower voltage (46kV) to initiate the ionisation
Delay time is short (less than 15 µs)	Delay time is long (greater than 40 µs)
Deionisation process is short (less than 150 µs)	Deionisation process is long (more than 1500 µs)

Furthermore, the initiation and propagation times under lightning surges are relatively short; however, under the switching voltage, the initiation time is predicted to be much longer than the propagation time, as the voltage takes a longer time to reach the critical level. Therefore, the effects of the impulse shape on the propagation velocity of the streamer need to be investigated in detail.

5.8 Discussion

Glass bubble material is a porous dielectric material that has similar behaviour to sandy soil. The wet material may have both linear and nonlinear behaviours based on the applied electric field and the amount of water, but the dry glass bubble material has only nonlinear behaviour under soil ionisation. In order to initiate the ionisation phenomenon and the streamer in the dry layer and then sustain the propagation of the streamer, the applied voltage on the active electrode must be adequately high. This propagation of the ionisation zone creates a low resistivity channel between the high voltage electrode and the wet section, which eventually leads to the breakdown of the dry layer.

There are four cases of discharge in the new glass bubble sample configuration. (a)The first one is when the applied voltage is low 55 kV; there

is either no ionisation or only a weak local ionisation around the electrode, so the generated electric field is insufficient to create a strong ionisation and a low resistivity path, i.e. there will not be any current flowing through the dry layer. (b) The second situation is when the applied voltage 62 kV is only able to drive the streamer to a limited distance from the active electrode, and it is then extinguished, i.e. the produced electric field is insufficient to sustain the ionisation propagation. This is because the applied voltage reduces very quickly, and thus there will not be a flow of current in this case either. (c) The third case is when the applied voltage has a higher value (66 kV), so that it can initiate the soil ionisation and sustain the propagation of the streamer up to the end of the dry layer; here, there will be a flow of current without the applied voltage collapse. Thus, the low resistivity path is created by the ionisation effect, which means that the high resistivity dry layer collapses, allowing the current to flow in this path. (d) The final discharge scenario is when the applied voltage is increased further 72 kV, which will be able to break down both the dry and wet layers.

The voltage applied to the wet layer after the dry layer failure is even higher, which then leads to the breakdown of the wet section as well. After that, the applied voltage will collapse at the instant the full sample breakdown, and the current will jump to a higher magnitude. The delay times due to the initiation and propagation of the ionisation phenomenon do not depend only on the applied electric field, but are also based on the mechanism of the initiation process. Different initiation and propagation times were found during the tests under similar applied voltages; this means also that the streamer could have variable velocities during the propagation as it proceeds down through the dry

glass microspheres. The proposed circuit of this sample was based on the behaviour of the sample under lightning voltage. The nonlinear resistance of the sample included both layers during the discharge, as both layers could have nonlinear behaviour, but the dry layer causes the main nonlinearity.

5.9   Conclusion

The proposed two-layer configuration of dry and wet layers in the sample was studied and analysed in detail. This new sample arrangement was very useful in studying the ionisation phenomenon, the streamer propagation, and the breakdown phenomenon. Multi-points voltage measurement was found an effective method to study propagation of the soil ionisation. Moreover, it was found that the ionisation phenomenon is initiated around the active electrode where the maximum electric field is expected and then propagates down towards the ground. Several stages of the discharge can be identified from this study; the first stage is the initiation of the soil ionisation, and then the initiation of the streamer in the ionised zone.

These two steps are represented by the time lag (t_1), and it is very difficult to distinguish between them, because as soon as the soil ionisation is initiated, the streamer will probably flow in the ionised area. If the electric field at the tip of the discharge was able to support the propagation of the streamer, then the third stage would begin, which is characterised with a part of the delay time (t_1) and all the delay time (t_2). Therefore, the breakdown in the dry layer occurred due to the propagation of the streamer through the whole layer, which also was found in [15, 16]. However, the wet material section helps prevent the full breakdown of the voltage in the case of no full breakdown of the

sample. This investigation suggests that initiation of the ionisation process and streamers may be attributed to field enhancement in the air voids between the glass bubble microspheres within the bulk material, as found in [13, 36], where the initiation time was very short and the dry layer contained a water percentage of zero, which could help with current flow to generate the heat ($I^2 \times R$). In addition, the dependence of the streamer propagation distance on the applied voltage value, as was seen in the case of half and complete streamer propagation in the dry layer, supports the theory of the electrical process.

Furthermore, the propagation velocity of the streamer varies once it proceeds through the microspheres, which could be due to either the streamer path, the electric field variations, or even the distribution of the material particles that may affect the field enhancement process during the propagation. Additionally, in this work, an estimation of the velocity of ionisation propagation was calculated from the measurement of the voltage at various points along the length of the dry layer. This velocity was found to be dependent mostly on the applied voltage.

An equivalent circuit for this test sample was proposed and simulated with EMTP software; the components of the circuit were derived based on the discharge behaviour under lightning impulse. The sample behaviour was mainly capacitive before soil ionisation starts, and then changed to a resistive behaviour after the full propagation of the ionisation in the dry layer. The simulation outcomes demonstrated a satisfactory agreement with the laboratory results, which indicated that the proposed circuit closely represented the performance of the sample under lightning impulse voltage.

Lastly, the proposed circuit proved that Nor's circuit model is a flexible model, which can be modified and used with different types of samples as was reported in [68].

Chapter Six

Soil Ionisation in Two-Layer Sand Samples

6.1 Introduction

There is a need to address the effect of multilayer soils and their resistivities on the earth electrode transient behaviour. The majority of the published studies investigating the soil ionisation phenomenon have assumed a uniform one-layer soil. However, investigating soil ionisation initiation and propagation in a multi-layered soil sample has not been sufficiently addressed. In real earthing systems, soils down to large depths consist of several layers with different moisture contents. ANSI/IEEE 80-1986 standard [85] suggests that representing the soil with two layers is considered reasonable for practical

applications. Therefore, this investigation considered laboratory tests to examine the key factors influencing the initiation and propagation of the ionisation phenomenon in the case of two-layer soil instead of the conventional one-layer soil. The sand samples consisted of two layers with different water contents. A rod-plane electrode configuration was utilized under standard lightning surges energization. The soil test sample was placed inside the vertical plastic tube between the two electrodes to facilitate the multi-point voltage measurement. In order to quantify the propagation of the ionisation inside the layers of the sample, potential transducers of the multipoint voltage measurement technique were installed along the tube at specific positions, such as the interface between the two layers and in the middle of the layers. Therefore, the voltage changes in the ionisation zone could be monitored in real time. After the ionisation initiation around the active electrode, the phenomenon propagates towards the ground electrode. However, the expansion of the ionisation zone is different in a dry medium from that in a wet medium, which could be attributed to the differences in the ionisation process in both conditions. In a dry medium, breakdown occurs after a delay time if the applied voltage is sufficiently high, causing a high current to flow. However, in the case of a wet medium, the current flows as soon as the voltage is applied. Then, the second current peak may appear with a higher current value when a considerable soil ionisation has taken place.

6.2 Test Setup

The test circuit used in this chapter is similar to the circuit shown in Figure 5-3. Lightning impulse voltage will only be used in this investigation, thus, the Haefely impulse voltage generator was employed. A potential divider with a

ratio of 27931:1 was used to measure the applied voltage at the active electrode, and two other dividers with ratios of 2000:1 and 1000:1 respectively were used to measure the dynamic voltages inside the sample during the discharge as shown in Figure 5-14. These two measured potentials made it possible to estimate the propagation distance of the ionisation zone; thus, confirming whether the soil ionisation propagated in the top layer only or crossed into the lower layer. Furthermore, the impulse impedance of the areas between the voltage probes will be calculated to examine if any reduction occurs due to the propagation of the ionisation discharge. A current transformer was used to measure the current flowing through the layers of the sample. The voltages and current signals were captured on a LeCroy digital oscilloscope.

6.3   Sample Preparation

Medium grain size sand was used in all the samples. Tap water was added to the dry sand to make the wetted layers. The water content (wc) was calculated as a percentage from the mass of the dry sand, as stated in [29]. The sand and water were thoroughly mixed so that a good moisture distribution among the sand grains was ensured. Then, this mixture was placed in the tube. Some pressure was manually applied to the sample to ensure that the mixture was adequately compacted and uniformly distributed in the tube; thus, preventing the formation of gaps inside the sample. A similar procedure was followed for making each layer.

6.4   Ionisation Propagation in One Wet Layer

Water content of 1% and 10% were used in the next tests, the aim of these

tests was to examine how these percentages would affect the initiation of the ionisation phenomenon in the sand under rod-plane electrode configuration. Each percentage of water content was mixed with the sand in separate tests to make the wetted column of sand in the tube. Voltage transducers were also used to track the initiation and propagation of the soil ionisation with each percentage.

6.4.1 One Wet Layer with a 1% wc

A one-layer sample with a 1% moisture percentage was prepared and then placed in the tube to a height of 30 cm. The two voltage probes were inserted in the tube, the first probe was located at a height of 20 cm, and the second at 10 cm height, as depicted in Figure 6-1. A lightning impulse voltage was applied to the sample in steps, and then measurements were taken for all three voltages and the current flowing in the sample.
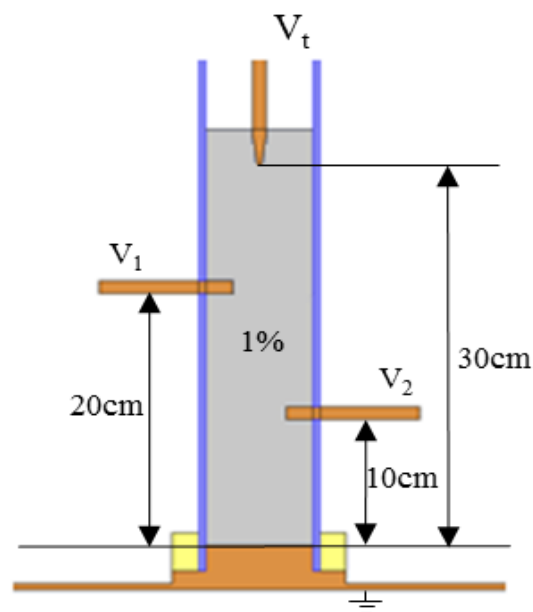

Figure 6-1 wet sand sample (1% wc) and voltage probes arrangement

Figure 6-2 shows an example of the behaviour of the sample under the applied voltage. There is a clear capacitive effect at the beginning of the current trace,

and then a resistive conduction is the dominant behaviour. No second current peak was observed in this test. It can also be seen that there is almost the same voltage difference between the three measured voltages, which is around 20 kV. This may be due to the same distances between the transducers and the effect of the water settling is negligible. Figure 6-3 shows the resistances calculated by dividing the applied voltage (V_t) by the current at the instant of current peak. These resistances tend to reduce with the increase in the current. As a result, the 1% wc was not considered a suitable moisture content to help initiate the ionisation phenomenon in the soil in this test arrangement.
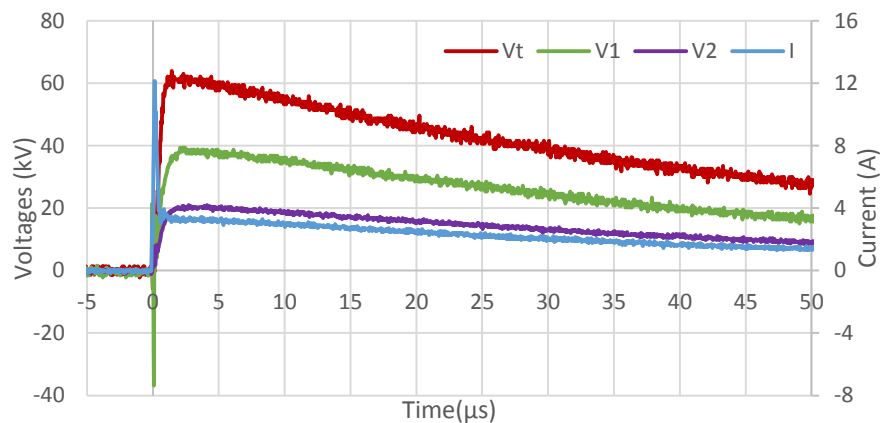

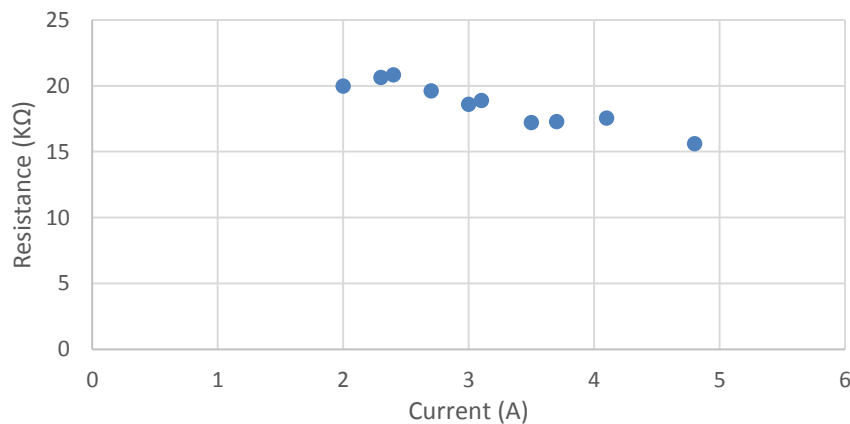**Figure 6-2 voltages and current traces for 1% wc sand sample**

Figure 6-3 resistance versus the current for 1% wet sand (V_{Ipeak}/I_{peak})

6.4.2   One Wet Layer with a 10% wc

In this experiment, a 10% wc was also tested. Figure 6-4 exhibits the arrangement used in this test, which is similar to that used in the previous test. Due to water settling, the test should be carried out directly after the sample preparation. Then, the impulse voltage was applied to the wetted sand with a 10% wc. The impulse impedances between the voltage transducers were calculated using the following equations:

$$Z_{t-1} = \frac{V_t - V_1}{I} \tag{6-1}$$

$$Z_{1-2} = \frac{V_1 - V_2}{I} \tag{6-2}$$

$$Z_2 = \frac{V_2}{I} \tag{6-3}$$
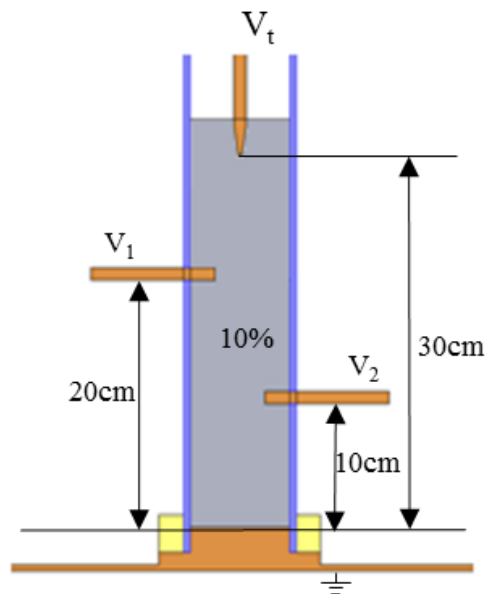

Figure 6-4 wet sand sample (10% wc) and voltage probes arrangement

At the beginning of the voltage application 39 kV, the behaviour was largely linear resistive, and the current had a shape similar to that of the applied voltage and the measured voltage (V_1 and V_2), (see Figure 6-5 (a and b)). However, after the voltage was increased to 55 kV, a second current peak

started to emerge in the current waveform, indicating the initiation of considerable soil ionisation near the HV electrode, but the soil ionisation propagation did not reach the first voltage transducer (V_1), as can be seen in Figure 6-5 (c and d). The impedance (Z_{t-1}), which is for the area between the rod electrode and voltage probe (V_1), reduced by the effect of soil ionisation, while the impedance (Z_{1-2}), which is for the area between the voltage probe (V_1) and voltage probe (V_2), remained constant, i.e. not affected by the soil ionisation. When the voltage increased more 61 kV, soil ionisation initiated and propagated up to around the first transducer (V_1) (see Figure 6-5 (e and f)), where the two impedances (Z_{t-1}) and (Z_{1-2}) have decreased. At higher applied voltage 63 kV; the ionisation phenomenon propagated to around the second voltage probe (V_2), as shown in Figure 6-5 (g and h), as the impedance (Z_2), which is the for the area under voltage probe (V_2), has reduced as well due to the ionisation propagation up to around (V_2). Equations (6-4) and (6-5) will be used to calculate the pre and post ionisation resistances.

$$R_1 = \frac{V_{Ipeak1}}{I_{peak1}} \tag{6-4}$$

$$R_2 = \frac{V_{Ipeak2}}{I_{peak2}} \tag{6-5}$$

The calculated pre-ionisation resistances (R_1) tend to decrease with the increase of the first current peak, which could be attributed to the thermal effect. Moreover, the post-ionisation resistances (R_2) significantly reduce with the increase of the second current peak, but this reduction was attributed to the soil ionisation phenomenon which agrees with the findings in [11]. (See Figure 6-6). Therefore, the 10% wc can be considered a suitable water content to initiate considerable soil ionisation in this test configuration.
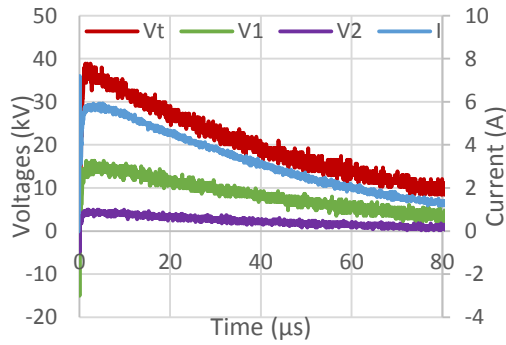
(a) discharge traces with V=39 kV
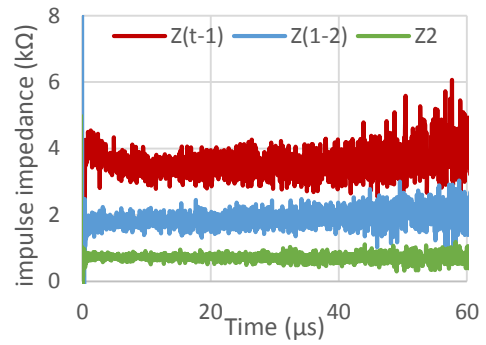
(b) impulse impedance when V=39 kV
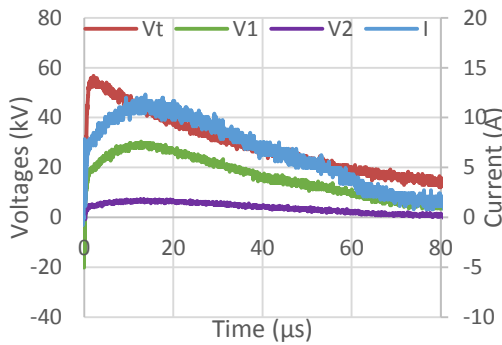
(c) discharge traces with V= 55kV
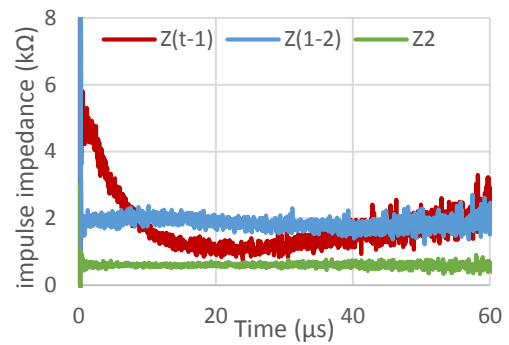
(d) impulse impedance when V=55 kV
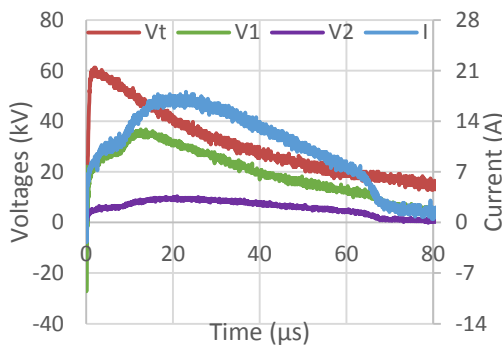
(e) discharge traces with V=61kV
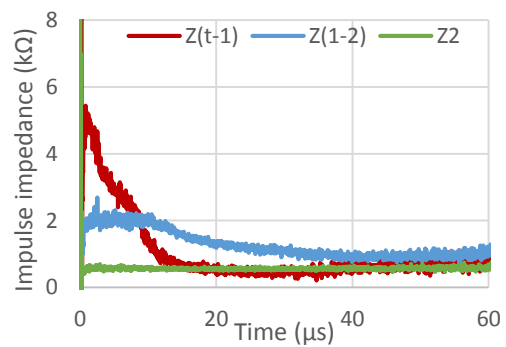
(f) impulse impedance when V=61 kV
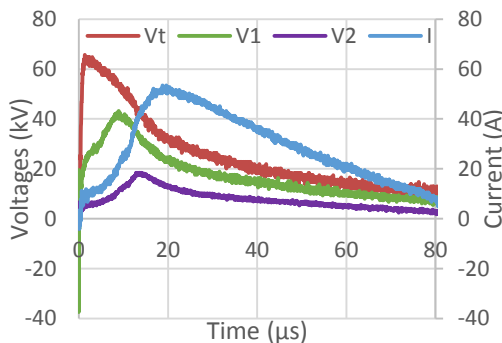
(g) discharge traces with V= 63kV
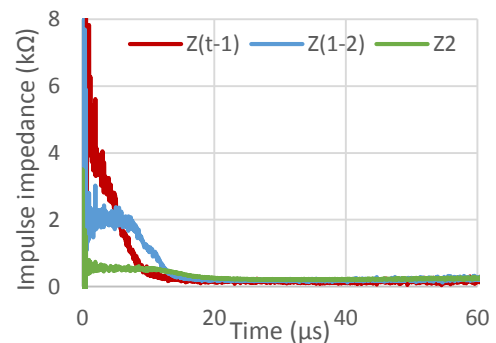
(h) impulse impedance when V=63 kV

Figure 6-5 soil ionisation propagation in 10% wetted sand sample
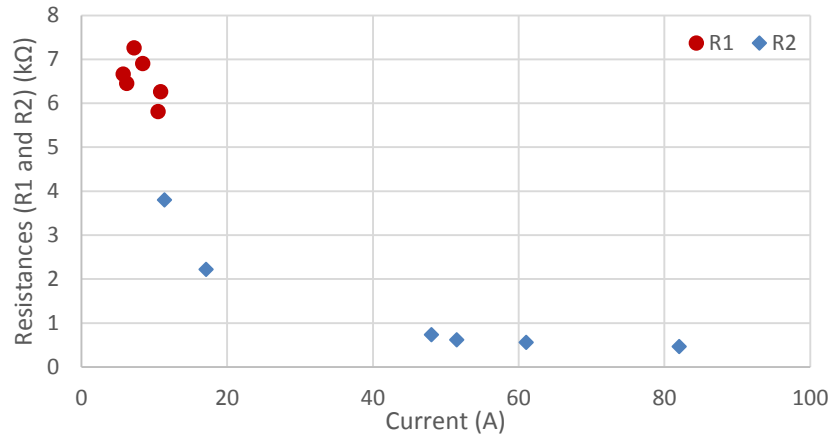
Figure 6-6 R₁ and R₂ versus current for 10% wc wet sand sample

Furthermore, there are different stages can be identified in this test. The behaviour was ohmic at relatively low voltages, but when the applied voltage became sufficiently high (55 kV), the soil ionisation initiated and propagated to a certain distance. As the applied voltage was increased, the propagation distance increased. Consequently, when the voltage at any point increases with the increase of current, it indicates the linear resistive behaviour in the area around that transducer. If the ionisation propagation reaches the voltage probe, the voltage starts to decrease despite the increase in current, indicating the nonlinear behaviour of the soil ionisation, where the impedance of the ionised zone drops due to this ionisation effect.

The above discussion is illustrated in Figure 6-7. During the current increase to the second crest, the ionisation phenomenon propagates further down to the first voltage probe, enlarging the ionisation zone and reducing the impedance even further. If the applied voltage was adequate to sustain the propagation, the soil ionisation would keep growing down until the second transducer. These results could be similar to the improved Liew's model [51],

where the discharge regions could be identified by the voltage transducers. The sparking region could be just around the electrode, and then the ionisation and deionisation zones would come after.
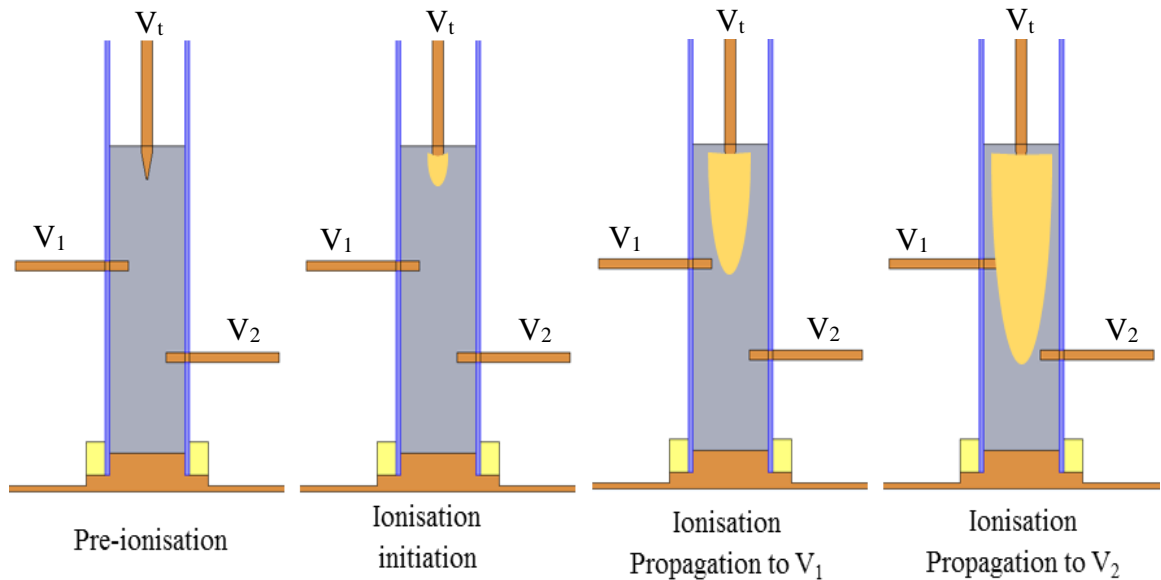
Figure 6-7 propagation stages in wet sand sample (10% wc)

6.5   Ionisation Propagation in Dry layer

The sample in this experiment consisted of dry sand to a height of 10 cm on top of 15 cm wetted sand column with a 5% wc. The first voltage divider (V_t) was connected to the active electrode, the second divider (V_1) was connected to the probe installed in the middle of the dry sand, and the third divider (V_2) was connected to the probe installed at the interface between the dry and wet layers, as depicted in Figure 6-8.

Therefore, the voltage transducers can allow the measurement of the development of the ionisation discharge while propagating in the upper dry layer. Lightning surges were applied in small voltage steps until a current was

detected with the CT. From the recorded waveforms, it can be seen that the current did not flow until the discharge had passed through the dry layer down to the second voltage transducer between the two layers. This means that the voltage (V_1) increased when the ionisation extended to the first transducer in the middle of the dry layer. The current and the voltage (V_2) increased at the same instant when the ionisation reached at the second probe, as shown in Figure 6-9. When calculating the voltage across the entire dry sand ($V_d = V_t - V_2$), this voltage collapsed when the ionisation propagation reached the wet layer indicating the breakdown of the dry sand layer by the effect of the soil ionisation. Once the dry layer breaks down, the applied voltage will be applied to the wet layer; this explains why the applied voltage did not show any sign of breakdown.
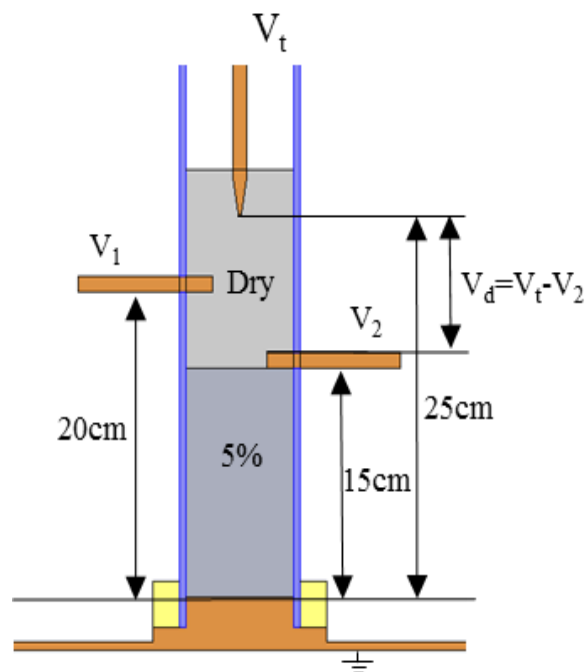
Figure 6-8 dry sand above wet sand sample (5% wc) and voltage probes arrangement
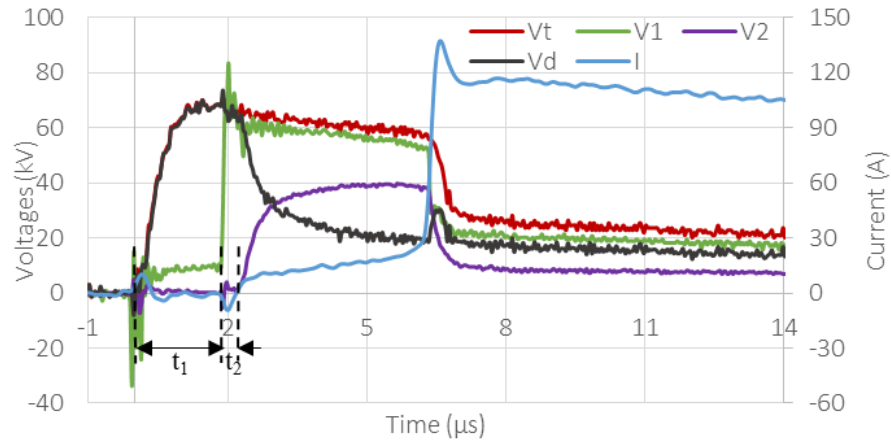
Figure 6-9 discharge traces for ionisation propagation in dry sand layer

Moreover, there are two different delay times (t_1, t_2) between the voltage probes that help understanding the ionisation propagation. These delay times indicate that the propagation of the ionisation discharge in the dry layer has various successive stages. The delay time (t_1 = 1.74 µs) represents not only the propagation, but also the initiation time of the ionisation at the electrode surface as was seen with the glass bubbles. Hence, (t_1) represents two stages of the discharge, whereas (t_2 = 0.84 µs), which represents the third stage, is the propagation of the ionisation between the voltage probes (V_1 and V_2) through the sand. The estimated velocity for this propagation is 6 cm/µs.

The total delay time for the current initiation (t_1+t_2) depends mainly on the applied voltage and the thickness of the dry layer. After about 3.9 µs from the current rise, a full breakdown of the sample occurred, the collapse of the three voltages was due to the breakdown of the wet layer as well. Similar initiation and propagation stages were seen in the sandy medium as described for the glass bubble material in the previous chapter, where the ionisation initiation

144

and propagation created a low resistivity channel for the current, which then caused the breakdown of the entire dry sand layer 10 cm in 2.58 µs.

6.6 Ionisation Propagation in the Configuration Dry over Wet Sand Layers

When 10% wc wetted sand was used under the dry layer, a second current peak was observed, which is thought to be caused by the soil ionisation initiation in this wet layer. Therefore, these experiments investigate how the soil ionisation could take place in the lower wetted sand layer below the dry layer. The HV electrode was inserted in the upper dry layer, and rearranging the positions of the two voltage probes in the lower layer, soil ionisation could be traced. A 1% and a 10% wc wet sands were tested separately in the lower layer below a dry sand layer to examine the initiation of the ionisation phenomenon in the lower layer with these water contents.

6.6.1 Wet Layer with a 1% wc under Dry Layer

The sample configuration consisted of a 10 cm dry sand layer above a 20 cm column of wetted sand with a 1% wc. The voltage transducers were installed at the interface between the two layers and at the middle of the wetted sand, as depicted in Figure 6-10. The first probe monitored the soil ionisation initiation on top of the wet layer, whereas the second probe tracked the propagation of the ionisation zone in the wet layer. Once the applied voltage was sufficient to breakdown the dry layer 73 kV, the current flowed in both layers after a delay time of 2.7 µs, and the potential transducers measured different voltages based on their location along the sample.

The voltage (V_1) had a faster rise time, possibly due to the breakdown of the dry layer. The current had an initial peak at the current rise, which was thought to be caused by the capacitive effect in the wet layer, as depicted in Figure 6-11 (a).

In Figure 6-11 (b) a full breakdown of the sample can be observed when the applied voltage was 74 kV. The dry layer broke down first after 2.48 µs delay time and then the current flowed without causing the collapse of the voltage. After 23 µs from the current rise, a full breakdown of the sample occurred which was due to the breakdown of the wet layer. Then, the applied voltage collapsed, and the current increased sharply. The breakdown of the wet layer could be due to the thermal effect of the conduction current, as the current flowed for 23 µs without any increase. This may indicate that soil ionisation may not have been initiated in the wet layer with a 1% wc below the dry sand.
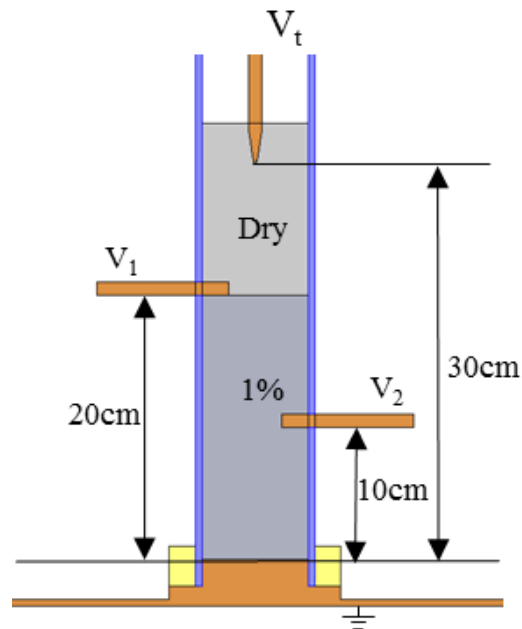
Figure 6-10 test arrangement of dry sand above 1% wc wetted sand
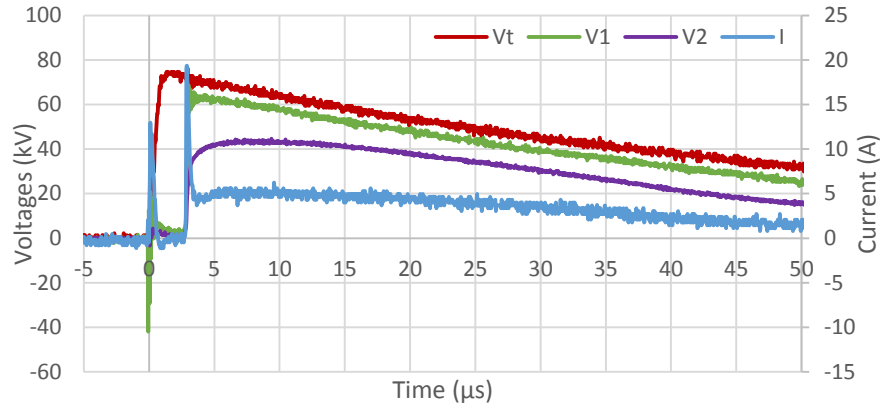
(a) with no full breakdown
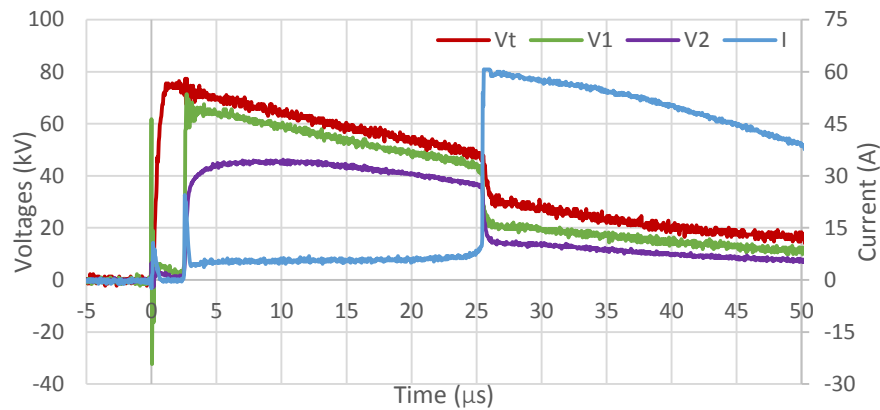
(b) with full breakdown

Figure 6-11 discharge traces in wet sand with 1% wc (20cm) below a dry sand (10cm)

6.6.2 Wet Layer with a 10% wc under Dry Layer

Figure 6-12 shows the configuration of the sample and the voltage probes, where the upper dry layer was 10 cm, as in the previous test, but the lower wetted layer contained a higher water percentage 10% and had a height of 20 cm. The first potential probe was inserted at the interface between the dry and wet layers, while the second probe was installed at the middle of the wetted layer. Thus, these two voltage transducers were able to measure the voltages in the expected ionisation zone in the wetted layer. Due to water settling, the

147

test should be carried out directly after the sample preparation. When the applied voltage was high enough to break down the upper dry layer 69 kV, soil ionisation initiated in the lower wetted layer, and the current jumped to the second peak. Once the ionisation reached the first probe between the two layers after a delay time 5.4 µs, the voltage (V_1) increased sharply, and then started to decrease at a faster rate, indicating the initiation of the ionisation phenomenon in the wet layer. The voltage (V_2) increased at the same time as (V_1), but it continued to grow as the current increased indicating linear resistive behaviour, up to the point where the ionisation propagation reached the second probe; then, (V_2) started to decrease also, as in Figure 6-13. At t = 34.1 µs, there was a slight increase in the current, which was due to the breakdown of the sand between the voltage probes (V_1 and V_2), where (V_1) decreased up to (V_2). The propagation time (t_p = 4.6 µs) between the two peaks of (V_1 and V_2) represents the propagation velocity of the ionisation between the two transducers in the lower layer.
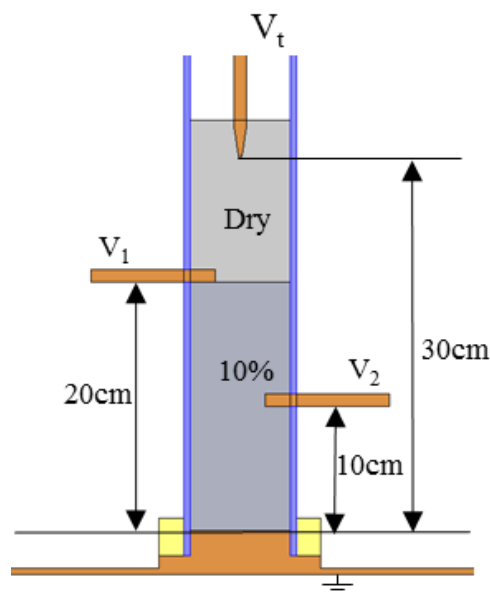
Figure 6-12 test arrangements of dry sand above 10% wetted sand
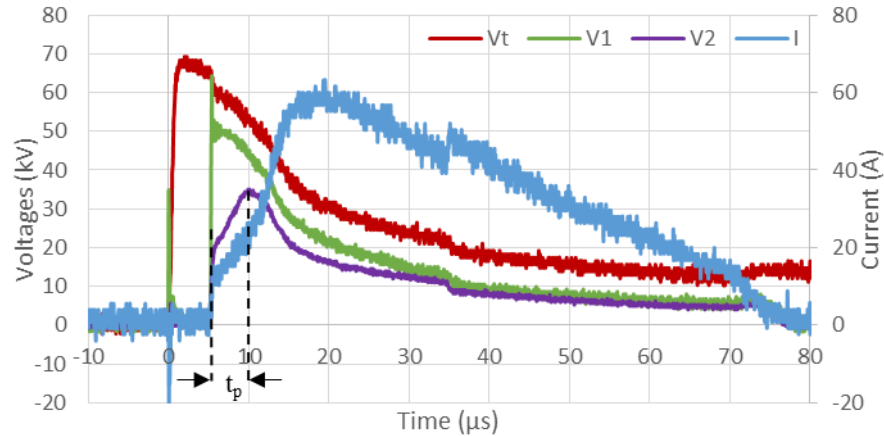
Figure 6-13 discharge traces in wet sand (20 cm) under dry sand (10 cm)

This test illustrates that despite the distance between the active electrode and the wet layer (10 cm dry sand), soil ionisation was found to initiate in the lower layer, which might be due to the availability of the ionisation conditions, such as the suitable amount of water, as It has already been proved that the 10% water content is adequate for soil ionisation tests. Figure 6-14 shows the impedances of the dry and wet layers based on the voltage measurements. The impedance of the upper dry layer [$Z_d = (V_t - V_1) / I$] dropped to a much lower level due to the initiation and propagation of ionisation in the dry sand layer. The ionisation propagation through the dry layer caused the breakdown of the dry layer. The impedance (Z_{1-2}), which is the impedance between voltage probes (V_1) and (V_2) as in Equation (6-2), dropped directly after the ionisation propagation arrived at the first probe. This could indicate that the soil ionisation initiated at the top of the wet layer. The impedance (Z_2), which is the impedance under the second probe as in Equation (6-3), started to reduce after a propagation delay time ($t_p = 4.6$ μs), where the ionisation took this time to initiate and propagation from probe (V_1) up to probe (V_2) in the lower layer. The impedance (Z_d) of the dry layer dropped very quickly due to

149

the breakdown, whereas in the wet layer the impedance took longer time to reach the minimum, where the ionisation propagated more than 10 cm below the second voltage probe, as (Z_2) confirms that.
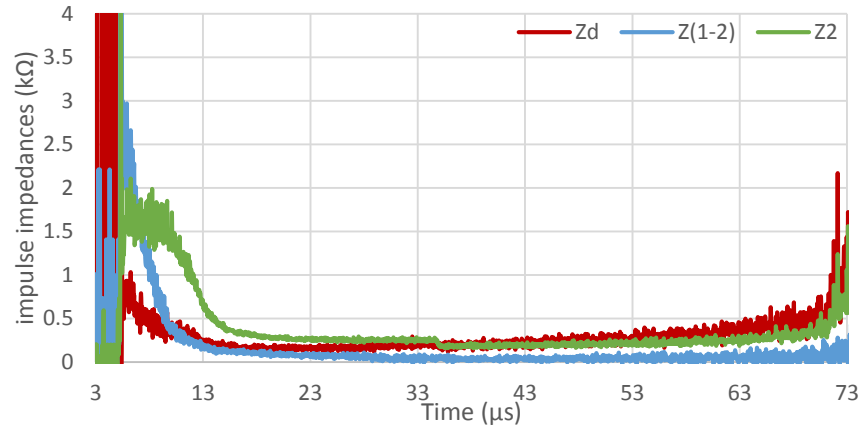
Figure 6-14 impulse impedances of the sample layers

6.7   Ionisation Propagation in Two Various Wet Layers

This investigation examines the scenarios when there are two wetted layers with various water contents in each layer; the water percentages considered in this study were 1% and 10%. These percentages were chosen to obtain a clear difference in the performance of the two layers under the applied lightning impulse voltages, given that it has already been demonstrated that the 1% wc is not suitable for the ionisation initiation in the adopted configuration, whereas the 10% wc was found very appropriate for the soil ionisation tests in this work. Therefore, these series of tests investigated the initiation and propagation of soil ionisation in two layers with distinctive water contents, where one layer contained a 10% wc and the other contained a 1% wc. The height of both layers was also changed to investigate the effect of the layer thickness on the initiation and propagation of soil ionisation in both layers. The active electrode was inserted on top of the upper layer, and the

two voltage transducers were utilized to track the initiation and propagation of the ionisation phenomenon in both layers.

6.7.1 The Upper Layer Contains Less Water Content

The upper layer contained a 1% wc and had a height of 10 cm, and the lower layer contained a 10% wc and had a height of 20 cm. The first voltage transducer (V_1) was installed at the interface between the two layers, and the second voltage probe (V_2) was installed in the middle of the lower layer, as depicted in Figure 6-15 (a). When the applied voltage was around 40 kV, a linear resistive behaviour was seen to dominate the current conduction. However, at 54 kV, a second peak started to appear in the current trace as shown in Figure 6-16 (c). It is obvious from the voltages (V_1 and V_2) that the soil ionisation crossed only the probe (V_1) to the lower layer, where (V_1) started with a behaviour similar to that of the current until the ionisation crossed the transducer, then the voltage (V_1) started to decrease. However, (V_2) showed exactly the same behaviour as the current, indicating a linear behaviour around the probe (V_2). (Z_{t-1}) in Figure 6-16 (d) confirms the initiation of soil ionisation in the upper layer, and (Z_{1-2}) confirms the propagation of soil ionisation up to around probe (V_1) only, as (Z_2) remained constant during the discharge without any reduction. When the applied voltage was further increased, the value of the second current peak increased as well. At 63 kV, the ionisation zone had propagated further down up to the second probe (V_2), as in Figure 6-16 (e and f). The major observation is that soil ionisation initiated in the upper 1% wc wet layer, which was not suitable for the ionisation, and then propagated down in the upper layer and crossed to the bottom layer as well. The adequate moisture content (10% wc) in the lower layer had possibly

created a suitable condition for the ionisation initiation in the upper layer. This is probably caused by the tendency of the current to flow and dissipate in the less impedance soil. The impedance of the upper layer dropped significantly during the ionisation propagation, which was the main impedance reduction in the sample, and then when the ionisation propagated in the lower layer, the impedance of the lower layer started to decrease as well.

In a similar test, the height of the upper layer was increased to 15 cm and the lower layer height was reduced to 15 cm, as depicted in Figure 6-15 (b). The required voltage to initiate the ionisation was increased up to 61 kV instead of 54 kV, as can be seen in Figure 6-17 (c and d), as a higher applied voltage was essential to drive the ionisation further down through the 15 cm thickness instead of 10 cm, as in the previous case. Figure 6-17 (e and f) confirms that the soil ionisation has crossed to the lower layer and propagated up to the second voltage probe (V_2) as the impulse impedance (Z_2) decreased due to the ionisation propagation in the lower layer.
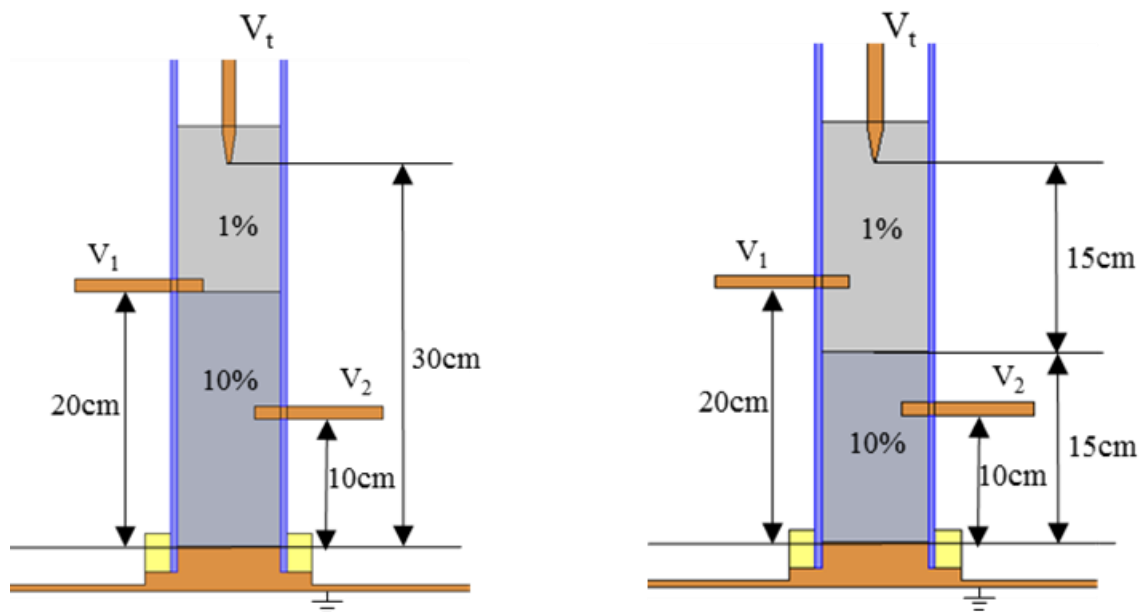
(a) 10 cm upper layer and 20 cm lower layer (b) 15 cm upper layer and 15cm lower layer

Figure 6-15 tests arrangements for 1% wetted sand above 10% wet sand
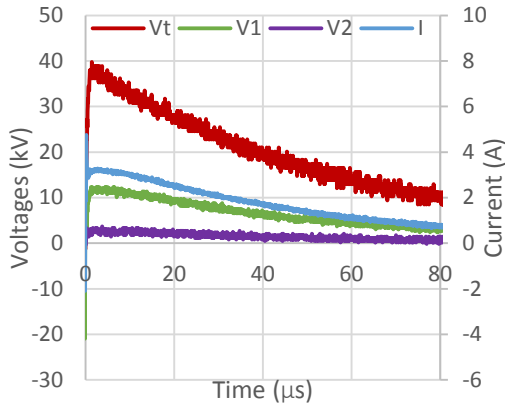
(a) discharge traces with V=40 kV
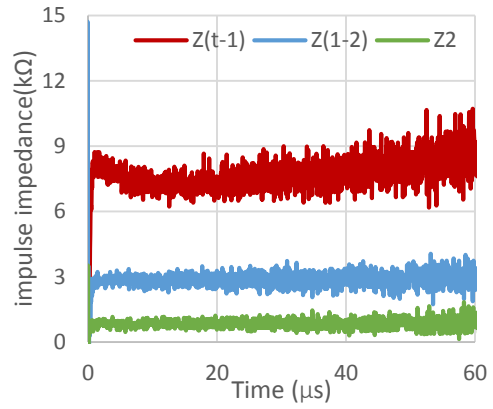
(b) impulse impedance when V=40 kV
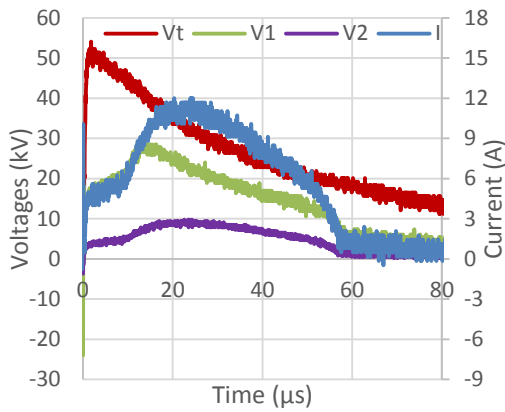
(c) discharge traces with V=54 kV
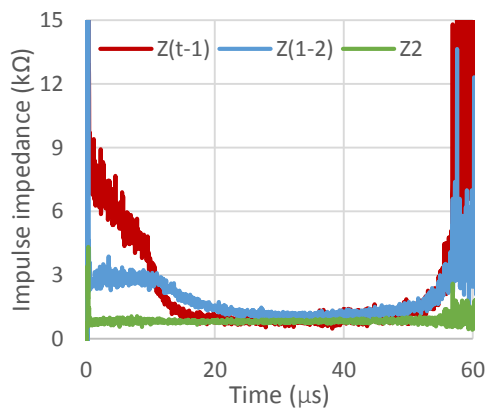
(d) impulse impedance when V=54 kV

(e) discharge traces with V=63 kV
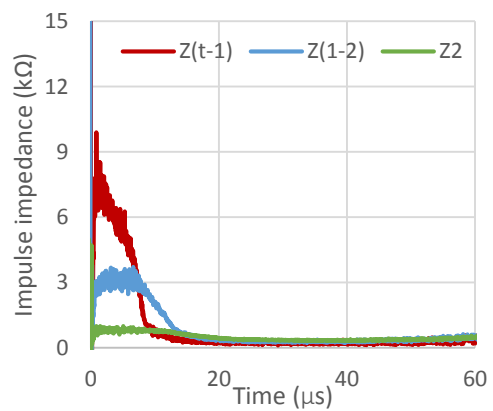
(f) impulse impedance when V=63 kV

Figure 6-16 ionisation propagation in 1% wet sand (10 cm) above 10% wet sand

(20 cm)
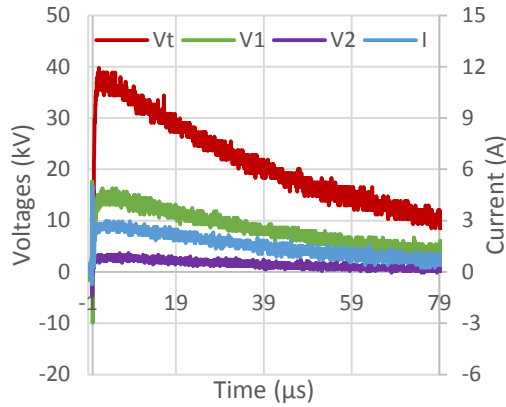
(a) discharge traces with V=40 kV

(b) impulse impedance when V=40 kV

(c) discharge traces with V=61 kV

(d) impulse impedance when V=61 kV

(e) discharge traces with V=62 kV

(f) impulse impedance when V=62 kV

Figure 6-17 ionisation propagation in 1% wet sand (15 cm) above 10% wet sand

(15 cm)

Consequently, it can be inferred that the height or the thickness of the two layers of the sample has a significant effect on the initiation and propagation of the soil ionisation phenomenon in a two-layer soil. The tendency of the current to flow and dissipate in the soil with less impedance (10% wc) has led to initiate the ionisation phenomenon in the upper poor sand layer (1%wc) where the active electrode was inserted, and then the ionisation propagated from around the HV electrode through both the upper and bottom layers.

As the applied voltage increases, the soil ionisation is initiated more quickly and propagated further down, thus reducing the impedance of both layers, which, in turn, allows higher current magnitudes to flow and dissipate in the lower less impedance layer. This scenario gives better resistivity reduction, further ionisation propagation, and higher dissipated current values.

6.7.2   The Upper Layer Contains Higher Water Content

The arrangement of the sample and the probes are shown in Figure 6-18. In this first experiment, the upper layer had a 10% wc and had a height of 10 cm, whereas the lower layer had 1% wc and had a height of 20 cm. The potential probe (V_1) was inserted at the interface between the two layers, while the transducer (V_2) was inserted in the middle of the lower layer. With this sample arrangement, it was expected that the soil ionisation would be initiated in the upper layer, because it contained the proper water percentage (10%) under a sufficiently high applied voltage.

However, as the applied lightning voltage increased, no second current peaks were observed. Figure 6-19 presents an example of this discharge, where 73 kV was applied, and still no second current peak was observed until the breakdown.

Nevertheless, the longer rise time of the current (5 µs) than the applied voltage may indicate that there was a weak ionisation had initiated only around the electrode, but it did not propagate far from the electrode and did not cross to the bottom layer. Where the two voltage probes (V_1 and V_2) had the same shape as the current, indicating the resistive conduction around these probes.

Although the applied voltage magnitude and the moisture percentage (10% wc) in the upper layer, were appropriate for the ionisation, but, it seems that these conditions were not enough. This is possibly due to the high resistivity of the lower 1% wc wet layer (292 Ω.m), which already proved to be a poor moisture content, that restricted the ionisation propagation by limiting the current increase.
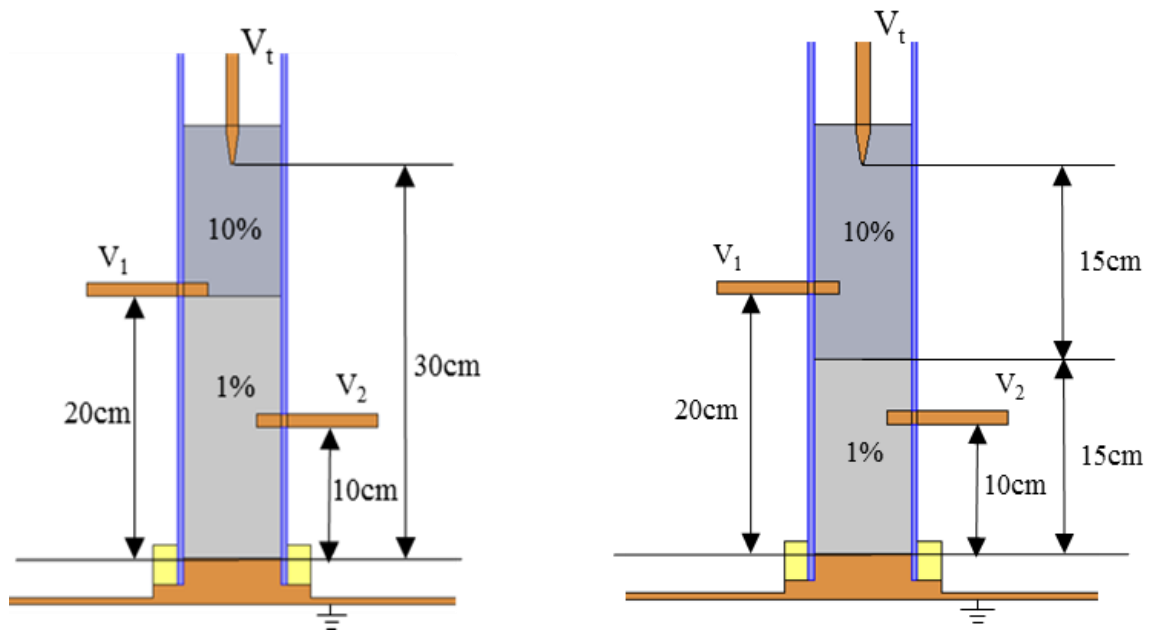
(a) 10 cm upper layer and 20 cm lower layer (b)15 cm upper layer and 15 cm lower layer

**Figure 6-18 tests arrangements of 10% wetted sand above 1% wet sand**
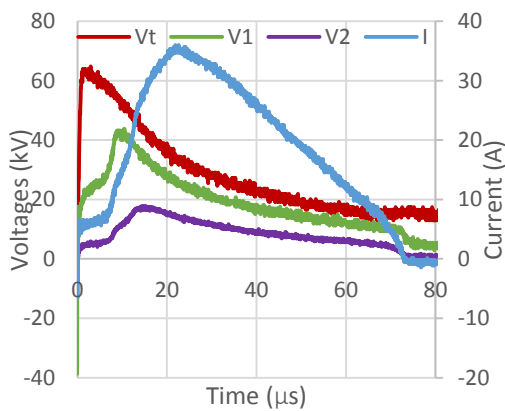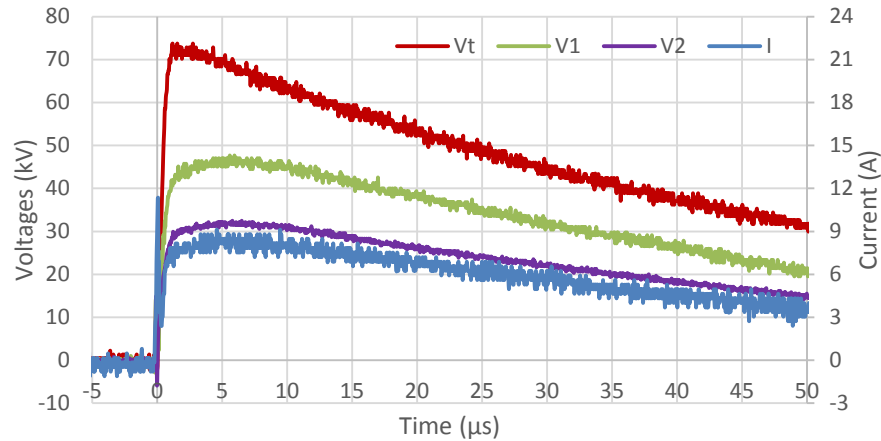
Figure 6-19 discharge traces in 10% wet sand (10 cm) above 1% wet sand (20 cm)

In the second test, the upper layer height was increased to 15 cm and the lower layer height was reduced to 15 cm, as shown in Figure 6-18 (b). The change in the thicknesses of both layers improved the outcomes of the discharge. A small second current peak was observed to begin at applied voltage 59 kV, as can be seen in Figure 6-20 (c). However, soil ionisation initiated and propagated only in the upper layer, and it did not cross to the bottom layer as shown in Figure 6-20 (d); the two voltage probes were still measuring linear resistive behaviour as the impulse impedances (Z_{1-2} and Z_2) did not have any reduction, indicating that there was no sign of soil ionisation around them.

At applied voltages of 61 kV and 69 kV, the ionisation propagated in the upper layer and passed the probe (V_1) as (Z_{1-2}) in Figure 6-20 (f and h) has decreased. However, the impulse impedances plotted in Figure 6-20 (h) support the idea that the soil ionisation initiated and propagated only in the upper layer, as the impulse impedance (Z_2) still has a constant value throughout the discharge without any sign of reduction up to the breakdown.
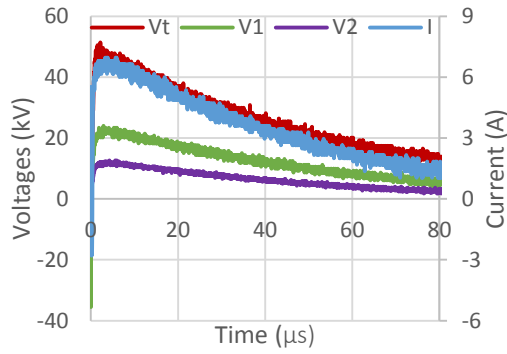
(a) discharge traces with V=50 kV
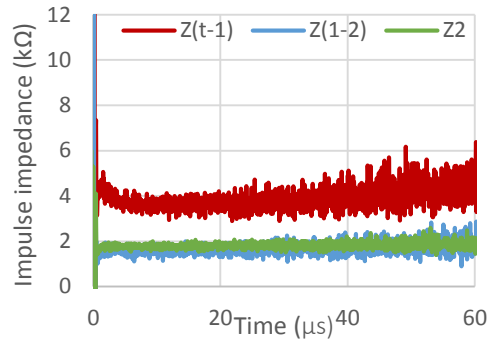
(b) impulse impedance when V=50 kV
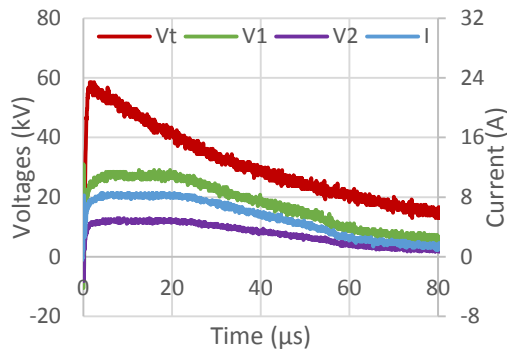
(c) discharge traces with V=59 kV
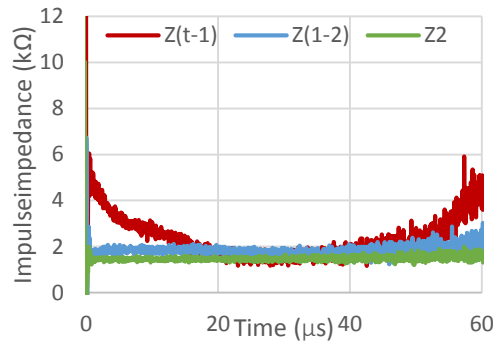
(d) impulse impedance when V=59 kV
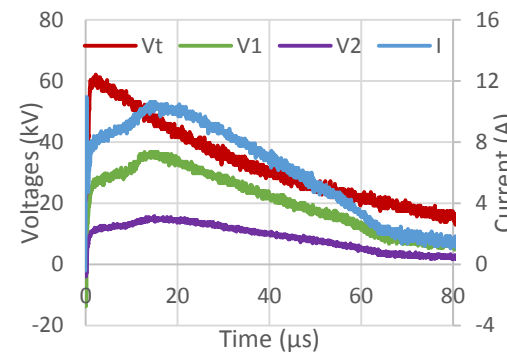
(e) discharge traces with V=61 kV
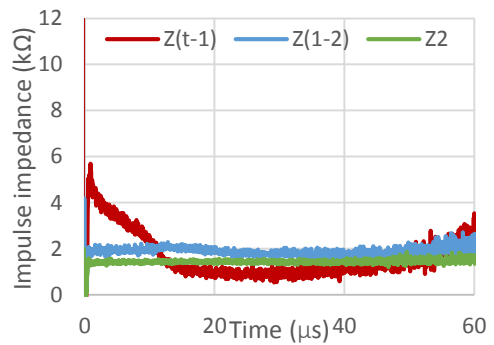
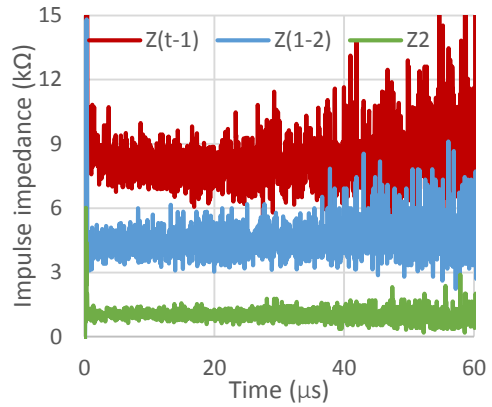(f) impulse impedance when V=61 kV
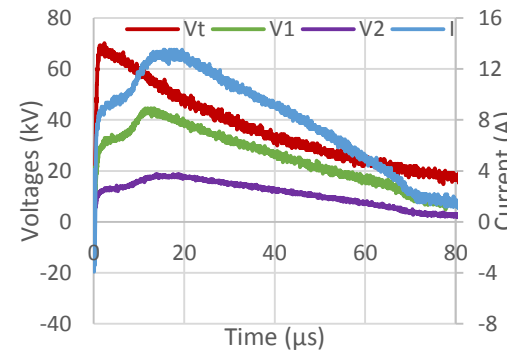
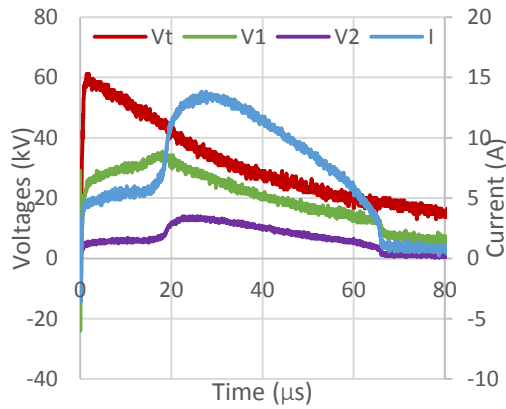(g) discharge traces with V=69 kV
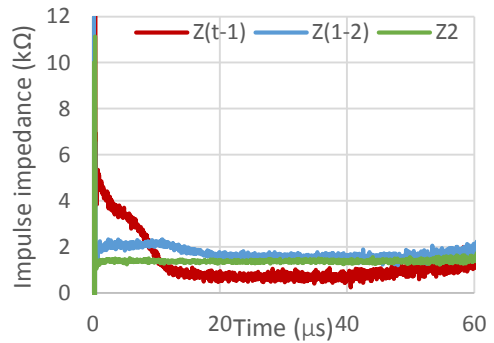
(h) impulse impedance when V=69 kV

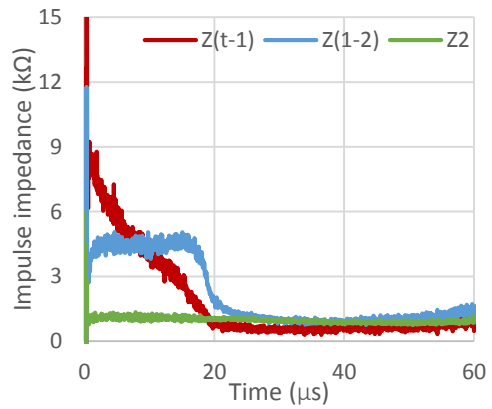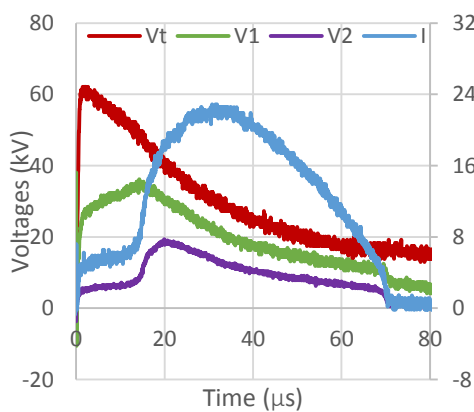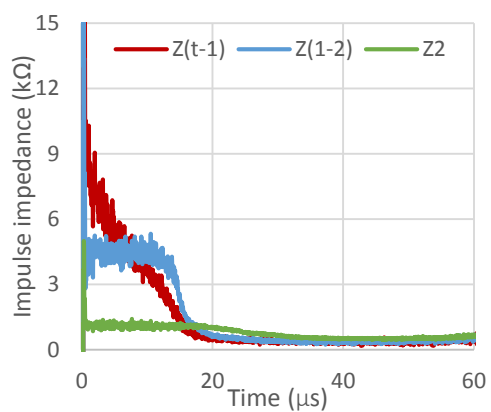**Figure 6-20 ionisation propagation in 10% wet sand (15 cm) above 1% wet sand (15 cm)**

Therefore, when the impedance of the lower poor layer was reduced by reducing its height (from 20 cm to 15 cm), this made it possible for the ionisation effect to appear by emerging the second current peaks. Despite the occurrence of soil ionisation, this was found to occur in the upper layer only, as the 1% wc wet sand in the lower layer was not affected by the ionisation. The second current peaks observed in this test were very low even at a voltage level near the breakdown, which is possibly due to the restriction exercised by the lower layer, which had a poor moisture content that does not help initiate soil ionisation.

6.8 Comparison between the Discharge in Dry and Wet Porous Media

The main cause of the differences between the dry and wet conditions is the water in the wet material; the water content constructs conductive channels among the material grains, thus reducing the resistivity of the material to a much lower value compared with the dry status by short-circuiting the air pockets between the particles. Therefore, the current will flow prior to the ionisation, creating what is called the 'pre-ionisation' peak, and then, during ionisation the current jumps to a second higher current peak. However, negligible current in the case of dry material may flow before soil ionisation takes place. Moreover, the relative permittivity of the wet soil is higher than that of the dry soil by the addition of the moisture content, as was described in [36, 86]. Therefore, in wet soil, there are two conduction mechanisms; the first is through the water channels among the grains, where this current conduction creates the first current peak and the pre-ionisation resistance. However, the

second mechanism is through the air voids after the ionisation initiation, and this leads to a second peak in the current trace and creates the post-ionisation resistance. Nevertheless, in dry porous materials, the only conduction mechanism is thought to be through the ionised air voids after the ionisation phenomenon is initiated, where the resistivity drop caused by the soil ionisation leads directly to breakdown of the soil, whereas in wet soil, soil ionisation reduces soil resistivity gradually until the breakdown voltage is reached.

The main differences in the soil ionisation process between wet and dry porous materials are briefly summarized in Table 6-1. This comparison was based on the behaviour of the discharges observed during the laboratory tests performed in section 6.4.2 and 6.6.2.

Table 6-1 comparison between ionisation process in wet and dry media

Wet porous material	Dry porous material
Ionisation occurs at lower voltage 55kV	Ionisation occurs at higher voltage (70kV)
High pre-ionisation current (7.2A)	Negligible pre-ionisation current
Easily occurs without breakdown	Occurs only with breakdown
Higher relative permittivity	lower relative permittivity
(ρ) decreases slightly as (V) increases	(ρ) drops dramatically at the breakdown
(ρ) takes longer time to reach the minimum (20 μs)	(ρ) takes shorter time to reach the minimum(12 μs)
Pre-ionisation (R) is relatively small (6.5kΩ)	Pre-ionisation (R) is large
Before soil ionisation mainly resistive	Before soil ionisation mainly capacitive
Current flows first through water channels and then through ionised air voids	Current flows only through ionised air voids
Thermal and electrical processes could cause soil ionisation	Mainly electrical process could cause soil ionisation

6.9 Thermal Calculations

In order to estimate the energy required to achieve the thermal effect during the discharge under lightning voltage, three cases were considered. Assuming that the water content is distributed uniformly between the soil grains and the initial temperature of the water is 20°C.

(i)   Energy required to evaporate 1ml of water

The estimated energy to evaporate 1ml of water was calculated as follows:

To boil 1ml of water from 20°C up to 100°C:

$$\Delta Q_1 = m.c_p.\Delta T \qquad\qquad (6\text{-}6)$$

Where:

m: mass of the water (1ml = 1g)

c_p: specific heat of the water (4.186 J/g.K)

ΔT: temperature difference (100-20=80 °C)

$$\Delta Q_1 = 1 \times 4.186 \times 80$$

$$\Delta Q_1 = 335 \text{ J}$$

To evaporate 1ml of water, the required energy is:

$$\Delta Q_2 = m.L_v \qquad\qquad (6\text{-}7)$$

L_v : specific latent heat of water (2260J/g).

$$\Delta Q_2 = 1 \times 2260$$

$$\Delta Q_2 = 2260 \text{ J}$$

$$\text{Total energy} \quad Q = \Delta Q_1 + \Delta Q_2$$

$$Q = 2.6 \text{ kJ}$$

Therefore, in order to evaporate 1ml of water in 100 µs, which is assumed the current conduction period in lightning impulse:

$$P = \frac{2.6 \times 10^3}{100 \times 10^{-6}}$$

$$P = 26 \text{ MW}$$

Very high power (26 MW) is estimated to evaporate 1ml of water in the soil under lightning impulse. This power could be obtained in real lightning strikes, however, yet to date, no experiment has been carried out under very high impulse currents to investigate the thermal effect in soil with high moisture content (15% wc or more) as was described in [20, 44].

(ii)   Energy required to evaporate the water in an assumed channel

The considered channel has a radius of 0.5 mm and a length of 30 cm. The water content in the whole soil sample is 10% wc. Therefore, by calculating the volume of this channel, then only 10% of that volume will be the considered water content in this case, which was found 0.02356 ml. Hence, the estimated energy required to evaporate 0.02356 ml of water was calculated as follows:

By using Equation (6-6), the energy required to boil 0.02356 ml of water from $20\,°C$ up to $100\,°C$ was determined.

$$\Delta Q_1 = 0.02356 \times 4.186 \times 80$$

Where:

m: mass of the water (0.02356 ml = 0.02356g)

$$\Delta Q_1 = 7.89 \text{ J}$$

To evaporate 0.02356 ml of water, Equation (6-7) will be used as follows:

$$\Delta Q_2 = 0.02356 \times 2260$$

$$\Delta Q_2 = 53.25 \text{ J}$$

$$\text{Total energy } Q = \Delta Q_1 + \Delta Q_2$$

$$= 61.14 \text{ J}$$

Thus, in order to evaporate 0.02356 ml of water in 100 µs under lightning impulse:

$$P = \frac{61.14}{100 \times 10^{-6}}$$

$$P = 611.4 \text{ kW}$$

611.4 kW is the calculated power needed to evaporate the water in a current channel in a sample with 10% wc under lightning impulse. However, for soil ionisation, the water in the current channel does not need to be all evaporated as was stated in [42]. Therefore, lower power is required to evaporate less amount of water (less than 0.02356 ml in this case). Moreover, for lower moisture percentages in the soil (less than 10% wc), the required power for the evaporation will also be reduced. Therefore, a small dry area could be created to initiate the ionisation.

(iii) Energy required to heat the water (10 °C) in an assumed channel

The measured tap water conductivity $\sigma_{20} = 0.28$ mS/cm

The resistivity of the water $\rho_{20} = 1/\sigma_{20} = 3571.4$ Ω.cm

The conductivity at different temperatures could be calculated by using Equation (6-8)

$$\sigma_T=\sigma_{20}(1+\alpha(T-20)) \hspace{3cm} (6\text{-}8)$$

Where:

α is the linear temperature coefficient = 2.5%/ $^\circ$C

The water in the considered channel was presumed to be heated up to 30°C, thus, the conductivity of the water at 30°C:

$$\sigma_{30}=0.28 \times 10^{-3}(1+0.025(30-20))$$

$$\sigma_{30}=0.35 \text{ mS/cm}$$

The resistivity of the water at 30°C

$$\rho_{30}=1/\sigma_{30} =2857 \ \Omega.\text{cm}$$

To heat 0.02356 ml of water from 20°C to 30°C, Equation (6-6) is used:

$$Q=0.02356*4.186*10$$

$$Q=0.986 \text{ J}$$

Therefore, the required power to heat 0.02356 ml of water 10°C in 100 µs:

$$P=\frac{0.986}{100\times10^{-6}}$$

$$P=9.86 \text{ kW}$$

The above-calculated power is required to reduce the resistivity of 0.02356 ml of water by 25% by heating it extra 10°C in 100 µs time. This power could be easily obtained at the beginning of the impulse discharge, which could lead to concentrate the current in fewer channels, where these channels will have lower resistivity due to the heat generated from the current flow as can be seen from the calculation above, and this supports what was described in [14].

6.10 Discussion

1% and 10% water contents have been selected to comprise the two-layer sand samples, as 1% wc is not appropriate water content to help initiate the ionisation phenomenon, while 10% wc is very suitable for initiating soil ionisation under the used test configuration. Therefore, different scenarios have been examined to investigate the ionisation phenomenon initiation and propagation in both layers of the sample.

The propagation of soil ionisation in both dry and wet soils is found when the sample consisted of dry layer at the top and wet layer (10% wc sand) at the bottom. Where the soil ionisation caused dry layer breakdown immediately after the propagation i.e. the impedance (Z_d) dropped very quickly causing the breakdown, while in the lower wet layer, the soil ionisation took longer time to reduce the impedance of the wet sand, as the impedance of the wet layer decreased gradually with the increase of the current.

Two-layer sand samples with very different water contents have shown a significant impact on the performance of the earthing electrode under the impulse voltages. The initiation and the propagation of the ionisation phenomenon in both layers of the sample have been greatly affected by the order of the layers and the thickness of each layer.

Table 6-2 shows the times for ionisation propagation (t_{t-1}), which is the initiation and propagation time from HV electrode (V_t) to probe (V_1) and (t_{1-2}) which is the propagation time from probe (V_1) to probe (V_2) when there was a propagation between them. It can be seen from the table (Scenarios 1 and 2) that the ionisation took longer time (t_{V1}) as the thickness of the upper 1% wet layer was increased from 10 cm to 15 cm. Moreover, from scenarios 2 and 3

the ionisation took shorter time to propagation in 10% wet layer (t_{V1} = 14.8 µs) than 1% wet layer (t_{V1} = 18 µs). This result conforms to the results found in [11, 20], which states that the initiation time of the ionisation decreases with the increase of the water content.

Table 6-2 propagation time comparison between the considered scenarios

No	Scenarios	Applied Voltage (kV)	t_{t-1} (µs)	t_{1-2} (µs)
1	(1%10cm)/(10%20cm)	54	14.8	/
		63	11.9	3.5
2	(1%15cm)/(10%15cm)	61	18	/
		62	14.9	5.1
3	(10%15cm)/(1%15cm)	61	14.8	/
		69	13.6	/

6.11 Conclusion

Investigations were conducted of soil ionisation initiation and propagation in several two-layer sand samples with a range of moisture contents. Multi-point voltage measurement technique was utilized to study the initiation and propagation of soil ionisation in the two layers of samples. It was found that 1% wc is not appropriate moisture content to help initiate considerable soil ionisation in the adopted test configuration, while 10% wc was very adequate to imitate significant soil ionisation under rod-plane electrode configuration as used in this work. Soil ionisation was found to cause the breakdown of the dry sand after just a few initiation and propagation stages. It was also found that the propagated ionisation discharge in dry soil can initiate soil ionisation in the wet sand below the dry layer if the wet layer contains an adequate moisture percentage.

The presence of 1% water content in the upper layer offers better performance, better impedance reduction, further ionisation propagation, and higher dissipated current values than does the other scenario with the 10% water content being in the upper layer of the sample. This result supports what was found in [76]. Furthermore, soil ionisation was found to initiate and propagate in the 1% wc layer when it was above the 10% wc. This was attributed to the tendency of the current to dissipate in the less impedance bottom layer. However, soil ionisation does not tend to propagate from 10% wc layer to 1% wc layer, which means that soil ionisation cannot continue the propagation in poor water content (1%wc) layers.

Finally, having different resistivity layers with different thicknesses in the soil was found to influence the process of the initiation and propagation of the soil ionisation either positively or negatively based on the order of the layers. Therefore, the voltage level, propagation distance, impedance reduction and dissipated currents will be significantly affected by these different layers.

Chapter Seven

General Discussion and Conclusions

7.1   Introduction

This thesis set out to obtain a wider understanding and better explanation of the complex soil ionisation phenomenon that influences earthing systems subjected to lightning strikes. It achieves this by first visually investigating this phenomenon to trace the dynamic developments of the discharge in a new dielectric porous material. Secondly, it investigates the initiation and propagation of the ionisation phenomenon in dry porous materials, and wet layer below the dry layer. Finally, it investigates the impact of a wetted two-

layer sand soil with different moisture contents on the initiation and propagation of the phenomenon in both layers.

7.2   Glass Bubble Material and High Speed Imaging

Glass bubble material is intended to be utilised in the plastic manufacturing process to improve specific properties. However, when used to investigate the soil ionisation phenomenon, it offers significant improvements to the task of capturing and imaging the development of the discharge under impulse voltages. The transmitted discharge light through the material made it possible to use high-speed camera to record the dynamic change of the discharge.

This new methodology was very effective in capturing details with 5.5 µs time, which is remarkably fast to record the lightning impulse discharge. The proposed method was found better alternative technique to visualise the discharge in the soil, instead of using the conventional sensitive films, such as x-ray films. In this project, for the first time, both glass bubble material with a high-speed camera were employed together in this type of investigation. Therefore, this high resistivity porous material proved its capability in transmitting the discharge light, which meant it could then be utilised to replace the soil as a test porous medium to investigate visually the ionisation phenomenon.

7.3   Visual Investigation of Soil Ionisation and Breakdown Phenomena

As discussed in the literature, imaging the ionisation phenomenon in the soil was considered a very helpful tool to eliminate some of the ambiguity and

complexity of this phenomenon. In this research, the discharge phenomenon was filmed with a high-speed camera, and analysed by the correlation between the recorded video frames and the measured voltage and current signals. Therefore, the discharge was captured gradually from the initiation of the current until the current approaches zero. This correlation process made it possible to visualize the dynamic developments and monitoring of the discharge phenomenon at various times through the discharge period. The ionisation and breakdown events were recorded and visualized in the high resistivity dry glass bubbles under lightning and switching impulse voltages. Moreover, there was a delay time before the current rise, which was thought to be the time the ionisation takes to initiate and propagate from the active electrode to the boundary between the two layers. Then, as soon as the ionisation creates a low resistivity channel for the current, the current rises. There is an obvious correlation between the current and the light intensity, so as the current value increases the light intensity increases as well, and vice versa. However, the high-speed camera did not capture the streamer during the propagation before the current onset. Thus, longer rise time surges and switching impulse voltages were applied in an attempt to delay the ionisation process, so that the camera could capture the propagation of the streamer from the beginning. Under these conditions, the camera recorded a similar behaviour.

Comparable results were obtained under lightning and switching voltages. The correlation between the current and the light intensity suddenly started to break after around 200 µs under switching voltage, as the brightness of the

discharge was increasing despite the continuation of the current decline. This was not understood and requires further detailed investigation.

7.4 The New Glass Bubble Sample Configuration

The resistivity of glass bubble material was experimentally measured with the parallel plate configuration under DC current. The test revealed that this material has a high resistivity value. This was the reason why the dry material did not demonstrate any considerable outcomes under impulse voltage for the imaging process, as no current was detected before the breakdown. Therefore, the new sample arrangement was prepared in order to overcome the problems related to the breakdown, and assist the high-speed camera to record better videos (regarding the clarity of the discharge light and the period of the discharge). Consequently, with the new sample arrangement, the camera was able to capture clearer frames of the discharge. Three different conduction scenarios were obtained through this sample configuration: conduction without a full breakdown of the sample, conduction with full sample collapse, and a long conduction period under switching impulse voltage. These three scenarios had a significant impact on the results obtained either by the high-speed camera or by electrical tests using the multipoint voltage measurement. Several tests have been carried out to obtain the best thickness of the dry layer and to study different parameters in both layers. Moreover, this arrangement was found very useful in studying the effect of the soil ionisation phenomenon on the dry material, and studying the initiation and propagation of the ionisation in the dry layer. The behaviour of the sample under lightning impulse voltage was also represented and simulated with an equivalent circuit, which was proposed based on the scenario of conduction without a full

171

breakdown of the sample. The components of the circuit were estimated from the discharge waveforms (voltage and current). The simulated voltage and current signals showed a good agreement with the actual discharge waveforms.

7.5   Soil Ionisation Propagation in Dry Porous Materials

After the discharge had been imaged in the dry porous material with a high-speed camera, a series of experiments were carried out to understand the impact of the ionisation phenomenon on the dry porous material, in particular, the case with no full sample breakdown. Besides, investigating the initiation and propagation of the soil ionisation phenomenon through the dry layer. Two voltage probes were installed in the dry layer to measure the voltage at different positions along the layer. This methodology of multi-point voltage technique was used to measure the dynamic voltage in the ionisation zone to track the propagation of the ionisation during the discharge. The impulse voltage across the dry layer could then be calculated to see what had occurred in this layer during the discharge process. The calculated voltage revealed that the dry layer broke down once the streamer had crossed the entire layer. Subsequently, the majority of the applied voltage was applied on the wet layer, which prevented the applied voltage from being collapsed. The breakdown of the dry layer was probably due to the propagation of the ionisation phenomenon by the creation of a low resistivity path for the current to flow along. In the case of the full sample breakdown, the dry layer broke first and then the wet layer. Moreover, from the voltage measurements, the ionisation was found to initiate around the active electrode where the electric field was expected to be at the highest value and then propagated towards the ground

through the particles of the medium. The initiation of the ionisation and the streamer have different delay times according to the delay time (t_1). Both delay times (t_1, t_2) revealed that the streamer also has a varying velocity during the propagation through the entire dry layer. Therefore, the initiation of the ionisation phenomenon does not depend only on the applied voltage, as there are other factors that may influence the initiation process.

7.6   Soil Ionisation Initiation in a Wet Layer below a Dry Layer

When 1% wc wet layer was below a 10 cm dry sand, soil ionisation was not observed in the lower layer as expected, because there was not enough water content (1%) in the lower layer. However, when the bottom wet layer had a 10% wc, the soil ionisation initiated at the boundary between the two layers and then propagated further down towards the ground. The initiation of the ionisation was very clear by the emergence of the second peak on the current trace. The voltage transducers tracked the propagation of the ionisation for more than 10 cm in the lower wet layer, as the calculated impulse impedances between the voltage probes revealed that there was a reduction in these impedances due to the ionisation propagation. In consequence, it can be said that the soil ionisation initiated around the electrode in the upper dry layer and then propagated down until reaching the wet layer boundary. At this point, the ionisation continued its propagation through the wet layer as well. The effect of the ionisation on both layers is different: the dry layer broke down directly due to the severe drop in the impedance, whereas the impedance of the wet layer decreased gradually over a longer time up to around the second current peak. This supports what was found in the literature [27, 28] concerning the

degree of the soil ionisation. The lower the resistivity of the soil is, the lower the effect of the ionisation phenomenon will be, and vice versa.

7.7   Soil Ionisation Propagation in Two-Layer Soil Samples

Two scenarios were examined and discussed to understand the behaviour of the soil ionisation initiation and propagation in two-layer sand samples. The first case considered a 1% wc in the upper layer and a 10% wc in the bottom layer, whereas the second case had the opposite. The thickness of both layers was also investigated by changing the thickness of both layers. As a result, significant different outcomes were obtained with each situation. The soil ionisation unexpectedly initiated and propagated in the upper soil with 1% wc and crossed to the bottom layer (10% wc wet layer), and then continued its propagation in the bottom layer. This initiation was attributed to the current's tendency to flow in the soil with less resistivity; thus, the soil ionisation was forced to initiate in the high resistivity soil to allow more current to be dissipated in the bottom layer, which had less resistivity. When the height of the top layer (1% wc wet layer) was increased and the height of the lower layer (10% wc wet layer) was decreased, the voltage required to initiate the ionisation was also increased. In this scenario, the ionisation will propagate in both layers of the sample (deeper distances), reducing the resistivity even more, which then allows more current to be dispersed.

The findings of the second scenario are completely different, as the soil ionisation did not show considerable soil ionisation initiation and propagation in the upper layer with adequate water content (10% wc), which indicates that the applied voltage and the moisture content were insufficient for the ionisation

174

initiation. The higher impedance soil in the bottom layer (1% wc wet layer) was thought to limit the ionisation initiation by restraining the current increase. However, when the upper layer height was increased and bottom layer height was reduced, the soil ionisation had a confined initiation and restricted propagation only in the upper 10% wc layer and did not cross to the lower 1% wc layer. This may indicate that the ionisation phenomenon does not tend to propagate from 10% wc layer to 1% wc layer, which means that soil ionisation cannot continue the propagation in a poor water content (1% wc) layer, as 1% wc was found not suitable for soil ionisation. Taken together, these results suggest that soil ionisation should be carefully studied when designing earthing systems in two-layer soil, taking in account the resistivity and thickness of each layer.

7.8 Future Work

- A visual investigation of the soil ionisation phenomenon in glass bubble material was performed under lightning and switching impulse voltages. However, a new phenomenon was observed during the switching discharge, represented by an unexpected increase in the discharge light intensity despite the decrease in the current. Further experimental studies are needed to investigate this new behaviour.

- In order to obtain more information about the discharge behaviour, the emitted discharge light could be examined and analysed. For instance, studying the correlation between the light intensity and the discharge time, the correlation between the light intensity and the current value, the temperature of the current channel, and determining the elements

of the ionised gas among the microspheres with the light analysis. Therefore, an interesting investigation could be performed using optical sensors to measure and analyse the light produced throughout the discharge.

- During the streamer propagation, the high-speed camera did not capture the development of the streamer; this is thought to be due to the small value of the current flowing in the streamer, which may produce very dim light. More research should be conducted to verify the current in the streamer during the propagation in dry materials, and to visualise the moment of initiation at the electrode surface.

- Three different impulse voltages were used in the visual study of soil ionisation in glass bubble material, and it was found that the longer the rise time of the wave, the longer the delay time is, so the initiation of the soil ionisation takes longer. However, the developments of the propagation of the soil ionisation and the streamer under the slow impulse voltages need to be investigated to understand the relation between the wave time characteristics and the initiation and propagation stages, including the propagation velocity.

- Two-layer soil was found to greatly influence the behaviour of the earthing systems under high impulse voltages. The resistivity and thickness of the layers can affect the soil ionisation around the earthing electrode. However, there is a need to conduct a larger test scale on selected sites considering the earth potential rise at the ground surface as a measure of the effectiveness of the soil ionisation initiation and propagation.

176

REFERENCES

[1]   F. E. Asimakopoulou, I. F. Gonos, and I. A. Stathopulos, "Experimental investigation on soil ionization," in *Proceedings of the 16th International Symposium on High-Voltage Engineering (ISH 2009), Cape Town, South Africa*, 2009.

[2]   F. E. Asimakopoulou, I. F. Gonos, and I. A. Stathopulos, "Methodologies for determination of soil ionization gradient," *Journal of Electrostatics,* vol. 70, pp. 457-461, 2012.

[3]   N. M. Nor, M. Trlep, S. Abdullah, R. Rajab, and R. Ramar, "Determination of Threshold Electric Field of Practical Earthing Systems by FEM and Experimental Work," *IEEE Transactions on Power Delivery,* vol. 28, pp. 2180-2184, 2013.

[4]   H. Jing, W. Xishan, and L. Lei, "Determination of critical electric field of soil under lightning impulse voltage," in *International Conference on Electrical Machines and Systems, ICEMS* 2008, pp. 265-268.

[5]   N. M. Nor, A. Haddad, and H. Griffiths, "Determination of threshold electric field Ec of soil under high impulse currents," *IEEE Transactions on Power Delivery,* vol. 20, pp. 2108-2113, 2005.

[6]   I. F. Gonos and I. A. Stathopulos, "Soil ionisation under lightning impulse voltages," *IEE Proceedings - Science, Measurement and Technology,* vol. 151, pp. 343-346, 2004.

[7]   N. M. Nor, S. Srisakot, H. Griffiths, and A. Haddad, "characterization of soil ionization under fast impulse," in *25th International Conference on Lightning Protection (ICLP)*, Rhodes - Greece, 2000, pp. 417-422.

[8]   N. M. Nor, A. Haddad, and H. Griffiths, "Factors affecting soil characteristics under fast transients," presented at the International Conference on Power Systems Transients - IPST, in New Orleans, USA, 2003.

[9]   N. Nor and A. Ramli, "Soil characteristics of wet sand under different impulse polarity and earth electrode's dimensions," *IEEE Transactions on Dielectrics and Electrical Insulation,* vol. 15, pp. 910-914, 2008.

[10]   N. M. Nor and A. Ramli, "Effects of moisture content, impulse polarity and earth electrode's dimension on dry and wet sand under high voltage conditions," *European Transactions on Electrical Power,* vol. 18, pp. 461-475, 2008.

[11]   B. H. Lee, G. H. Park, H. G. Kim, and K. S. Lee, "Analysis of soil ionization behaviors under impulse currents," *Journal of Electrical Engineering and Technology,* vol. 4, pp. 98-105, 2009.

[12]   Y. Gao, J. He, J. Zou, R. Zeng, and X. Liang, "Fractal simulation of soil breakdown under lightning current," *Journal of Electrostatics,* vol. 61, pp. 197-207, 2004.

[13]   D. P. Snowden, E. S. Beale, and V. A. J. van Lint, "The Effect of Gaseous Ambient on the Initiation of Breakdown in Soil," *IEEE Transactions on Nuclear Science,* vol. 33, pp. 1669-1674, 1986.

[14]   V. A. J. van Lint and J. W. Erler, "Electric Breakdown of Earth in Coaxial Geometry," *IEEE Transactions on Nuclear Science,* vol. 29, pp. 1891-1896, 1982.

[15]   T. M. Flanagan, C. E. Mallon, R. Denson, and I. Smith, "Electrical Breakdown Characteristics of Soil," *IEEE Transactions on Nuclear Science,* vol. 29, pp. 1887-1890, 1982.

[16]   T. M. Flanagan, C. E. Mallon, R. Denson, and R. E. Leadon, "Electrical Breakdown Properties of Soil," *IEEE Transactions on Nuclear Science,* vol. 28, pp. 4432-4439, 1981.

[17]   T. L. T. dos Santos, R. M. S. de Oliveira, C. L. da S S Sobrinho, and J. F. Almeida, "Soil ionization in different types of grounding grids simulated by

FDTD method," in *International Microwave and Optoelectronics Conference (IMOC), 2009 SBMO/IEEE MTT-S* 2009, pp. 127-132.

[18]   C. Yaqi, H. Jinliang, and Z. Bo, "Analysis on impulse characteristics of independence grounding devices for lightning protection," in *8th International Symposium on Antennas, Propagation and EM Theory. ISAPE 2008. ,* 2008, pp. 1248-1251.

[19]   S. Sekioka, M. I. Lorentzou, M. P. Philippakou, and J. M. Prousalidis, "Current-dependent grounding resistance model based on energy balance of soil ionization," *IEEE Transactions on Power Delivery,* vol. 21, pp. 194-201, 2006.

[20]   N. M. Nor, A. Haddad, and H. Griffiths, "Characterization of ionization phenomena in soils under fast impulses," *IEEE Transactions on Power Delivery,* vol. 21, pp. 353-361, 2006.

[21]   A. Geri, G. M. Veca, E. Garbagnati, and G. Sartorio, "Non-linear behaviour of ground electrodes under lightning surge currents: computer modelling and comparison with experimental results," *IEEE Transactions on Magnetics,* vol. 28, pp. 1442-1445, 1992.

[22]   J. He and B. Zhang, "Progress in Lightning Impulse Characteristics of Grounding Electrodes with Soil Ionization," *IEEE Transactions on Industry Applications,* pp. 1-1, 2015.

[23]   J. He, J. Yuan, and B. Zhang, "Photographic Investigations on Lightning Impulse Discharge Phenomena in Soil," *IEEJ Transactions on Power and Energy,* vol. 133, pp. 947-953, 2013.

[24]   X.-m. Han, M.-f. Peng, B.-j. Pu, C.-z. Xia, J.-h. Yu, Y.-f. Wang*, et al.*, "The experimental study of spark breakdowns in soil," in *Power Engineering and Automation Conference (PEAM), 2011 IEEE*, 2011, pp. 36-40.

[25]   M. Víctor and M. Cabrera, "Photographic investigations of electric discharges in Sandy media," *Journal of Electrostatics,* vol. 30, pp. 47-56, 1993.

[26] M. Hayashi, "Observation of Streamer in the Soil by Surge Current," *The Journal of the Institute of Electrical Engineers of Japan,* vol. 87, pp. 133-141, 1967.

[27] N. M. Nor and R. Rajab, "Correlation Between Steady State and Impulse Earth Resistance Values," *American Journal of Applied Sciences,* vol. 6, pp. 1139-1142, 2009.

[28] N. Mohamad Nor, M. Trlep, S. Abdullah, and R. Rajab, "Investigations of earthing systems under steady-state and transients with FEM and experimental work," *International Journal of Electrical Power & Energy Systems,* vol. 44, pp. 758-763, 2013.

[29] "Methods of test for soils for civil engineering purposes Part 1: General requirements and sample preparation," *British standard BS 1377-1,* 1990.

[30] G. Ala, M. L. D. Silvestre, F. Viola, and E. Francomano, "Soil ionization due to high pulse transient currents leaked by earth electrodes," *Progress In Electromagnetics Research B,* pp. 1-21, 2009.

[31] J. C. Salari and C. Portela, "Grounding Systems Modeling Including Soil Ionization," *IEEE Transactions on Power Delivery,* vol. 23, pp. 1939-1945, 2008.

[32] A. Habjanic and M. Trlep, "The simulation of the soil ionization phenomenon around the grounding system by the finite element method," *IEEE Transactions on Magnetics,,* vol. 42, pp. 867-870, 2006.

[33] L. Yaqing, M. Zitnik, and R. Thottappillil, "An improved transmission-line model of grounding system," *IEEE Transactions on Electromagnetic Compatibility,* vol. 43, pp. 348-355, 2001.

[34] A. C. Liew and M. Darveniza, "Dynamic model of impulse characteristics of concentrated earths," *Proceedings of the Institution of Electrical Engineers,* vol. 121, pp. 123-135, 1974.

[35]   F. E. Asimakopoulou, I. F. Gonos, and I. A. Stathopulos, "I-V Curves for the Determination of the Ionization Voltage in Soil Samples " in *XVII International Symposium on High Voltage Engineering*, Hannover, Germany, 2011.

[36]   A. M. Mousa, "The soil ionization gradient associated with discharge of high currents into concentrated electrodes," *IEEE Transactions on Power Delivery,* vol. 9, pp. 1669-1677, 1994.

[37]   N. M. Nor, "Review: Soil Electrical Characteristics Under High Impulse Currents," *IEEE Transactions on Electromagnetic Compatibility,* vol. 48, pp. 826-829, 2006.

[38]   G. Ala, P. L. Buccheri, P. Romano, and F. Viola, "Finite difference time domain simulation of earth electrodes soil ionisation under lightning surge condition," *IET Science, Measurement & Technology,* vol. 2, pp. 134-145, 2008.

[39]   R. E. Leadon, T. M. Flanagan, C. E. Mallon, and R. Denson, "Effect of Ambient Gas on Arc Initiation Characteristics in Soil," *IEEE Transactions on Nuclear Science,* vol. 30, pp. 4572-4576, 1983.

[40]   N. Mohamad Nor and A. Ramli, "Electrical properties of dry soil under high impulse currents," *Journal of Electrostatics,* vol. 65, pp. 500-505, 2007.

[41]   N. A. Idris, H. Ahmad, and M. N. Isa, "Impulse impedance tests on laboratory model earth electrode," in *Asia-Pacific Conference on Applied Electromagnetics. APACE,* , 2005, p. 5

[42]   D. P. Snowden and J. W. Erler, "Initiation of Electrical Breakdown of Soil by Water Vaporization," *IEEE Transactions on Nuclear Science,* vol. 30, pp. 4568-4571, 1983.

[43]   J. W. Erler and D. P. Snowden, "High Resolution Studies of the Electrical Breakdown of Soil," *IEEE Transactions on Nuclear Science,* vol. 30, pp. 4564-4567, 1983.

[44]   N. M. Nor, "Investigations of Soil Characterisation under High Impulse Currents," PhD Thesis, Cardiff University, 2001.

[45] N. M. Nor, "Ionisation gradient of low resistivity soils and liquids," in *17th International Zurich Symposium on Electromagnetic Compatibility, EMC Zurich 2006*, pp. 409-412.

[46] C. W. G. o. Lightning, *Guide to Procedures for Estimating the Lightning Performance of Transmission Lines*: Cigre, 1991.

[47] J. L. C. Lima and S. Visacro, "Experimental developments soil ionization: new findings," in *International conference on grounding and earthing & 3th international conference on lightning physics and effects*, Florianopolis- Brazil, 2008.

[48] M. Loboda and V. Scuka, "On the transient characteristics of electrical discharges and ionization processes in soil," in *23rd Int. Conf. Lightning Protection*, Firenze, Italy, 1996, pp. 539-544.

[49] H. Jin-Liang, M. Qing-Bo, and T. You-Ping, "Surge breakdown properties of soil," in *Proceedings of International Symposium on Electrical Insulating Materials, *, 1998, pp. 429-432.

[50] J. He, X. Wang, R. Zeng, and X. Peng, "Influence of impulse breakdown delay of soil on lightning protection characteristics of transmission line," *Electric Power Systems Research,* vol. 85, pp. 44-49, 2012.

[51] W. Junping, L. Ah Choy, and D. Mat, "Extension of dynamic model of impulse behavior of concentrated grounds at high currents," *IEEE Transactions on Power Delivery,* vol. 20, pp. 2160-2165, 2005.

[52] H. Jinliang, Z. Baoping, Z. Rong, and Z. Bo, "Experimental Studies of Impulse Breakdown Delay Characteristics of Soil," *IEEE Transactions on Power Delivery,* vol. 26, pp. 1600-1607, 2011.

[53] Z. Song, J. He, and M. R. Raghuveer, "Experimental study on lightning breakdown channels in the soils," in *Eleventh International Symposium on High Voltage Engineering* 1999, pp. 426-429 vol.2.

[54] M. Víctor, M. Cabrera, S. Lundquist, and V. Cooray, "On the physical properties of discharges in sand under lightning impulses," *Journal of Electrostatics,* vol. 30, pp. 17-27, 1993.

[55] K. J. Nixon and I. R. Jandrell, "Quantifying the lightning transient performance of an earth electrode," in *6th IEEE Africon Conference in Africa* 2002, pp. 665-670 vol.2.

[56] V. P. Androvitsaneas, I. F. Gonos, and I. A. Stathopulos, "Transient impedance of grounding rods encased in ground enhancing compounds," in *International Conference on Lightning Protection (ICLP)*, 2014, pp. 359-363.

[57] I. F. Gonos, F. V. Topalis, and I. A. Stathopulos, "Transient impedance of grounding rods," in *Eleventh International Symposium on High Voltage Engineering,* 1999, pp. 272-275 vol.2.

[58] I. F. Gonos, M. K. Antonioy, F. V. Topalis, and I. A. Stathopulos, "Behaviour Of A Grounding System Under Impulse Lightning Current," in *Proceedings of the 6th International Conference on Optimization of Electrical and Electronic Equipments, OPTIM. ,* 1998, pp. 171-174.

[59] N. Harid, H. Griffiths, N. Ullah, M. Ahmeda, and A. Haddad, "Experimental Investigation of Impulse Characteristics of Transmission Line Tower Footings," *Journal of Lightning Research,* vol. 4, pp. 36-44, 2012.

[60] L. Grcev, "Impulse Efficiency of Ground Electrodes," *IEEE Transactions on Power Delivery,* vol. 24, pp. 441-451, 2009.

[61] N. M. Nor, S. Abdullah, and R. Rajab, "Performance of earthing systems at steady-state and under impulse conditions," in *IEEE 7th International Power Engineering and Optimization Conference (PEOCO),,* 2013, pp. 1-6.

[62] N. Harid, H. Griffiths, and A. Haddad, "Effect of ground return path on impulse characteristics of earth electrodes," in *7th Asia-Pacific International Conference on Lightning (APL),* 2011, pp. 686-689.

[63]   B.-H. Lee, D.-C. Jeong, S.-B. Lee, and K.-C. Chang, "Effective Impulse Impedances of Deeply Driven Grounding Electrodes," *KIEE International Transactions on Electrophysics and Applications,* vol. 4, pp. 207-214, 2004.

[64]   E. E. Oettle, "A new general estimation curve for predicting the impulse impedance of concentrated earth electrodes," *IEEE Transactions on Power Delivery,* vol. 3, pp. 2020-2029, 1988.

[65]   B. R. Gupta and B. Thapar, "Impulse Impedance of Grounding Grids," *IEEE Transactions on Power Apparatus and Systems,* vol. PAS-99, pp. 2357-2362, 1980.

[66]   Z. Rong, G. Xuehai, H. Jinliang, Z. Bo, and G. Yanqing, "Lightning Impulse Performances of Grounding Grids for Substations Considering Soil Ionization," *IEEE Transactions on Power Delivery,* vol. 23, pp. 667-675, 2008.

[67]   W. Kalat, M. Loboda, and Z. P. ke, "Implementation of the dynamic model of surge soil conduction for transient behaviour of grounding electrodes simulations using ATP version of EMTP," in *22nd International Conference on Lightning Protection*, Budapest, 1994, pp. 375-380.

[68]   E. P. Nicolopoulou, F. E. Asimakopoulou, I. F. Gonos, and I. A. Stathopulos, "Comparison of equivalent circuit models for the simulation of soil ionization," *Electric Power Systems Research,* vol. 113, pp. 180-187, 2014.

[69]   W. Sima, S. Liu, T. Yuan, D. Luo, P. Wu, and B. Zhu, "Experimental Study of the Discharge Area of Soil Breakdown under Surge Current Using X-ray Imaging Technology," *IEEE Transactions on Industry Applications,* pp. 1-1, 2015.

[70]   J. He, R. Zeng, and B. Zhang, *Methodology and Technology for Power System Grounding*, first ed. india: John Wiley & Sons, 2013.

[71]   G. M. Petropoulos, "The high-voltage characteristics of earth resistances," *Journal of the Institution of Electrical Engineers - Part II: Power Engineering,* vol. 95, pp. 59-70, 1948.

[72] M Hayashi and T Higuchi, "Grounding Resistance Reduction Study," in *Fifth Intrnational Symposium on High Voltage Engineering*, Germany, 1987, pp. 1-4.

[73] B. Zhang, J. He, and R. Zeng, "Spatially discontinuous ionization phenomenon in inhomogeneous soil," *Science China Technological Sciences,* vol. 53, pp. 918-921, 2010.

[74] J. He and B. Zhang, "Soil Ionization Phenomenon around Grounding Electrode under Lightning Impulse," in *Asia-Pacific International Symposium and Exhibition on Electromagnetic Compatibility APEMC* Australia, 2013, pp. 94-98.

[75] S. Zeqing, M. R. Raghuveer, and H. Jingliang, "Influence of the nature of impulse current propagation in soils on transient impedance characteristics," in *Annual Report Conference on Electrical Insulation and Dielectric Phenomena,* , 2000, pp. 739-742 vol.2.

[76] Y. Liu, N. Theethayi, R. Thottappillil, R. M. Gonzalez, and M. Zitnik, "An improved model for soil ionization around grounding system and its application to stratified soil," *Journal of Electrostatics,* vol. 60, pp. 203-209, 2004.

[77] K. J. Nixon, I. R. Jandrell, and A. J. Phillips, "A simplified model of the lightning performance of a driven rod earth electrode in multi-layer soil that includes the effect of soil ionisation," in *Industry Applications Conference, 2006. 41st IAS Annual Meeting. Conference Record of the 2006 IEEE*, Tampa, FL, 2006, pp. 1821-1825.

[78] H. Jinliang, Z. Rong, G. Yanqing, T. Youping, S. Weimin, Z. Jun*, et al.*, "Seasonal influences on safety of substation grounding system," *IEEE Transactions on Power Delivery,* vol. 18, pp. 788-795, 2003.

[79] M. G. Unde and B. E. Kushare, "Impact of seasonal variation of soil resistivity on safety of substation grounding system," in *Fifth International Conference*

on Advances in Recent Technologies in Communication and Computing (ARTCom 2013),, 2013, pp. 173-182.

[80] "High-voltage test techniques Part 1 : General definitions and test requirements," *international standard IEC60-1 1989-11,* 1989.

[81] E. Kuffel, W. S. Zaengl, and J. Kuffel, *High Voltage Engineering Fundamentals*, second ed. Oxford: Newnes, 2001.

[82] I. Yuki, M. Shigeyasu, K. Akiko, I. Hisatoshi, and H. Kunihiko, "Shack–Hartmann type laser wavefront sensor for measuring two-dimensional electron density distribution over extinguishing arc discharge," *Journal of Physics D: Applied Physics,* vol. 45, p. 435202, 2012.

[83] A. F. Rogers, "Sand Fulgurites with Enclosed Lechatelierite from Riverside County, California," *The Journal of Geology,* vol. 54, pp. 117-122, 1946.

[84] L. Yaqing, N. Theethayi, R. M. Gonzalez, and R. Thottappillil, "The residual resistivity in soil ionization region around grounding system for different experimental results," in *IEEE International Symposium on Electromagnetic Compatibility*, 2003, pp. 794-799 vol.2.

[85] "IEEE Guide for Safety in AC Substation Grounding," *ANSI/IEEE Std 80-1986,* 1986.

[86] S. Srisakot, "Characterisation of Soil Ionisation in Earthing Systems," PhD Thesis, Cardiff University, 2001.